

Effect of Pile Embedment Length on the Connection Behavior and Precast Pile Footing

ALDOT Project Number: 930-924

Submitted to:

Alabama Department of Transportation
1409 Coliseum Boulevard
Montgomery, Alabama 36110

Prepared by:

Vidya Sagar Ronanki, PhD Student
Gabrielle Willis
Sriram Aaleti, Ph.D.

Department of Civil, Construction, and Environmental Engineering,
College of Engineering,
The University of Alabama

Prepared by

UTCA

University Transportation Center for Alabama

The University of Alabama, The University of Alabama at Birmingham,
and The University of Alabama in Huntsville

UTCA Report Number 16409
October 2018

TABLE OF CONTENTS

Chapter 1: Introduction	1
1.1 Background	1
1.2 Overview of Precast Concrete and Accelerated Bridge Construction	1
1.3 Overview of Pile Embedment Depth in Foundations	3
1.4 Project Objectives and Scope.....	3
1.5 Organization of the Report.....	3
Chapter 2: Literature review	5
2.1 Introduction.....	5
2.2 Review of Studies using HP Piles.....	5
2.2.1 Shama, Mander and Aref (2002)	5
2.2.2 Xiao, Wu, Yaparak, Martin & Mander (2006)	8
2.2.3 Xiao, Chen (2013).....	11
2.3 Review of studies using other than HP piles	14
2.3.1 Steunenbergh, Sexsmith, & Stierner (1998)	14
2.3.2 Silvia & Seible (2001)	15
2.3.3 Stephens & Mckittrick (2005)	18
2.3.4 Rollins & Stenlund (2010)	20
2.4 Summary of Research studies	22
2.5 Review of various state DOT requirements on minimum pile embedment depth.....	27
2.5.1 Colorado DOT	27
2.5.2 Connecticut DOT	27
2.5.3 Delaware DOT	28
2.5.4 Georgia DOT	28
2.5.5 Idaho DOT	28
2.5.6 Illinois DOT	28
2.5.7 Indiana DOT	29
2.5.8 IOWA DOT	29
2.5.9 Kansas DOT	29
2.5.10 Kentucky DOT.....	30
2.5.11 Michigan DOT	30
2.5.12 Minnesota DOT	30
2.5.13 Montana DOT	30
2.5.14 Nevada DOT	30
2.5.15 New Hampshire DOT	31
2.5.16 NY State DOT.....	31
2.5.17 North Carolina DOT	32
2.5.18 North Dakota DOT	32
2.5.19 Ohio DOT	32
2.5.20 Oregon DOT	32
2.5.21 Rhode Island DOT	33
2.5.22 South Carolina DOT (same as Nevada DOT details)	33

2.5.23	Vermont DOT	33
2.5.24	Washington State DOT	33
2.5.25	West Virginia DOT	34
2.5.26	Wisconsin DOT	34

Chapter 3: Identification of a Prototype Bridge and Development of 3D Finite Element Models

.....		35
3.1	Introduction.....	35
3.2	Expected range of loading values on top of footings.....	35
3.2.1	Input Parameters	36
a)	Girder type	36
b)	Span.....	36
c)	Girder Spacing	36
d)	Width of the bridge deck.....	36
e)	Overhang width.....	36
f)	Thickness	36
g)	Average haunch thickness.....	36
h)	Wearing surface thickness	36
i)	Parapet height and cross sectional area.....	36
j)	Unit weight of concrete.....	37
3.2.2	Load calculations	37
a)	Dead Loads	37
b)	Live loads.....	38
c)	Braking force	39
d)	Wind loads	39
e)	Limit state load combinations.....	41
3.2.3	Summary of expected loads and selection of Prototype Bridge	41

Chapter 4: Evaluation of effect of pile embedment depth using 3D finite element methods and test specimen selection.....

4.1	Introduction.....	44
4.2	Finite element model properties.....	44
4.2.1	Material models in ATENA.....	45
a)	Concrete material model	45
b)	Reinforcement material model.....	46
c)	Interface material model	46
4.2.2	Element types in ATENA	47
4.2.3	Material model verification and modelling of other concrete systems.....	48
a)	Compression cylinder test and dog bone coupon tension test	48
b)	Verification of crack prediction capabilities of ATENA	49
4.3	Finite element model of Prototype Bridge foundation	50
4.4	Results of FEA of Prototype Bridge foundation.....	52
4.4.1	Principal stress contours	52
4.4.2	Rebar Stresses	54
4.4.3	Shear stresses in main foundation.....	54

4.5	Effect of reducing the pile embedment length	55
4.5.1	Comparison of maximum principal stresses in concrete	55
4.5.2	Comparison of rebar stresses	57
4.5.3	Comparison of shear stresses	57
4.6	Selection of test specimens	57
Chapter 5: Fabrication and testing of experimental specimens		61
5.1	Introduction	61
5.2	Material Properties	61
5.2.1	Steel	61
5.2.2	Concrete	62
5.2.3	Grout	63
5.3	Fabrication of test specimens	63
5.4	Test Setup and Instrumentation	67
5.4.1	Specimen #1 and Specimen #2	67
5.4.2	Specimen #3 and Specimen #4	68
5.4.3	Gauge placement	70
a)	Steel Strain Gauges	70
b)	Concrete strain gauges	71
5.4.4	Load Application	71
Chapter 6: Results and discussion		72
6.1	Introduction	72
6.2	Specimen #1 Test Results	72
6.3	Specimen #2 Test Results	75
6.4	Pile-concrete interface properties and post construction analysis	78
6.5	Specimen #3 Test Results	80
6.6	Specimen #4 Test Results	85
Chapter 7: Summary and conclusions		88
7.1	Summary	88
7.2	Conclusions	89
7.3	Recommendations for Future Research	89
Chapter 8: References		90

List of Tables

Table 1-1 Table showing minimum embedment length requirements as per various state DOTs .	3
Table 3-1 Selection of girder shape for various span lengths	36
Table 3-2 Load combinations and factors as per AASHTO LRFD specifications (2017)	41
Table 3-3 Expected maximum vertical loads on footings for various spans	42
Table 3-4 Expected loads on top of foundation for Prototype bridge.....	42
Table 4-1 Material properties of concrete used in modelling of Prototype Bridge foundation	52
Table 5-1 Reinforcing bar and structural steel properties.....	62
Table 5-2 Concrete material Properties	62
Table 5-3 Measure concrete compressive strengths	62
Table 5-4 Measured compressive strengths of grout	63
Table 6-1 Table showing calculation of cohesion value, C	79

List of Figures

Figure 1-1 Figure showing precast construction projects implemented by various state DOTs. (Graybeal, 2014; Culmo, 2009)	2
Figure 2-1 Specimen details for the tests conducted by Shama, Mander and Aref (2002)	5
Figure 2-2 Test Setup used by Shama, Mander and Aref (2002)	6
Figure 2-3 Observed failure in test specimens with existing connection details (Shama, Mander, & Aref, 2002)	6
Figure 2-4 Observed force vs lateral displacement behavior of the test specimens with existing connection details (Shama, Mander, & Aref, 2002)	7
Figure 2-5 Observed failure and force vs lateral displacement behavior of the retrofitted test specimens (Shama, Mander, & Aref, 2002)	7
Figure 2-6 Prototype foundation used for testing, Xiao et al (2006)	9
Figure 2-7 Test specimen and pile anchorage details, Xiao et al (2006)	9
Figure 2-8 Results and observations from the cyclic vertical load tests, Xiao et al (2006)	10
Figure 2-9 Observed failure and experimental results of specimens with lateral load, Xiao et al (2006)	11
Figure 2-10 Geometry and reinforcement of test models (Xiao & Chen, 2013) (dimensions in mm)	12
Figure 2-11 Test setup and loading condition for piles, (Xiao & Chen, 2013)	13
Figure 2-12 Observed failure in test specimens, (Xiao & Chen, 2013)	13
Figure 2-13 Tests specimen details, Steunenberg et al. (1998)	15
Figure 2-14 Figure showing test setup details and observed failure in piles, Steunenberg et al. (1998)	15
Figure 2-15 Standard CalTrans details for CISS piles, (Silva & Seible, 2001)	17
Figure 2-16 Test setup and specimen details, (Silva & Seible, 2001)	17
Figure 2-17 Limit states of test specimen STD2, (Silva & Seible, 2001)	18
Figure 2-18 Limit states of test specimen STD3, (Silva & Seible, 2001)	18
Figure 2-19 Test Matrix giving the specimen details for experimental investigation, Stephens & Mckittrick (2005)	19
Figure 2-20 Test setup – plan view, Stephens & Mckittrick (2005)	20
Figure 2-21 Test specimen details, Rollins & Stenlund (2010)	21
Figure 2-22 Typical test setup, Rollins & Stenlund (2010)	22
Figure 3-1 Screen shot showing the input page of the excel sheet for calculating loads on top of footings	35
Figure 3-2 Geometry of parapet as per ALDOT standards	37
Figure 3-3 Screen shot showing the dead load calculations performed in the excel sheet for calculating loads on top of footings	38
Figure 3-4 HL 93 loading of design truck (Indicated in blue) and design lane load (indicated in black)	38
Figure 3-5 Screen shot showing the live load calculations performed in the excel sheet for calculating loads on top of footings	39
Figure 3-6 Screen shot showing the braking force calculations performed in the excel sheet for calculating loads on top of footings	39

Figure 3-7 Screen shot showing the wind load calculations performed in the excel sheet for calculating loads on top of footings	40
Figure 3-8 Screen shot showing load combination calculations performed in the excel sheet	41
Figure 3-9 Figure showing details of the prototype bridge selected.....	43
Figure 4-1 Expected cracking in an ATENA model of a simply supported beam failing in shear	44
Figure 4-2 Bi linear stress-strain relationship used for rebar modelling	46
Figure 4-3 Figure showing interface element parameters.....	47
Figure 4-4 Figure showing element types in ATENA (2016)	47
Figure 4-5 Truss element with 2 or 3 node formulation in ATENA (2016).....	48
Figure 4-6 FE model details of the compression cylinder and dog bone coupon test	48
Figure 4-7 Figure showing output stress strain curves for compression and tension obtained from ATENA FEA	49
Figure 4-8 FE model of BT-78	49
Figure 4-9 Figure showing comparison of experimentally observed cracking to results from ATENA FEA	50
Figure 4-10 Figure showing details of the finite element model built in ATENA	51
Figure 4-11 Figure showing principal stress contours in Prototype Bridge foundation	53
Figure 4-12 Stresses in main reinforcement layer above the piles	54
Figure 4-13 Shear Stresses in foundation	55
Figure 4-14 Figure comparing principal stresses in foundation for different embedment depths	56
Figure 4-15 Figure comparing stresses in bottom reinforcement layer for different embedment depths	57
Figure 4-16 Figure comparing shear stresses in foundation for different embedment depths.....	57
Figure 4-17 Figure showing details of specimen #1 and specimen #2	58
Figure 4-18 Figure showing details of specimen #3	59
Figure 4-19 Figure showing precast foundation details.....	60
Figure 5-1 Figure showing tensile testing of rebar	61
Figure 5-2 Figure showing the rebar deformation pattern	62
Figure 5-3 Figure showing grout preparation in a concrete mixer	63
Figure 5-4 Figure showing the form work of all the test specimens	64
Figure 5-5 Figure showing casting details of Specimen #3 and Specimen #4	65
Figure 5-6 Figure showing details of concrete casting	66
Figure 5-7 Figure showing test setup for specimens #1 and #2.....	67
Figure 5-8 Figure showing strain gauge locations for piles in specimens #1 and #2	68
Figure 5-9 Figure showing typical test setup for specimens #3 and #4.....	69
Figure 5-10 Details of the hold down plates.....	70
Figure 5-11 Location of concrete gauges.....	70
Figure 5-12 Figure showing placement of steel and concrete gauges	71
Figure 6-1 Figure showing the condition of pile concrete interface for specimen #1 at maximum loading.....	72
Figure 6-2 Graph showing the experimentally obtained load vs pile displacement data for Specimen #1	73
Figure 6-3 Figure showing the strains recorded at various embedment depth on the pile in specimen #1.....	74

Figure 6-4 Figure showing the strains recorded along the depth of the pile for Specimen #1	75
Figure 6-5 Figure showing the condition of pile concrete interface for specimen #2 at maximum loading.....	75
Figure 6-6 Graph showing the experimentally obtained load vs pile displacement data for Specimen #2.....	76
Figure 6-7 Figure showing the strains recorded at various embedment depth on the pile in specimen #2.....	77
Figure 6-8 Figure showing the strains recorded along the depth of the pile for Specimen #2	78
Figure 6-9 Figure showing post construction Finite Element Analysis details of Specimen #3 ..	79
Figure 6-10 Comparison of experimental results with FEA for Specimen #3	82
Figure 6-11 Figures showing no visible damage to the concrete surrounding the pile in Specimen #3.....	83
Figure 6-12 Graph showing the experimentally observed longitudinal rebar stresses and comparing with FEA in Specimen #3	83
Figure 6-13 Graph showing load vs deflection from experimental observations and FEA for Specimen #3.....	84
Figure 6-14 Figure showing graphs of concrete strains observed at critical locations for Specimen #3.....	85
Figure 6-15 Figure showing cracking in Specimen #4	86
Figure 6-16 Figure comparing the critical parameters of Specimen #3 and Specimen #4	87

CHAPTER 1: INTRODUCTION

1.1 Background

Rapid economic and population growth, along with deteriorating bridge infrastructure, is putting a persistent strain on the nation's transportation network. Federal and state transportation departments (DOTs) are looking for new ways to build, repair, or replace bridges quickly and with minimal interruption to the traveling public. The FHWA has begun an attempt to shorten the time it takes to put new bridges into operation and to increase the design life of bridges from 50 to 75 years. In response to these changes and to facilitate accelerated bridge construction (ABC) practices, several State Departments of Transportation (DOTs), including Alabama DOT (ALDOT), have developed a variety of structural connection details for prefabricated bridge elements ranging from full-depth precast deck panels to precast girders to precast integral abutments.

1.2 Overview of Precast Concrete and Accelerated Bridge Construction

Precast concrete is a natural progression from the more traditional construction method of cast-in-place concrete. There are various advantages to casting in plant-controlled environments. It could lead to improved material and construction quality monitoring. This enhanced manufacturing quality has a positive impact on the service life and enables enhanced architectural treatments of manufactured bridge components. In addition, the consistent production process and workflow of precast manufacturers provide a safer working environment for construction crews. By reusing molds, precast concrete can reduce production costs. Prefabricated elements that are connected in-situ to other parts can reduce the number of employees that must be mobilized on the construction site, hence decreasing the number of days or frequency of lane closures while the construction project is active. In addition, it expedites construction by eliminating the need to wait for the strength of concrete components to develop. Therefore, the economics of bridge construction are enhanced using prefabricated materials.

The use of prefabricated bridge elements also enables ABC techniques, which lead to significantly reduced construction times when compared to traditional construction methods. ABC techniques have been used in bridge construction to successfully reduce the disruption caused to users. Several experimentally validated connection details to facilitate accelerated construction are available in the literature for connecting different prefabricated superstructure and substructure bridge elements. Figure 1-1 shows some of these details which have already been implemented in existing bridge construction projects by several departments of transportation. Figure 1-1a shows precast deck panels joined together at the site. This was part of a rapid bridge deck replacement project carried out by NYSDOT on four bridges on I-81 (Graybeal, 2014). Figure 1-1b shows a precast pier cap joined together at the site to the cast-in-situ columns. This project was carried out to replace an aging bridge over Lake Belton by TxDOT. Also, notice in this figure that the pier cap has curved edges, this custom architectural detail was easily implemented as the cost of the form was spread out over 62 identical prefabricated caps (Culmo, 2009). Figure 1-1c shows the installation of the precast concrete pier. Multiple sections like these were sealed and bonded

together using epoxy and detailed with shear keys for shear transfer in the prefabricated sections. Once all the sections were installed and sealed the pier was post-tensioned (Culmo, 2009). ALDOT has also recently initiated two Accelerated Bridge Construction (ABC) projects including; 1) rapid bridge replacement in Dothan, AL using lateral bridge sliding technology, and 2) rapid bridge construction using prefabricated column elements connected to cast-in-place pile footings using bar couplers.

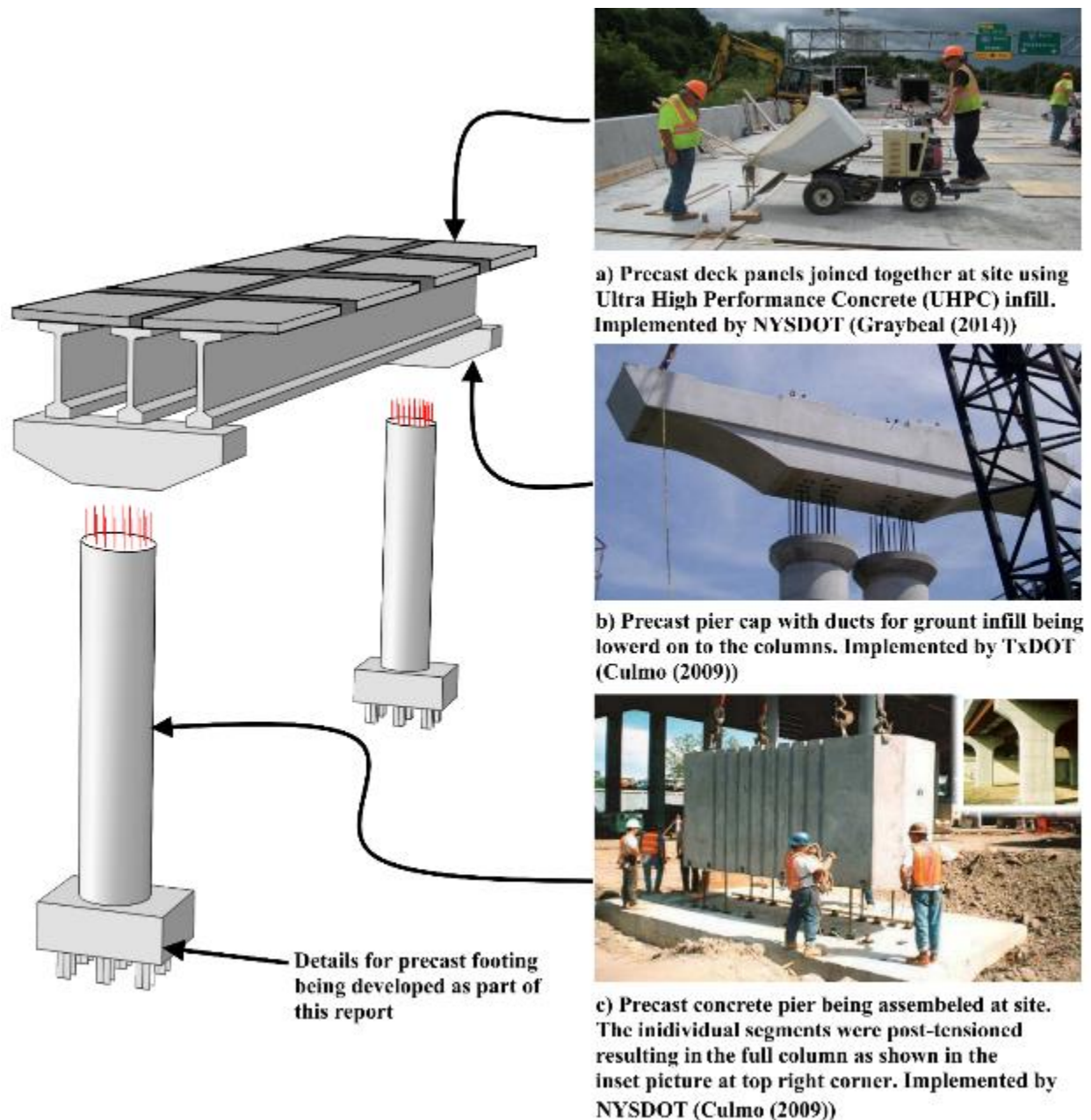


Figure 1-1 Figure showing precast construction projects implemented by various state DOTs. (Graybeal, 2014; Culmo, 2009)

1.3 Overview of Pile Embedment Depth in Foundations

ALDOT standard design assumes that the connection between pile and footing is a pinned connection. Additionally, ALDOT specifies that steel piles be embedded at least 24 in. into the foundation. In this context, Aaleti et al. (2012) found that a 24 in. embedment may result in a fixed connection and may influence the load transmission mechanism and local stresses surrounding the piles. In addition, most other states mandate a minimum embedment depth of 12 in. (see Table 1-1). Any reduction in the required minimum embedment depth will result in a reduction in overall footing thicknesses. This reduction in material consumption will aid in reducing the weight of precast elements used in future ABC construction projects and reduce production costs for both precast and cast-in-place projects.

Table 1-1 Table showing minimum embedment length requirements as per various state DOTs

State Code	Embedment Length (min)
CO, MI, WI	6 in.
NC	9 in.
CT, DE, GA, IL, IA, KS, MN, MO, NV, NH, NY, ND, OR, RI, SC, VT, VA, WA, WV	12 in.
IN, OH, ID, KY, AL	24 in.
MT	20 in.

1.4 Project Objectives and Scope

This research project's primary objective was to examine the viability of reducing the minimum embedment depth requirements for steel piles in foundations and to provide the ALDOT Bridge Bureau with a dependable and cost-effective substructure system that can be implemented for accelerated bridge construction. These objectives were accomplished by combining a 3D Finite Element Analysis (FEA) with the experimental results of evaluating four distinct specimens. Four specimens were cast in the Large-Scale Structures Laboratory (LSSL) at the University of Alabama and loaded to surpass more than twice the piles' permitted load limit. These specimens were monitored with internal and external strain gauges to ensure their performance was adequate at all load levels. In addition, a comprehensive analysis of the present practices of several state DOTs and other accessible research material was conducted as part of this study.

1.5 Organization of the Report

Chapter 2 reviews the current pile embedment regulations of several state DOTs in the United States, and it follows this introductory chapter. The experimental and analytical research that have been conducted to determine the factors that control the length of the pile embedment into the footings are also reviewed. The expected bridge loads for different bridge configurations such span, spacing, number of lanes, and supporting pier configuration are analyzed in detail and presented in Chapter 3. The loads were calculated using the AASHTO Long-Range Bridge Design Specifications (2017). The prototype base that was used as a starting point for the test specimens' design and construction is also described in this section. In Chapter 4, we go over the FEA methods that were utilized to model the test specimen's behavior. All the test specimens included in this

investigation have detailed designs presented in Chapter 5. The specifics of the instrumentation scheme employed to record the behavior of these specimens are also provided in this chapter. The testing apparatus is described in detail in Chapter 6. In this chapter, we also present the data gathered from the instruments used in the testing process.

CHAPTER 2: LITERATURE REVIEW

2.1 Introduction

This chapter presents a comprehensive literature analysis about the performance and behavior of various pile to footing connections, as well as a discussion of the minimum embedment length criteria of many state DOTs. While HP steel pile-to-footing connections are the primary focus of this study, other types of pile-to-footing connections have also been investigated. This was done so that a full picture could be formed of the effects of various testing methods, the effects of confining rebar and detailing, the various types of loading scenarios, etc. As a result, this chapter is broken up into three sections: a review of studies involving HP piles; a review of research involving other pile types; and a discussion of state DOT standards.

2.2 Review of Studies using Steel HP Piles

2.2.1 Shama, Mander, and Aref (2002)

Shama et al. (2002) examined the behavior and performance of existing pile cap connection details with a 12-inch embedment length (300 mm). Two experimental programs were built and evaluated for this investigation. The first program evaluated the performance of two existing connection details under cyclical lateral loads to construct a hypothesis supported by FEM comparisons. This hypothesis addresses the stress distribution along the length of the connection embedment. The second program utilized the established theory to retrofit the specimens. These were then evaluated to see whether the proposed retrofit detail is successful or unsuccessful.

The test specimens consisted of two HP 10 x 42 piles, one for weak axis testing and the other for strong axis testing. As indicated in Figure 2-1, both piles were embedded in a rectangular concrete block. In these rectangular blocks, transverse steel was welded to an L2xL2x3/8 angle to demonstrate the steel's continued sufficiency in this direction.

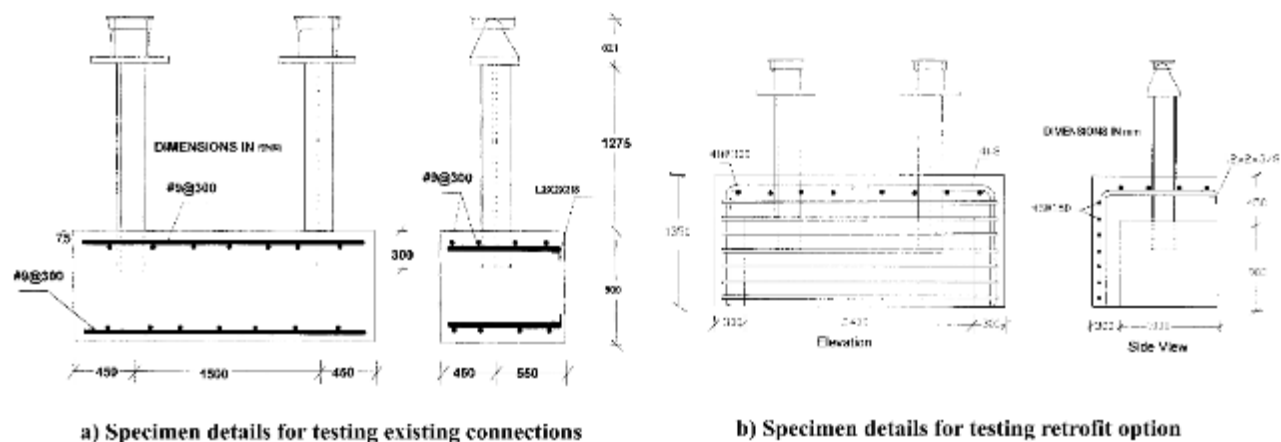


Figure 2-1 Specimen details for the tests conducted by Shama, Mander and Aref (2002)

The setup for these tests consisted of a hybrid setup combining the vertical component of the diagonal actuator force with a variable axial force from vertical actuator acting via a lever beam system (see Figure 2-2). This was done to account for the additional vertical thrust typically experienced by exterior piles, and to accommodate a small lab testing space. A W10X88 was used as anchorage to prevent translation and uplift during testing. The concrete used in this study was found to have a compressive strength of 4.35ksi (30 MPa) and was used in conjunction with Grade 60 steel reinforcement. The Steel HP pile specimens that were tested had an average yield strength (f_y) of 45.6 ksi (315 MPa) and an ultimate strength (f_u) of 68.9 ksi (475 MPa).

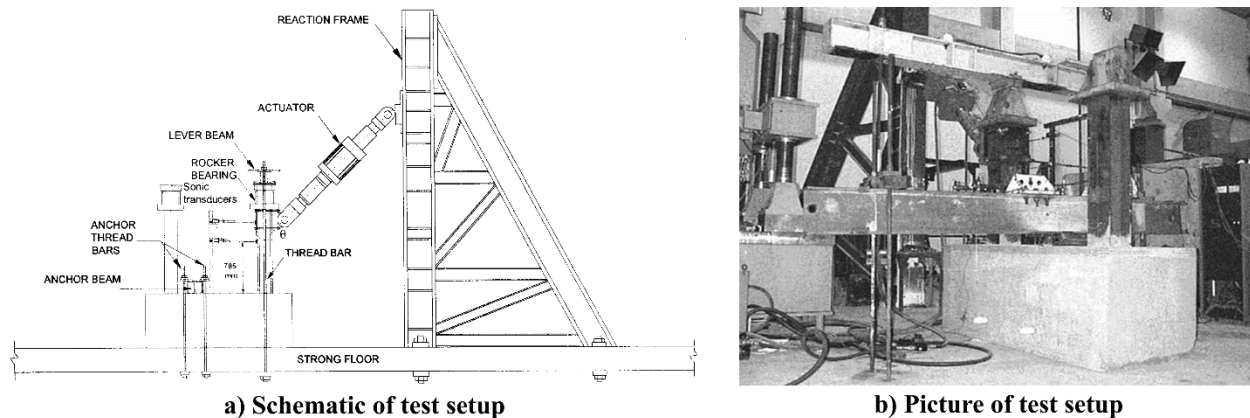


Figure 2-2 Test Setup used by Shama, Mander and Aref (2002)

Specimens were tested with two reversed cycles at displacement amplitudes of 0.25%, 0.55, 1%, 2%, 3%, 4%, and 5% drift. The cyclic period lasted for one minute. For the tests of existing connection details, it was found that the failure of the specimens occurred due to cracking of concrete surrounding concrete in the concrete pile caps and not due to the failure of steel piles (see Figure 2-3).

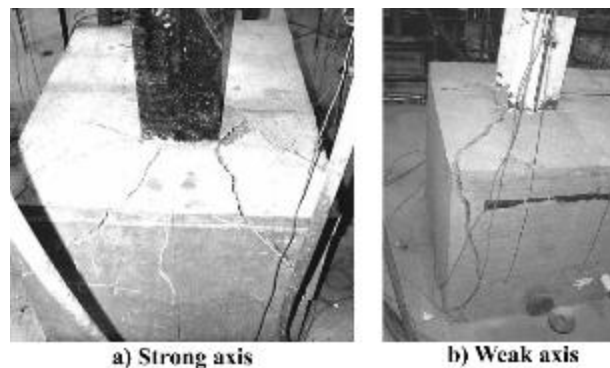


Figure 2-3 Observed failure in test specimens with existing connection details (Shama, Mander, & Aref, 2002)

The experimentally obtained force vs lateral displacement graphs for both the strong axis and weak axis specimens are shown in Figure 2-4. It was observed that for the specimen tested along its strong axis, linear behavior was exhibited prior to 1% drift, but at 2% drift brittle concrete failure occurred. As the test progressed, steel slippage occurred around 4 and 5% drift. For the specimen

tested along its weak axis, it was observed that the inelastic behavior of the steel began at 2% drift, and brittle failure did not occur until 3% drift. Strength dropped from this point until steel slippage began at 5% drift.

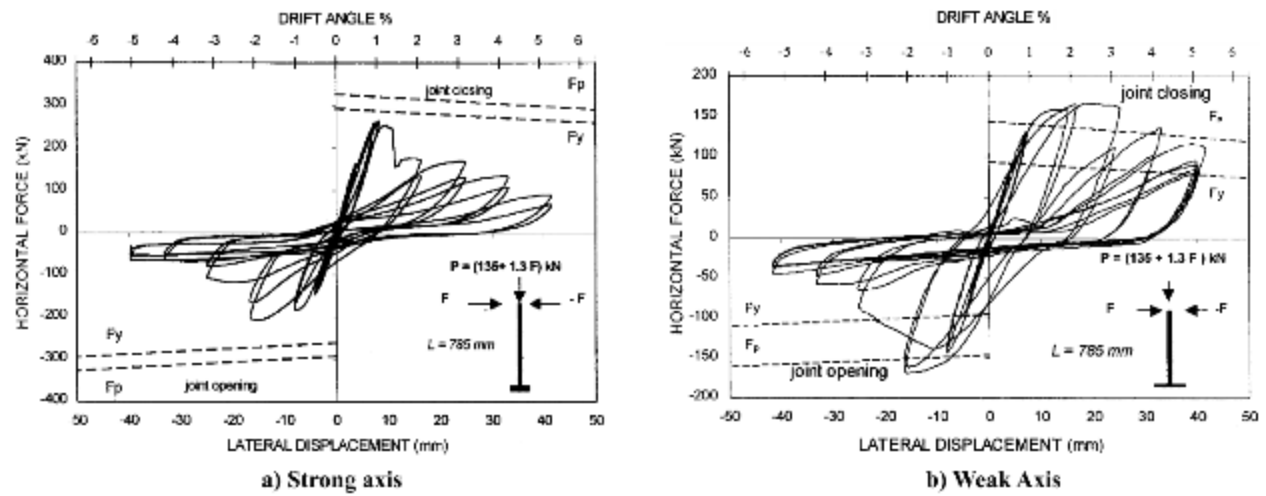


Figure 2-4 Observed force vs lateral displacement behavior of the test specimens with existing connection details (Shama, Mander, & Aref, 2002)

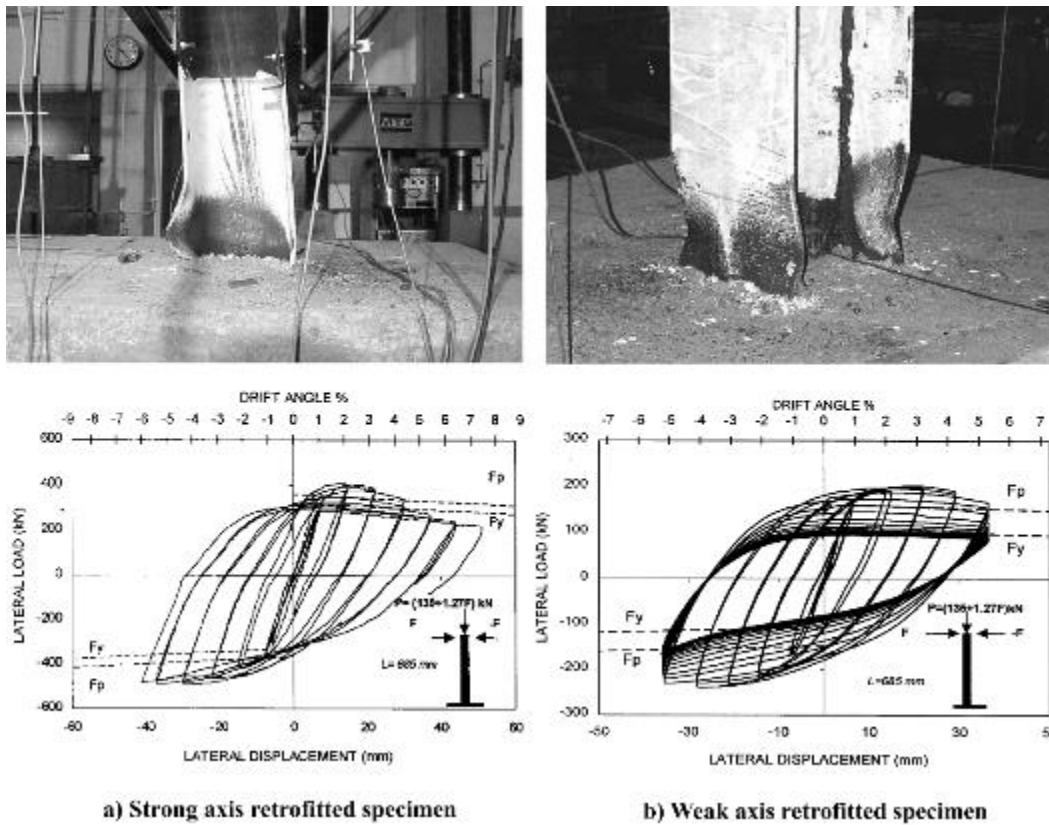


Figure 2-5 Observed failure and force vs lateral displacement behavior of the retrofitted test specimens (Shama, Mander, & Aref, 2002)

Based on these observations, a theoretical model was created with an assumed linear stress distribution. This model permitted the calculation of concrete compressive stresses. Using this model, retrofitting test specimens were designed and constructed. By relocating the plastic hinge from the concrete cap to the steel pile, the objective of the retrofitting was to improve the performance under seismic conditions. Thus, encouraging a connection that is more ductile, able to resist higher deformation and dissipate more seismic energy. The modified specimens were examined using the same loading techniques as the originals. The modified strong-axis specimen failed because of local pile buckling, with only minor surface cracking of the cover concrete observed. The modified weak-axis specimen also failed due to local buckling in the steel pile, but the concrete pile cover was unharmed (see Figure 2-5).

This investigation concluded that a simplified linear elastic theory created in this study was able to accurately predict the performance of connections under lateral load. The upgraded pile-to-pile-cap connections demonstrated more ductile behavior and were subjected to rigorous drift amplitude testing. In actuality, the structure may not experience a 6 percent drift, and the local buckling failure that occurred due to cycle fatigue under lateral loading may not occur.

2.2.2 Xiao, Wu, Yaparak, Martin & Mander (2006)

In a FHWA-NCEER funded study (Xiao et al. (2006)), researchers at the University of Southern California and The State System of New York (SUNY) studied the connection behavior of H-Piles embedded in concrete pile caps, focusing on a shallow embedment and V-shaped anchorage bars. The connection details were modelled after a prototype bridge in California (see Figure 2-6), and a total of five full-scale specimens were constructed and tested to failure. The details of the test specimens are shown in Figure 2-7a. Two of these specimens were tested under vertical cyclic loading, two under lateral cyclical force combined with a constant vertical load, and one specimen was tested under varying horizontal and vertical loads. The constructed specimens were meant to simulate the corner piles on large footings. The specimens used HP 14x89 piles embedded 5 in. into the footing and anchored as per the details shown in Figure 2-7b. The V-shaped anchorage bars were welded to the piles, ensuring the bars were in contact with the edges of the holes closest to the end of the pile. For testing, when combined loading was necessary, the actuator was set to an angle of 47 degree to apply both horizontal and vertical loading. The testing matrix used in this study is shown in Table 2-1. The vertical loading tests failed in both the weak and strong axes, by V-bar rupture. The force-displacement curves for both the strong axis and weak axis specimens are shown in Figure 2-8a and Figure 2-8b, and the observed failures are shown in Figure 2-8c and Figure 2-8d. The capacities of both specimens were much less than the predicted capacity, but that was assumed to be caused by the V-bars not acting at the same time and not developing the full strength for the connection before one ruptured.

For the lateral load tests, the strong axis specimen was allowed to rock and large cracks formed in the pile cap. Final failure for this specimen was due to push-out rupture of the concrete at the footing edge (Figure 2-9a). The weak axis specimen could not rock and failed from the HP-pile yielding in the flanges near the connection. The horizontal loading specimens showed capacities that were close to the estimated values. The force-displacement curves for both the strong axis and

weak axis specimens subjected to lateral loading are shown in Figure 2-8a and Figure 2-89b, and the observed failures are shown in Figure 2-89c and Figure 2-89d.

In the various loading specimen (HP-S-VL), one of the anchor bars ruptured, resulting in a much lower than anticipated capacity. Xiao et al. (2006) recommended the use of a single v-bar instead of two in calculating the design tensile capacity of the system, to ensure the tensile capacity can be adequately calculated and eliminate the risk of underestimating the strength due to one bar rupturing before the other. Another finding is confirmation that the pile-to-pile cap connection can sustain quite a bit of moment and idealizing the connect as a pin is highly unrealistic. Upon concrete rupture, it was also discovered that there is still flexural resistance, even after the embedment resistance disappears. It was recommended that; V-bars are generally to be avoided for anchorage in new bridges and welding the anchor bars to the pile could be considered; block rupture strength along the pile-cap edges is essential in evaluating the bridge pile foundation and for a more elaborate assessment of the pile foundation behavior, the moment resistance of the pile end with the shallow embedment should be considered.

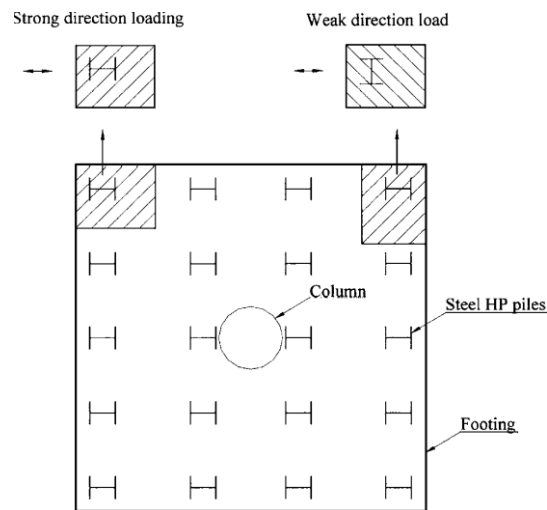


Figure 2-6 Prototype foundation used for testing, Xiao et al (2006)

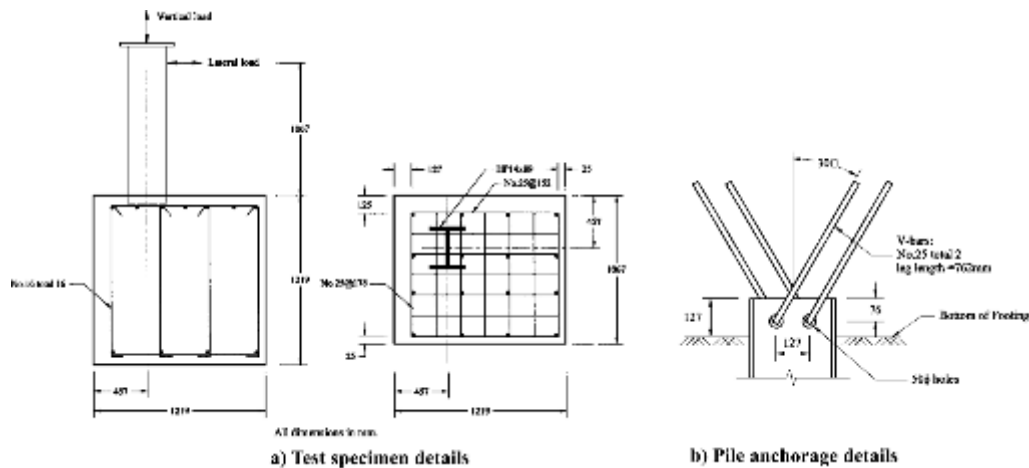
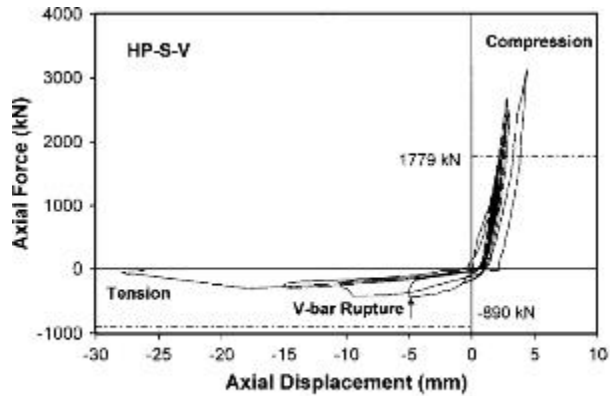


Figure 2-7 Test specimen and pile anchorage details, Xiao et al (2006)

Table 2-1 Details of the test matrix used in Xiao et al. (2006) study

Model Specimens	Orientation of HP pile	Loading Condition	Concrete Strength f'_c (MPa)	Axial load (kN)
HP-S-V	Strong direction	Cyclic vertical loading only	41.1	Varies
HP-W-V	Weak Direction	Cyclic vertical loading only	37.9	Varies
HP-S-L	Strong direction	Cyclic lateral loading with constant vertical load	41.1	1,779
HP-W-L	Weak direction	Cyclic lateral loading with constant vertical load	41.1	1,779
HP-S-VL	Strong direction	Proportionally varied cyclic loading and vertical loading	37.9	Varies ^a

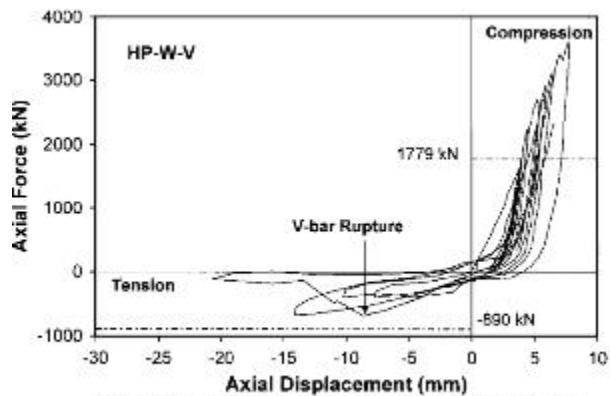
^aInitial axial load was 890 kN; 1 MPa = 0.145 ksi; 1 kN = 0.225 Kip



a) Force vs displacement of strong axis specimen



c) Observed cracking on the specimen

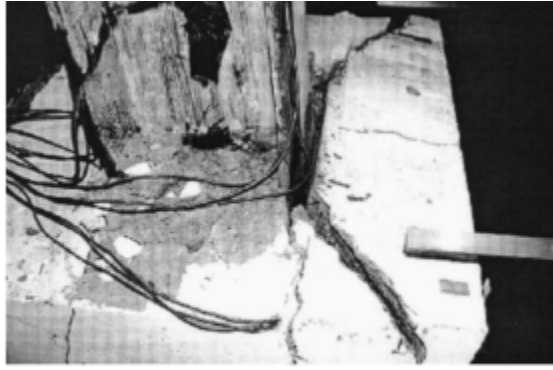


b) Force vs displacement of weak axis specimen

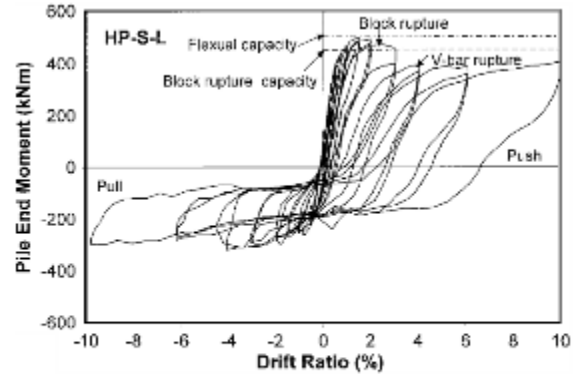


d) Rupture of the anchor bar

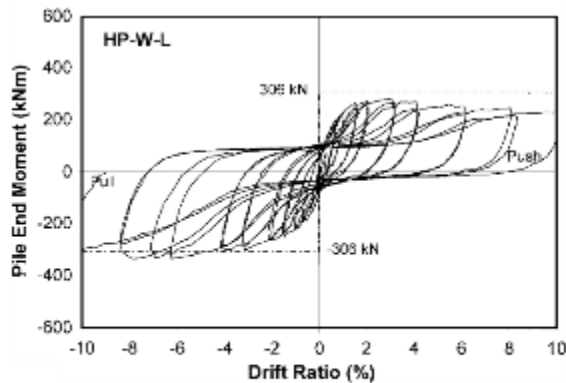
Figure 2-8 Results and observations from the cyclic vertical load tests, Xiao et al (2006)



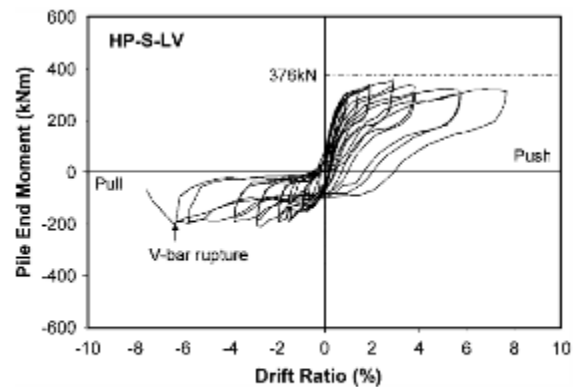
a) Observed failure of concrete block in specimen with constant vertical load and cyclic lateral load



b) Observed pile end moments vs drift ratio for constant vertical load and cyclic lateral load of strong axis specimens



c) Observed pile end moments vs drift ratio for constant vertical load and cyclic lateral load of weak axis specimens



d) Observed pile end moments vs drift ratio for cyclic vertical and lateral load

Figure 2-9 Observed failure and experimental results of specimens with lateral load, Xiao et al (2006)

2.2.3 Xiao, Chen (2013)

This study extended the work carried out by Xiao et al (2006). Previously validated equations were used to predict capacities of a new connection type. In past studies, Xiao et al. (2006), investigated the usage of V-shaped anchorage bars and concluded that type of anchorage was not practical due to the difficulty in securing the bars to the steel piles. This paper investigates welding straight bars to the steel piles and whether this connection type provides additional strength and certainty in calculations. Four straight bars were welded to HP piles along the web for each specimen. The straight bars extended through the entire depth of the pile cap, but the HP sections were only embedded 25mm, in the hopes of creating a connection closer to the behavior of a pin. A full, 16-pile foundation specimen was used, and both middle and corner piles were tested, in both the strong and weak axes, as well as tensile-only tests. The test model and anchorage details are shown in Figure 2-10. Self-balancing loading was used in testing, with setup shown in Figure 2-11. The corner weak axis pile failed from concrete crushing on the back of the pile. The corner strong axis pile failed from concrete cover spalling off. Both middle piles failed from arc cracking on the pile caps, and the tensile specimens failed from pull out and eventual anchor bar rupture. Failure can be seen in Figure 2-12. Overall, the specimens showed considerable improvement compared to the

V-shaped anchorage connection system and did not experience early failure of the anchorage bars. However, other issues may still arise which are unrelated to anchorage bar rupture, so there is still a concern for bond failure, concrete cone pullout, and other issues. Even though the embedment was very small for this study, the connection could still sustain considerable moment, and a pin model is still not accurate. However, because the embedment was so small, concrete block rupture was able to prevail as a governing failure mode for some of the specimens.

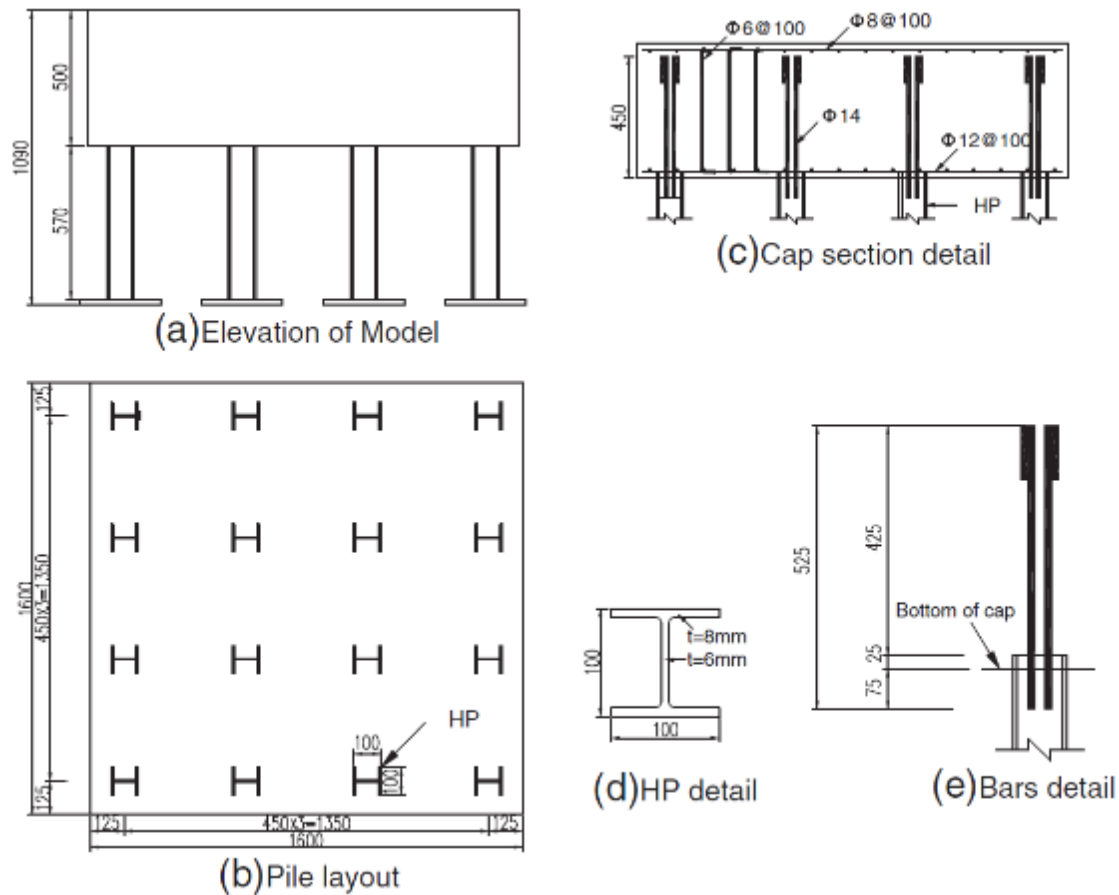


Figure 2-10 Geometry and reinforcement of test models (Xiao & Chen, 2013) (dimensions in mm)

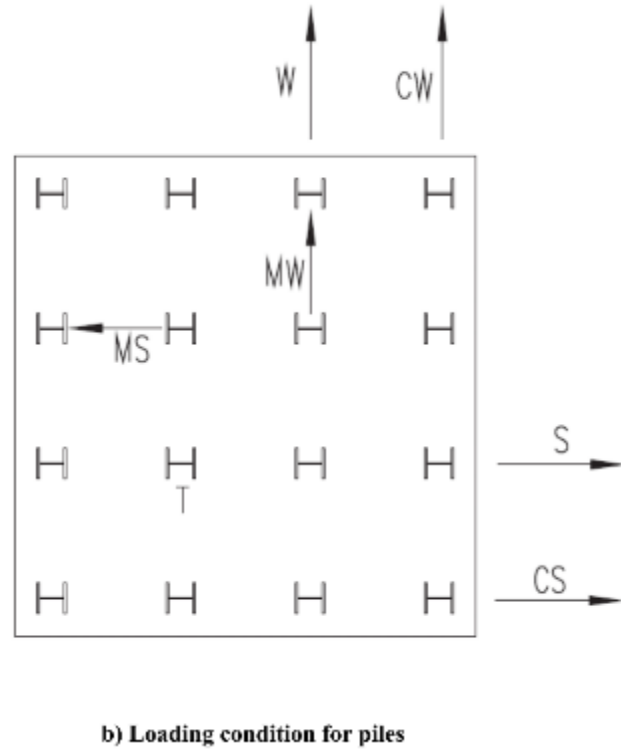
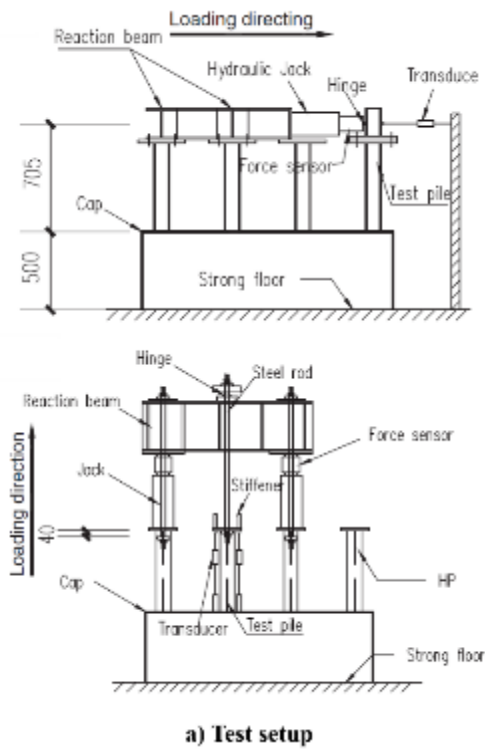


Figure 2-11 Test setup and loading condition for piles, (Xiao & Chen, 2013)

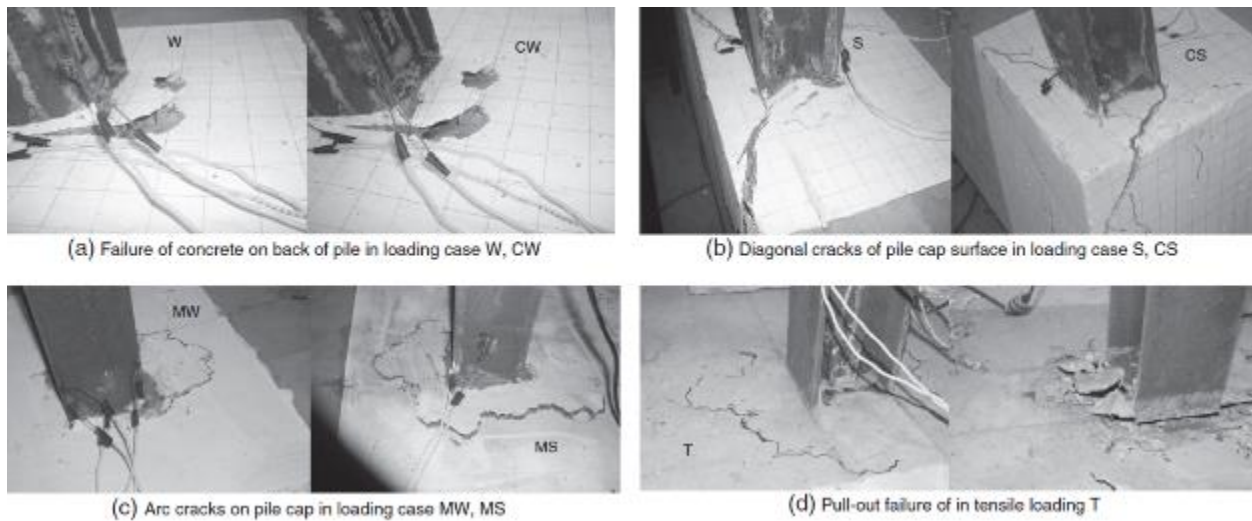


Figure 2-12 Observed failure in test specimens, (Xiao & Chen, 2013)

2.3 Review of studies using other than HP piles

2.3.1 Steunenberg, Sexsmith, & Stierner (1998)

A study conducted for the Ministry of Transportation and Highways of British Columbia (MoTH) investigated the connection behavior of steel pipes embedded in precast concrete cap beams under seismic loading. The goal was to evaluate the design at the time and make recommendations for improvements. Emphasis was placed on ensuring the failure mode of both the MoTH design and the improved design was ductile, specifically, hinging at the piles. Another objective of the study was to observe the behavior of the anchorage system embedding the steel pipe within the concrete. The anchorage system consisted of welding 30 15M x 600 mm deformed wire bars to a steel plate, which was then welded to the end of the pipe pile. Only the plate and the deformed wire bars were embedded into the concrete to facilitate an easier precast construction process. The study tested a single specimen, a full-scale specimen that followed the typical specifications of a MoTH design. Details of the specimen can be seen in Figure 2-13. The specimen was tested under horizontal cyclic loading with no applied vertical loading. Load control was used to get to 75 percent of the yield load, then displacement control was used for the following cycles. The specimen failed from plastic hinging in the pile but results also showed the deformed wire bars undergoing bond slip. Both test setup and failure of the pile can be seen in Figure 2-14. Despite the observed bond slip, the connection was both as strong and as ductile as needed, and the modelled predictions agreed well with the experimental results. Steunenberg et al. recommended more testing to increase the design behavior certainty and investigate the bond development of the anchor bars. A thicker base plate for the pile was recommended to distribute strains to the deformed anchor bars more adequately. Steunenberg et al. also urge MoTH to increase the pile overstrength factor for a more accurate design.

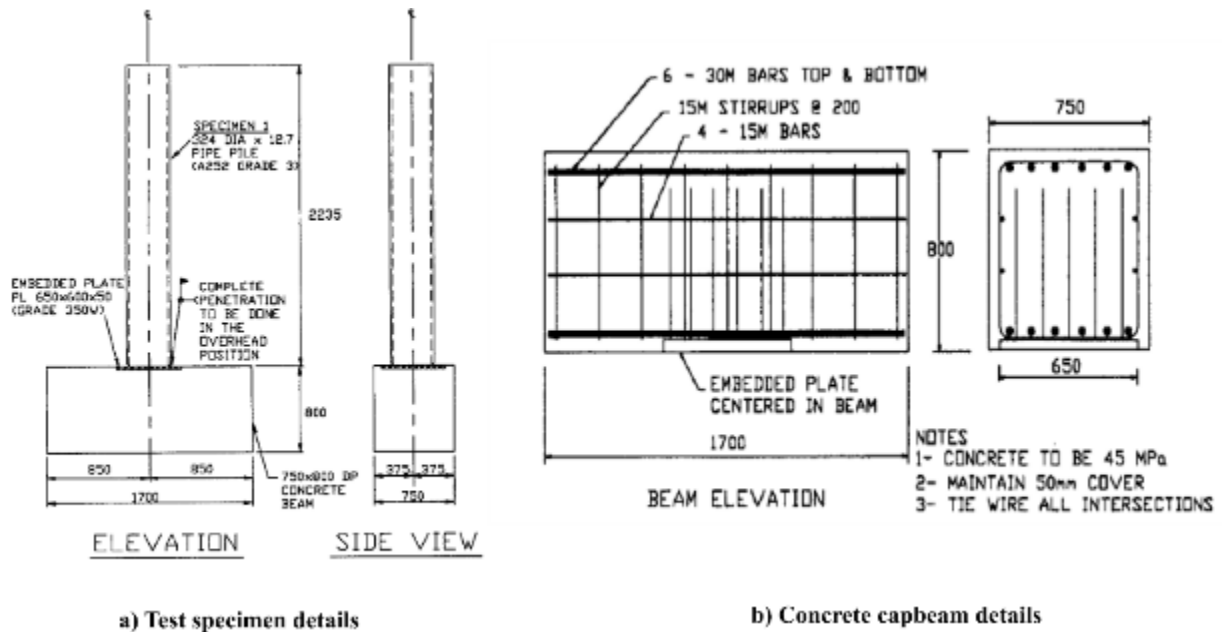


Figure 2-13 Tests specimen details, Steunenberg et al. (1998)

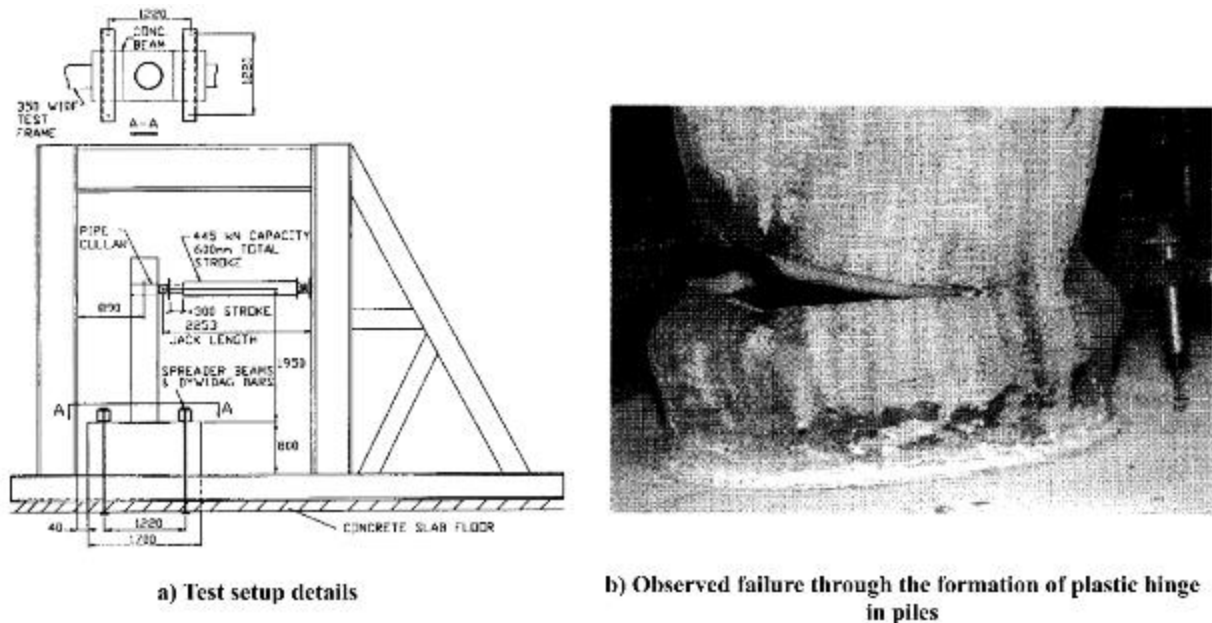


Figure 2-14 Figure showing test setup details and observed failure in piles, Steunenberg et al. (1998)

2.3.2 Silvia & Seible (2001)

Researchers at the University of California San Diego investigated the behavior of CISS piles under seismic loading. Two typical Caltrans pile connections were built and tested, then compared to analytical models. Both specimens were based on a viaduct replacement project in Oakland, California, one with an unreinforced concrete core within the pile and one with a reinforced

concrete core. The unreinforced concrete core specimen used two #8 V-shaped bars as anchorage into the pile cap. Specimen and testing details are shown in Figures 2-15 and 2-16. Specimens were loaded to typical service axial loads, then over four cycles, loaded seismically to theoretical first yield in force control. From that point, three cycles were conducted in displacement control at various displacement ductility levels. The connection with V-shaped anchorage bars was tested in both the weak and strong directions to account for the unilateral direction of the bars.

Silva and Seible established limit states for the pile and the pile cap. The limit states for the pile were the pile elastic limit state, the pile functional evaluation limit state, and pile safety evaluation. The pile elastic limit state was based on the point where there began to be sustained damage during or after a seismic event. The criteria for this limit state was qualitatively based on small (unrepairable) crack widths and quantitatively on steel strain reaching first yield. The pile functional evaluation limit state was based on moderate sustained damage, in which the pile is still function and there should not be any damage that exposes additional steel to corrosion. Repair should still not be required. The pile safety evaluation limit state signifies damage to the pile that would cause it to become unsafe. At this limit state, repairs or even replacement would be necessary to prevent corrosion as steel would become exposed. In the pile cap, limit states of pile cap concrete cover spalling, pile cap joint region cracking, and pile cap joint region failure limit states were identified. Pile cap concrete cover spalling limit state is reached when the concrete directly around the steel casing begins to spall off due to rotation of the steel shell. Pile cap joint region cracking limit state corresponds to when cracking begins to occur around the joint, as defined by principle tensile stresses. Pile cap joint region failure limit state occurs when the joint region cracking becomes excessively large and shear failure begins.

The unreinforced connection failed when the V-Shaped anchor bars failed prior to reaching the design axial tensile load. During cyclic loading, the concrete around the V-shaped bars crushed, and the bars rocked against the holes as the cyclic loading progressed. The limit states observed, in order of occurrence, were pile elastic limit state, pile cap cover concrete spalling control, pile function evaluation, and pile safety evaluation limit states. For the reinforced connection, failure in the joint region occurred and the specimen was also unable to reach the design tensile load. The limit states for this specimen were pile elastic limit state, pile cap joint region cracking limit state, pile functional evaluation limit state, pile cap joint shear failure limit state, pile cap cover concrete spalling control limit state, and pile safety evaluation limit state. These limit states are illustrated for both specimens in Figures 2-17 and 2-18.

Overall, Silva and Seible recommended lowering the design tensile loads for both of these connection details, as well as adding more V-shaped anchor bars when traditional longitudinal reinforcement is not used. Researchers also recommended additional shear reinforcement should be included at the joint for reinforced connections, and these connections should both generally be designed such that the pile elastic state is never reached to prevent the need for repairs.

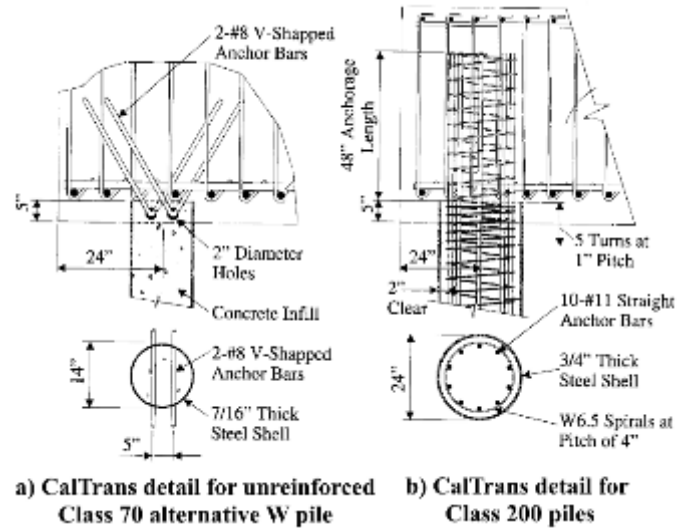


Figure 2-15 Standard CalTrans details for CISS piles, (Silva & Seible, 2001)

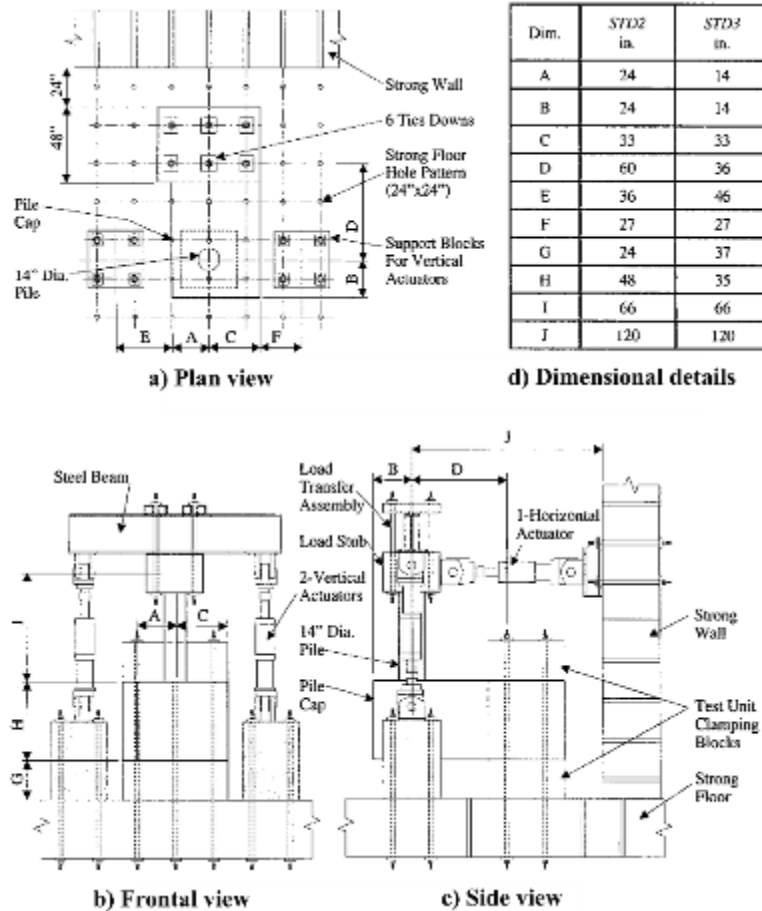


Figure 2-16 Test setup and specimen details, (Silva & Seible, 2001)

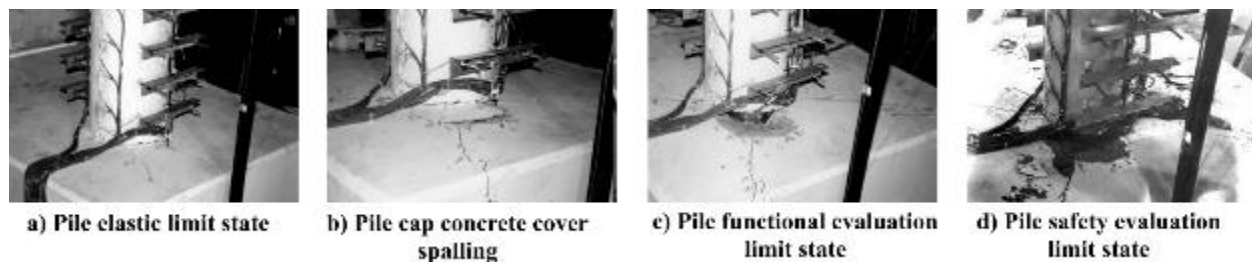


Figure 2-17 Limit states of test specimen STD2, (Silva & Seible, 2001)

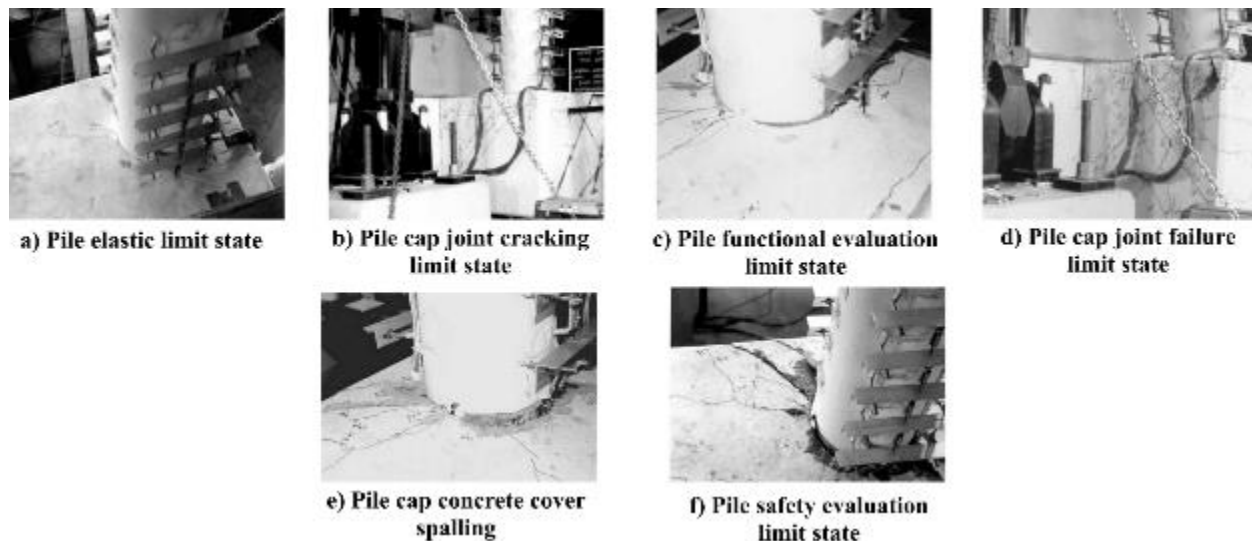


Figure 2-18 Limit states of test specimen STD3, (Silva & Seible, 2001)

2.3.3 Stephens & Mckittrick (2005)

In a study for Montana's Department of Transportation (MDOT), steel pipe piles were filled with concrete and their connection with concrete pile caps were investigated under lateral loading. The specific connection was based off a typical short or medium span MDOT bridge design. Both analytical and experimental methods were used to this end, with analytical methods ranging from strut-and-tie modelling and FEM, to hand calculations. In the experimental phase, five specimen were constructed and tested at Montana State University. Specimen details are shown in Figure 2-19, and test setup is shown in Figure 2-20. Loading was applied laterally with a hydraulic jack. PC-1 was a "typical" full-sized design, and failed through concrete cracking adjacent to the pile. PC-2 was similar to PC-1, but featured a pipe pile with a smaller thickness and failed in a similar manner. PC-3 employed three times the pile cap reinforcement and lower strength concrete compared to PC-1. Failure for this specimen occurred from cracking in the cap concrete and excessive deformation of the cap steel. PC-3a used 5 times the reinforcement of PC-1 and failed similarly to PC-3. PC-4 used seven times the longitudinal reinforcement of PC-1 and failed from plastic hinging in the pile.

From the analytical methods, each had advantages and drawbacks. Hand-written calculations usually adequately predicted capacities and failure mode, but underestimated capacity of lightly reinforced sections by up to 70 percent. Presumably this is from ignoring the tensile capacity of concrete. Strut and tie models once again were inaccurate for lightly reinforced pile caps but could provide more insight into the internal stresses and forces within the sections. FEM was valuable in providing a 3D snapshot of the stresses at every point in the pile-cap but did not track nonlinear behavior in the concrete very well when compared to the other methods.

Overall, several conclusions were reached in this investigation. As more reinforcement was added, the ductility of the connection increased, whereas the lighter reinforced sections had steel that underwent large amounts of plastic deformation and strains. For the compression of the concrete, the stresses surpassed the ACI limiting factor of $0.85f'_c$ by at least a factor of 2. All of the analysis methods used were beneficial in various ways, but each had their own limitations, especially concerning lightly-reinforced sections.


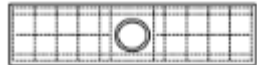
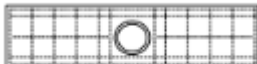
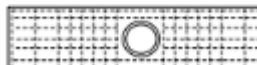


Item	Pipe Pile Wall Thickness, in	Longitudinal Steel Ratio ^a , %	Transverse Steel Ratio ^a , %	Yield Strength of Pile Steel ^b , psi	Concrete Strength ^b , psi	Comments	Reinforcing Layout
Full Size	0.5	0.40	0.09	35,000	4,000 ^b	Timber Creek Bridge, Powder River County, MT	
PC-1	0.32	0.41	0.09	53,000	4,832	Relative amount of reinforcement similar to that in full size structure	
PC-2	0.25	0.41	0.09	56,000	5,326	Same reinforcement as in PC-1, reduced wall thickness for pipe pile	
PC-3	0.25	1.09	0.24	53,000	3,150	Reinforcement increased by a factor of 3 compared to PC-1, concrete strength noticeably low compared to other models	
PC-3a	0.25	2.11	0.65	53,000	3,945	Reinforcement increased by a factor of 5 compared to PC-1	
PC-4	0.25	2.83	0.70	60,000	4,682	Longitudinal reinforcement increased by a factor of 7 compared to PC-1	

Figure 2-19 Test Matrix giving the specimen details for experimental investigation, Stephens & Mckittrick (2005)

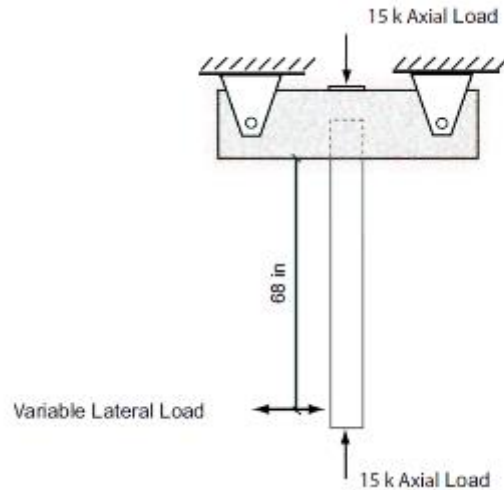


Figure 2-20 Test setup – plan view, Stephens & Mckittrick (2005)

2.3.4 Rollins & Stenlund (2010)

Research at Brigham Young University (BYU) for Utah Department of Transportation (UDOT) was conducted to investigate the behavior of pile-to-pile cap connection behavior, including embedment length, to develop a connection able to resist lateral loading while still developing the pile capacity. Test specimens were constructed and tested in-situ, which is not frequently done. Four pile foundations were constructed, with concrete-filled steel pipe piles embedded into the pile cap. The first specimen had an embedment of 6 inches and standard reinforcement within the concrete in the pile. The second specimen used a 12 inch embedment length and the same standard pile reinforcement. The third specimen used a 12 inch embedment length as well, but contained no concrete within the pile. The fourth and final specimen had a 24 inch embedment and concrete in the pile, but no additional reinforcement within the pile concrete. These details are shown in 2-21. All specimens were tested laterally with a hydraulic ram one above grade, as shown in Figure 2-22. The first specimen failed by excessive deformation, caused by the piles pulling out of the ground. However, the observed shear and moment capacity were still adequate when compared to the design values so the connection details were good. The second specimen performed very similarly to the first, but the failure mode was difficult to determine, either pile pullout from the ground or slippage of the piles from the concrete. The third specimen, without concrete infill, failed due to large shear and tensile cracks. The capacity of this specimen was much lower than the first two specimens, as expected. The fourth and final specimen failed from pile pullout from the ground, and the added embedment length was more than adequate to develop the full capacity of the connection. The load-deflection curve for the fourth specimen was only slightly better than the first two specimens, which had more steel but half to a quarter of the embedment length. Overall, these tests showed that a longer embedment length is the best way to guarantee the full capacity develops, but the addition of reinforcement, as in the first and second specimens, can decrease the need for such a long embedment length, compared to the fourth specimen.

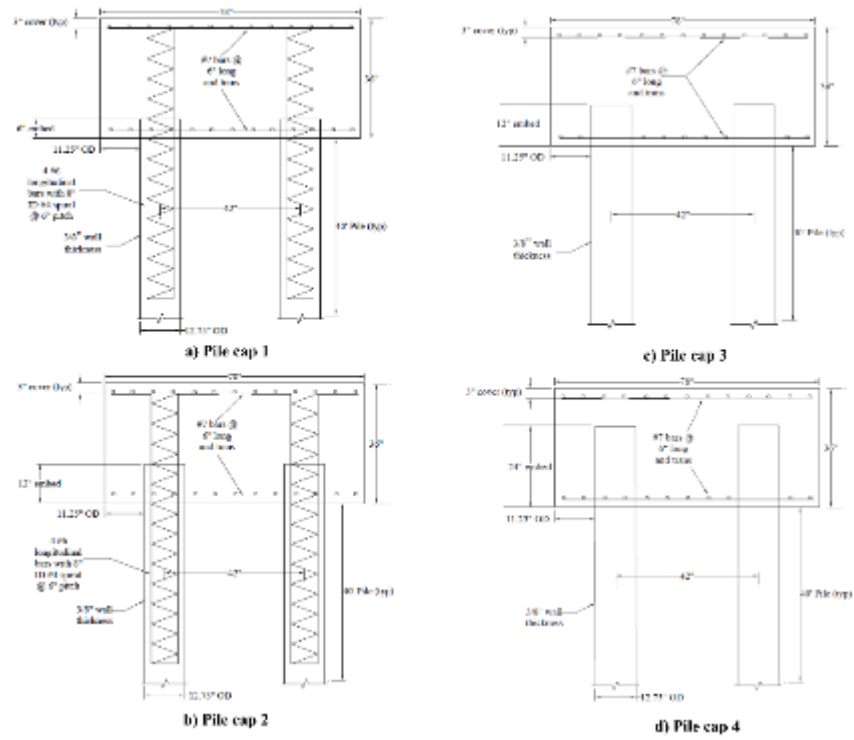


Figure 2-21 Test specimen details, Rollins & Stenlund (2010)

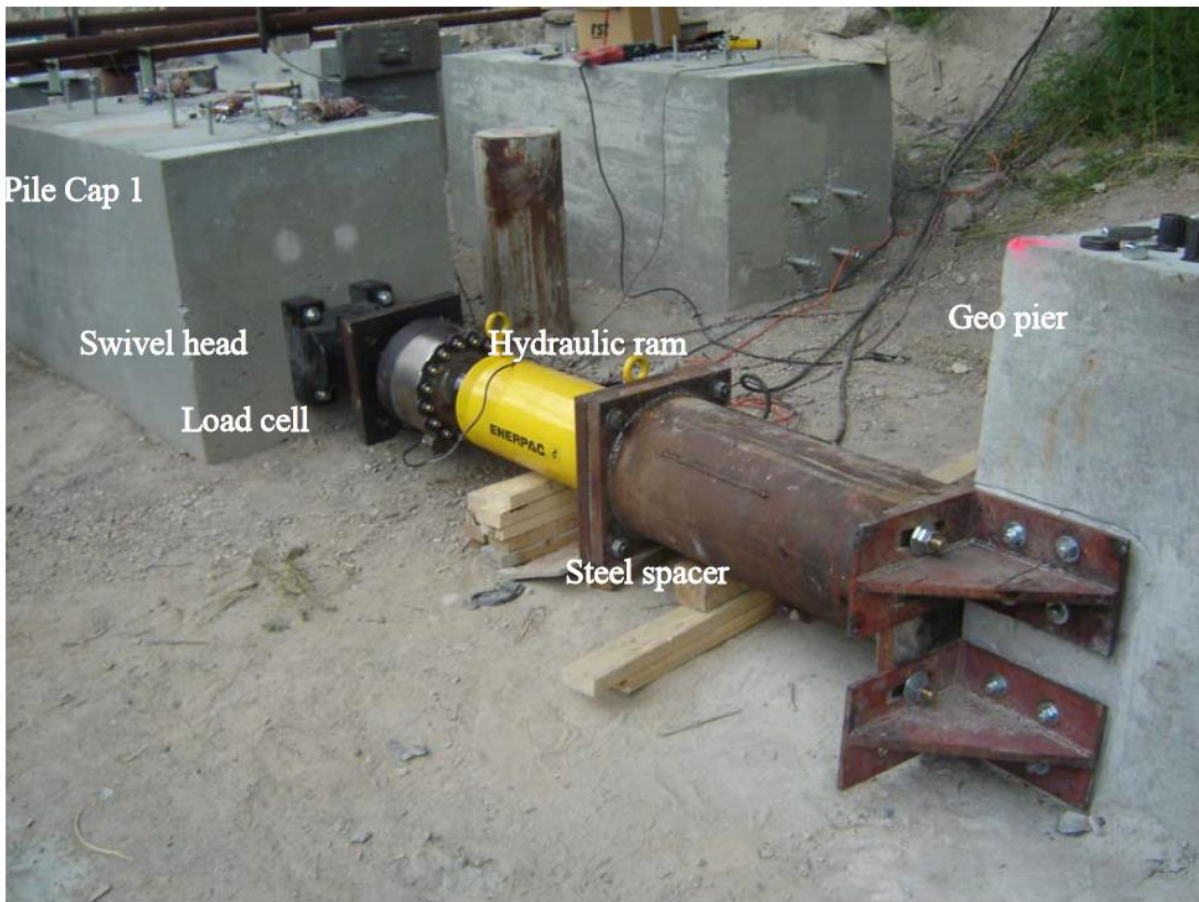
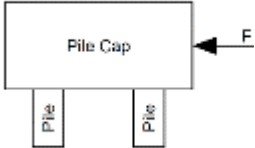
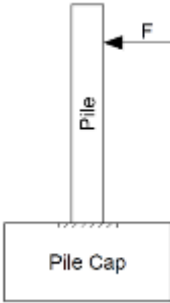
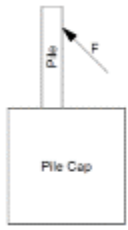


Figure 2-22 Typical test setup, Rollins & Stenlund (2010)

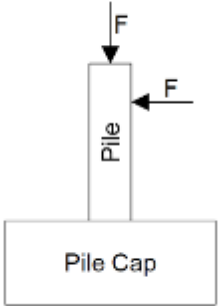
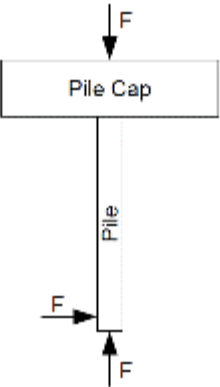
2.4 Summary of Research studies

Presented below is a table summarizing the research studies examined in sections 2.2 and 2.3.

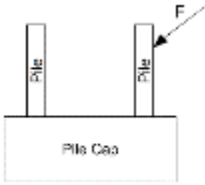


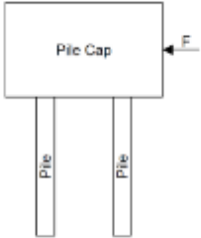
Summary of Existing Research on Pile-to-Pile Cap Connections

Study	Testing Methods	Pile Details		Cap Details	Connection Details	Test Details		Results
		General	Specifics			Setup	Examined Parameters	
Rollins and Stenlund (2010)	In-situ experimental testing, LPILE and GROUP softwares for analysis	Steel pipe	40ft long, 12.75in outside diameter, 3/8" wall thickness	3ft (H) x 2ft (W) x 6.5ft (L)	Pile 1 6" embedment 4-#6 bars, 6.25ft long, #4 spiral @ 6" pitch		Embedment length, pile-to-pile cap connection details, and the ability of analysis softwares to predict testing results	6-12" embedment length only develops 40-60% of the pile's moment capacity. 24" embedment is the smallest length that requires no additional reinforcement
					Pile 2 12" embedment 4-#6 bars, 6.25ft long, #4 spiral @ 6" pitch			
					Pile 3 12" embedment No concrete in the pile			
					Pile 4 24" embedment Concrete fill in pile			
Steunenbergh, Sexsmith, and Stierner (1998)	Experimental testing combined with an FEM tested behavioural model	Steel pipe	324φ x 12.7mm, 2235mm long	800mm (H) x 750mm (W) x 1700mm (L)	Steel pipe was welded to a steel plate measuring 600 x 650 x 50mm that was embedded into the concrete. 30 15M x 600mm long deformed wire bars served as anchors for the plate into the pile cap.		Investigated the adequacy of design connection for the Ministry of Transportation and Highways of British Columbia	Plate thickness inadequate to prevent yielding at pipe edge and ensure strains are adequately distributed to the anchor bars. Pile over-strength factor was low.
Xiao, Wu, Yaprak, Martin, and Manger (2006)	Experimental testing, comparisons to previous studies	HP Piles	100T, or HP 14x89, 1067mm long	7-9.3m (L) x 6.4-8.5m (W) x 1.75-1.92m (H). Based on prototype bridge in California, measurements are listed in ranges	Piles embedded 127mm into concrete, with holes drilled into web, 127mm apart. No. 25 V-shaped anchor bars threaded through holes, 762mm leg length, 30 degree angle from vertical		Shallow embedment combined with the use of V-shaped anchor bars	V-shaped bars ruptured first, much below the ultimate design capacity

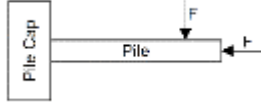
Summary of Existing Research on Pile-to-Pile Cap Connections

Study	Testing Methods	Pile Details		Cap Details	Connection Details	Test Details		Results
		General	Specifics			Setup	Examined Parameters	
Silva, Seible (2001)	FEM analysis, experimental testing	Cast in Steel Shell (CISS) Piles	Pile 1	14" diameter 7/16" thick steel pipes, concrete infill	48" (H) x 120" (L) x 57" (W)		Adequacy of two common connection designs for CISS piles	Anchor bars fractured for Pile 1 before design tensile axial load, were insufficient for Pile 2. Loss of contact between anchor bars and steel shell at large rotations.
			Pile 2	24" diameter 3/4" thick steel pipe, reinforced concrete infill	35" (H) x 110" (L) x 47" (W)			
Stephens, McKittrick (2005)	FEM analysis, strut and tie modeling, and experimental testing	Steel Pipe	PC-1	0.32" pipe wall thickness	0.41% longitudinal steel ratio, 0.09% transverse steel ratio, 4.83 ksi concrete		Lateral load behavior of Montana DOT steel pipe-to-concrete pile caps. Evaluated different analysis methods for efficacy.	PC-1 and PC-2 failed from large strains of reinforcement near the pile, PC-3 and PC-3a failed from tensile concrete cracking in the cap, along with excessive deformation of the cap steel. PC-4 failed from plastic hinge formation at the pile.
			PC-2	0.25" pipe wall thickness	0.41% longitudinal steel ratio, 0.09% transverse steel ratio, 5.326 ksi concrete			
			PC-3	0.25" thickness	1.09% longitudinal steel ratio, 0.24% steel ratio, 3.15 ksi concrete			
			PC-3a	0.25" thickness	2.11% longitudinal steel, 0.65% transverse steel, 3.945ksi concrete			
			PC-4	0.25" thickness	2.83% longitudinal steel, 0.70% transverse steel, 4.682ksi concrete			

Summary of Existing Research on Pile-to-Pile Cap Connections

Study	Testing Methods	Pile Details		Cap Details	Connection Details	Test Details		Results
		General	Specifics			Setup	Examined Parameters	
Shama, Mander, and Aref (2002)	Experimental testing and FEM analysis	HP Piles	HP 10x42, 1275mm long	900mm (H) x 1000mm (W) x 2400mm (L)	Piles embedded 300mm into pile caps,		Studied existing pile-to-pile cap connections, focusing on shallow embedment length	Brittle concrete failure began at 2% drift in the strong axis and at 3% drift in the weak axis direction.
Teguh, Duffield, Mendis, Hutchinson (2006)	FEM analysis, Time History Analysis, comparison to previous experimental studies	Pre-stressed concrete	0.45m x 0.45m square piles, R12 spiral reinforcement, 1/2" low relaxation strand tendons	2.14m x 0.92m x 2.14m	P1 embedded 0.61m, P2 embedded 0.45m. No additional reinforcement		Compared experimental results to FEM analytical models to refine the Australian design standards	Recommends a more flexible foundation system to reduce ductility demand on columns.
Xiao, Chen (2012)	Experimental testing, FEM analysis, comparison to previous studies	HP Piles	$b_f = 100\text{mm}$, $h = 100\text{mm}$, $t_w = 6\text{mm}$, $t_f = 8\text{mm}$, extended 570mm beyond pile	1600mm (L) x 1600mm (W) x 500mm (H)	Piles embedded 25mm, with welded anchor bars continuing 425mm past that		Tested lateral and axial capacity of new connection, then compared results to previous study's results	Straight anchor bars were able to fully develop the tensile capacity. Shallow embedment can cause the governing failure mode to be concrete block rupture near the edges or corners of the footing
Mokwa, Duncan (2003)	Proofs validated through experimental testing	HP Piles	Piles were either 6m or 3m long, 0.13m cover concrete near piles	1.5m (L) x 1.5m (W) x 0.9m (H)	Piles embedded 0.8m, no special connection details		Tested for verification of the rotational stiffness factor.	Method for determining rotational stiffness was proved valid for the testing conditions given, further testing needed.

Summary of Existing Research on Pile-to-Pile Cap Connections

Study	Testing Methods	Pile Details		Cap Details	Connection Details	Test Details		Results
		General	Specifics			Setup	Examined Parameters	
Harries, Petrou (2001)	Experimental Study, comparison of exiting methods	Precast, prestressed concrete	18in square, 18ft length	7ft (L) x 3ft (H) x 7ft (W)	One pile had 24in embedment length, the other had 18in		Investigated the viability of a connection without special details	Longer embedment length is sufficient without any extra connection details

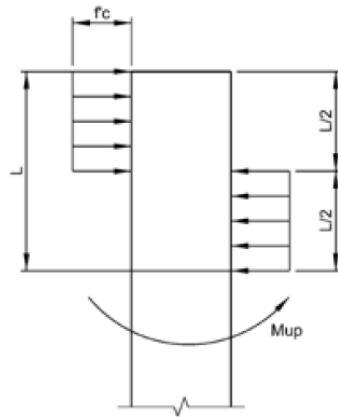
2.5 Review of various state DOT requirements on minimum pile embedment depth

In this section a review of other state DOT requirements on minimum pile embedment depth is provided. These details have been obtained by examining the available structural design manuals of all 51 states in the US. It has to be noted that some state DOTs including ALDOT do not explicitly state any minimum requirements in their structural design manuals. The requirements stated here are in verbatim, and in relevant places the clause number of the respective states design manual is provided. The web links to access these manuals are provided in the references section at the end of this report.

2.5.1 Colorado DOT

10.5.3 Top of Pile Fixity

The following simplified method may be used to calculate the minimum pile embedment required to classify the connection at the top of the pile as fixed.



$$M_{up} = \phi f'_c b_f \left(\frac{L}{2} * \frac{3L}{4} - \frac{L}{2} * \frac{L}{4} \right)$$

$$M_{up} = \phi f'_c b_f L^2 \left(\frac{3}{8} - \frac{1}{8} \right)$$

$$4M_{up} = \phi f'_c b_f L^2$$

$$L = \sqrt{\frac{4M_{up}}{\phi f'_c b_f}}$$

Figure 10-1: Pile Fixity

Where:

L = Required pile embedment into cap (in.)

ϕ = Strength reduction factor for concrete bearing = 0.7 (AASHTO 5.5.4.2.1)

f'_c = 28-day compressive strength of concrete (ksi)

M_{up} = Plastic moment capacity of pile about strong axis (kip-in.)

b_f = Pile flange width (in.)

2.5.2 Connecticut DOT

5.14.4 Driven Piles

Pile foundations supporting abutments shall have a minimum of two rows of piles, unless the piles are incorporated into a fully integral abutment. Piles shall be anchored to and embedded in the footings a minimum of twelve inches.

2.5.3 Delaware DOT

107.3.4.4 Steel H-Piles

Steel H-piles shall be embedded into the pile cap a minimum of 12 inches.

2.5.4 Georgia DOT

Minimum criteria provided only for seismic zone as shown below

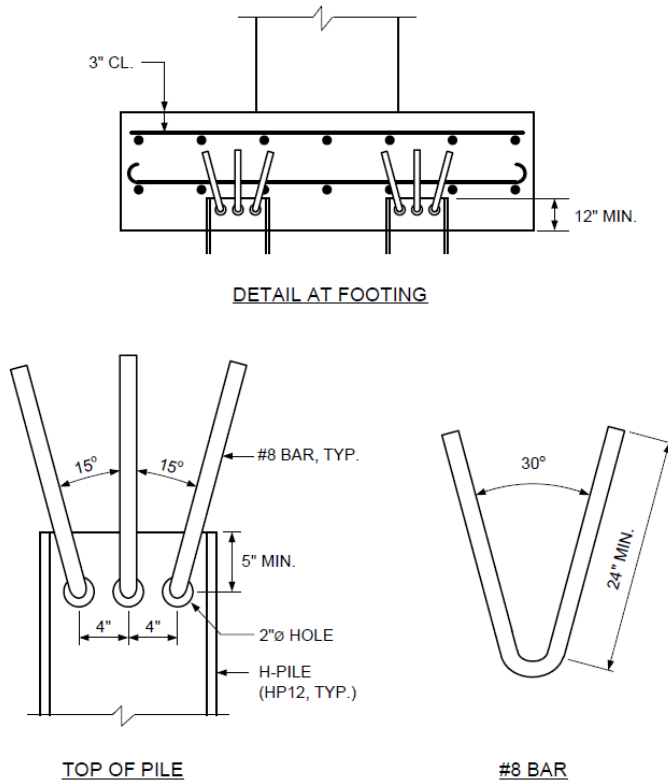


Figure 9B-3 H-Pile Connection Detail for Seismic Zones 2, 3, and 4

2.5.5 Idaho DOT

11.6.1.3 DESIGN GUIDELINES FOR INTEGRAL ABUTMENTS

Foundations: Abutments shall be supported on a single row of steel H-piles, steel smooth hollow pipe pile or steel-encased concrete piles utilizing smooth steel tubes. Piles should be embedded into the abutment concrete at least 2 feet

2.5.6 Illinois DOT

3.10.1.12 Pile Connection to Abutments, Piers and Footings

Piles supporting footings or non-integral abutments shall extend 12 in. into the structure. Integral abutment piling shall extend 2 ft. into the abutment to assure pile fixity. Reinforcement shall be placed to maintain 3 in. clearance from the bottom of the footing

and arranged in such a manner to allow the pile to project into the footing or abutment. Pile bent piers shall have their piling extend through the individual or solid wall encasement 12 in. into the pier cap. Where piles are required to resist large lateral loadings by soil/structure interaction (also known as pile flexure or pile fixity), the piles may be embedded 2 ft. into the abutment or footing to ensure top of pile fixity and reduce deflection.

2.5.7 Indiana DOT

409-5.03(11) Piles: A footing on piles shall be analyzed to consider the structural contribution of the concrete below the tops of the piles. Bottom-mat reinforcement shall be placed 4 in. above the bottom of the footing. The pile type shall be based on the recommendations provided in the geotechnical report. Pile spacing shall be as described in Chapter 408. Pile embedment into the footing shall be at least 1.5 ft

2.5.8 IOWA DOT

Table 6.2.5. Minimum pile embedment and pile head reinforcing

Substructure element	Minimum embedment	Pile head reinforcing
Integral abutment for A or B pretensioned prestressed concrete beams (PPCBs)	2 feet (600 mm)	Spiral ⁽¹⁾
Integral abutment for C, D, BTB, BTC, BTD, or BTE pretensioned prestressed concrete beams (PPCBs)	2 feet (600 mm)	Spiral ⁽¹⁾ and bent p bars ⁽²⁾
Integral abutment for steel plate girders	2 feet (600 mm)	Spiral ⁽¹⁾⁽³⁾ and bent p bars ⁽²⁾⁽³⁾
Stub abutment on timber piles	2 feet (600 mm)	Spiral ⁽³⁾
Stub abutment on steel piles	2 feet (600 mm)	None ⁽⁴⁾
Pier footing	1 foot (300 mm)	None ⁽³⁾
Continuous concrete slab pile bent cap (not monolithic with slab)	1.5 feet (460 mm)	None ⁽³⁾
Continuous concrete slab pile bent cap (monolithic with slab)	1 foot (300 mm)	Cap steel (bent dowels) ⁽⁵⁾

Table notes:

- (1) Spiral is placed around each pile head as detailed on standard sheets [OBS SS 2078-2091]. The spiral should not be epoxy coated.
- (2) For the bent p bars see the Abutment Pile Plan on standard sheets [OBS SS 2085-2091].
- (3) No standard sheet is available.
- (4) See standard sheets for C or D beams [OBS SS 2092-2105].
- (5) Cap steel (bent dowels) is detailed on a standard sheet [OBS SS P10L].

2.5.9 Kansas DOT

Cut-off elevation (top of pile): This elevation is shown on the Construction Layout in the profile view. This locates the top of the pile within the pile cap, abutment or pile bent. Usually, the embedment is between 2 feet to 3 feet in an abutment; one foot (1'-0") in a footing.

2.5.10 Kentucky DOT

PILE BENT ABUTMENTS: Pile Bent Abutments are generally more economical than Open Column Abutments on spread footings. Therefore, if there is a choice between the two types of abutment, choose the Pile Bent Abutment even if the number of piles to be driven is small. Preferably, use Integral Pile Bent Abutments. Obtain current details from the Division of Structural Design. Embed piles a minimum of 2 feet into the pile cap.

2.5.11 Michigan DOT

7.03.09

5. Pile Embedment Piles are to be extended into the footing a distance of 6". When a tremie seal is used, the piles are to be extended into the footing a distance of 1'-0"

2.5.12 Minnesota DOT

[10.7.1.5] Clear Spacing and Minimum Concrete Cover The minimum concrete cover for piles is 9 inches. To facilitate pile driving operations, the minimum center-to-center pile spacing is 2'-6" with 3'-0" minimum preferred. It may be necessary to increase the plan dimensions of a footing or pile cap when using battered piles to provide the minimum concrete cover of 9 inches. The standard embedment into a pier or high parapet abutment footing for a driven pile is one foot and should be dimensioned in the plans. Assume the piles are pinned supports. The standard pile embedment for a low parapet abutment footing is 2'-4".

2.5.13 Montana DOT

Embedment.

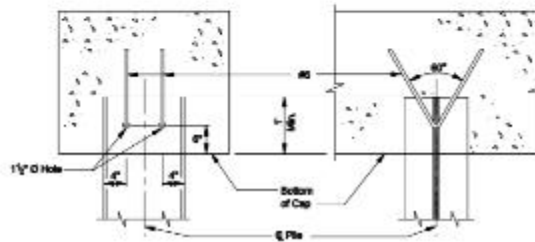
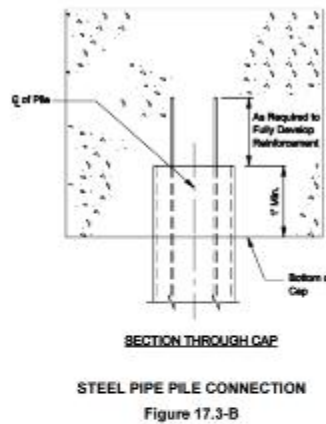
Embed piles a minimum of 500 mm into the footing after all damaged pile material has been removed. If pile reinforcement is extended into the footing, satisfying the provisions of LRFD Article 5.13.4.1, the embedment length may be reduced. Pile connections with high tensile loads or moments require additional design considerations.

2.5.14 Nevada DOT

The following applies to the connection of piles to pile caps or to bent caps unless seismic analysis dictates otherwise:

1. Steel Pipe Piles. The reinforcing steel must be extended into the pile cap and fully developed through adequate development length or standard hooks. The reinforcing steel extends to the minimum tip elevation of the pile. See Figure 17.3-B.
2. Steel H-Piles. Two V-shaped #6 reinforcing bars should be used to anchor steel piles to pile-supported footings or caps. The diameter of the hole should be 1½ in. The reinforcing bars shall be tied or wedged tightly against the top of the hole to reduce the possibility of slip between the reinforcing bar anchor and the pile. The

reinforcing bars should extend into the cap or footing a minimum of 1ft-8in beyond the bottom mat of reinforcement. See Figure 17.3-C.



2.5.15 New Hampshire DOT

A. Pile Embedment, Clearance, and Rebar Mat Location

All piles shall have an embedment in the concrete sufficient to resist moment, shear, and axial loads. Steel to concrete working stress shear bond strength can be estimated at 40-psi (276 kPa) for dry conditions and 20-psi (138 kPa) for tremie conditions of contact surface in checking pile embedment. The addition of shear studs to the embedded pile section can increase shear resistance. Typically, extend piles 1.5-ft. (0.450-m) into stub abutments, 2-ft. (0.6-m) into integral abutments, and 1-ft. (0.3-m) into pier or other footings including through foundation seals. Cast-in-place concrete piles with reinforcing extending into footings are embedded a minimum of 6-in. (150-mm). Piles should be a minimum of 9 inches from any edge of the footing (AASHTO LRFD 10.7.1.2) with 12 inches being typical to accommodate the layout tolerance. Reinforcing mat shall be placed at the top and bottom of the footing with a 3-in. (75-mm) clear distance and placed to clear piles.

2.5.16 NY State DOT

11.1.4.2 Pile Spacing and Placement Details

The tops of C.I.P. piles shall be embedded 6" into the footing. The tops of all other piles shall be embedded 1'- 0" into the footing.

2.5.17 North Carolina DOT

Article 4.5.15

12 in. prestressed concrete piles shall not be spaced less than 2'-9" center to center in footings. In general, embed pile heads into concrete as follows:

Type of Structure	Timber	Steel HP	Steel Pipe	Prestressed Concrete	Prestressed Concrete, larger than 12"
Abuts. & Ret. Walls	9"	9"	12"	9"	12"
End Bent & Bent Caps	12"	12"	12"	12"	12"
Pile Footings	9"	9"	12"	9"	12"

2.5.18 North Dakota DOT

IV-02.03.07 Pile Spacing

To facilitate pile-driving operations, the minimum center-to-center pile spacing is 2'-6" with a 3'-0" minimum preferred. It may be necessary to increase the plan dimensions of a footing or pile cap when using battered piles. The standard embedment into a pier or abutment footing for a driven pile is 1'-0" and shall be dimensioned in the plans.

2.5.19 Ohio DOT

303.4.2.3 Pile Embedment

Piles supporting capped pile piers shall be embedded 1'-6" [450 mm] into the concrete cap. Other substructure units on a single row of piles should have the piles embedded 2'-0" [600 mm] into the concrete. A 1'-0" [300 mm] embedment depth into the concrete footing is required for all other cases. In every case, there shall be at least 1'-6" [450 mm] cover over top of pile

2.5.20 Oregon DOT

Piling Details

(1) Steel Pile footing embedment to develop fixity

It may be necessary to develop lateral load resistance in piles or pile groups. To develop required lateral load capacities piles must be embedded in pile caps or footings adequately to develop the full moment capacity of the pile section.

If lateral load capacity is not needed a pile embedment length of 12 inches is sufficient

2.5.21 Rhode Island DOT

10.6.1.2 Footing Depth and Thickness

In general, the thickness of pile supported footings shall not be less than 2'-6". Piles must be positively anchored into the footing and shall extend a minimum of 12 inches into the footings. The bottom layer of footing reinforcement may be placed above the top of the piles to avoid interference with the piles.

2.5.22 South Carolina DOT (same as Nevada DOT details)

19.2.6.3 Pile Connection Details

The following applies to the connection of piles to pile-supported footings and to bent caps unless seismic analysis dictates otherwise:

1. Steel H-Piles. Two V-shaped #6 reinforcing bars should be used to anchor steel piles to pile-supported footings or bent caps. The diameter of the hole should be limited to 2 times the bar diameter (1½ in). The reinforcing bars shall be tied or wedged tightly against the top of the hole to reduce the possibility of slip between the reinforcing bar anchor and the pile. The reinforcing bars should extend into the cap or footing a minimum of 1'-8" beyond the bottom mat of reinforcement.

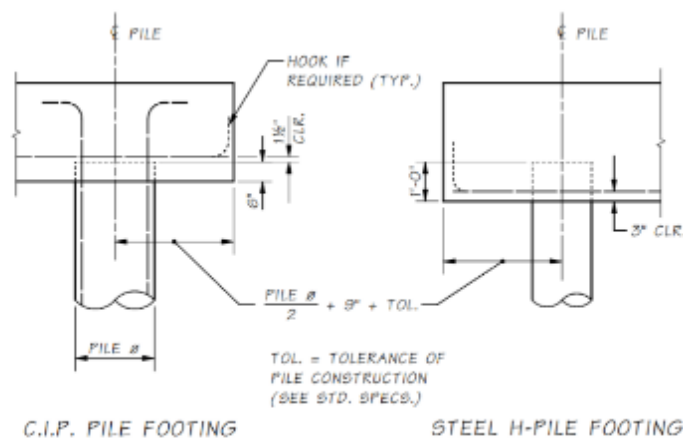
2. Steel Pipe Piles. A fillet-welded square steel end plate, as shown in Figure 19.2-3 should be used to anchor steel pipe piles to pile-supported footings or bent caps. The end plate and fillet weld is sized according to the specific requirements of the foundation. The pipe pile shall be embedded a minimum of 1'-3".

2.5.23 Vermont DOT

10.2.4.3 Pile Spacing and Clearances

Minimum pile spacing shall be 2'-6" or 2.5 pile diameters. Piles shall extend a minimum of 1'-0" vertically into the footing.

2.5.24 Washington State DOT



Pile Embedment and Reinforcing Placement
Figure 7.7.5-2

2.5.25 West Virginia DOT

3.12.3 Pile Foundations

In order to facilitate the driving of non-predrilled steel bearing piles the following minimum size of piles shall be specified:

- HP 10x42 for lengths up to 40 FT
- HP 12x53 for lengths between 40 and 80 FT
- HP 14x73 for lengths over 80 FT

The design may require larger piles, for the above lengths, based on vertical and/or lateral loads.

The minimum piling length shall be 10 FT. The pile embedment is a minimum of 1 FT into the cap.

2.5.26 Wisconsin DOT

11.3.1.2 Pile Spacing

The distance from the side of any pile to the nearest edge of footing shall not be less than 9". Piles shall project at least 6" into the footings.

CHAPTER 3: IDENTIFICATION OF A PROTOTYPE BRIDGE AND DEVELOPMENT OF 3D FINITE ELEMENT MODELS

3.1 Introduction

Bridge foundation loads can vary based on parameters such as girder span, girder spacing, number of supporting piers, width of deck, etc. Due to the vast variety of possible bridge configurations, it was necessary to develop a prototype bridge that would represent the standard design and detailing procedures utilized by ALDOT. This prototype design would serve as the basis for constructing practical and adequately sized test specimens, which could then be studied utilizing the facilities available at the University of Alabama's large scale structures lab (LSSL). In this context, it is also important to note that a comprehensive understanding of the strength and service level requirements for various bridge configurations, including the prototype bridge, would enable us to accurately characterize the performance of the test specimens under various limit states.

This chapter shows the specifics of the analysis performed to investigate the range of expected loading values on top of the foundations and the prototype bridge.

3.2 Expected range of loading values on top of footings

An excel sheet was developed in-house to calculate the loading on top of the foundations for various span lengths. The primary inputs for this excel sheet are as shown in Figure 3-1 and discussed below.


1	UNIVERSITY OF ALABAMA-				Calculation of loads on top of			
2	RESEARCH PROJECT				footings			
3								
4								
5								
6	1 Input Parameters							
7								
8	GIRDER TYPE			=	ASHTO III			
9	Span			=	90 ft			
10	Girder Spacing			=	6 ft			
11	No. of Griders			=	4			
12	Width (gutter to gutter)			=	24 ft			
13	Overhang width			=	2 ft			
14	Deck Thickness			=	8 in			
15	Average Haunch Thickness			=	4 in			
16	Wearing Surface thickness			=	2.5 in			
17	Parapet Cross sectional Area			=	5.4 ft ²			
18	Parapet Height			=	3 ft			
20	Unit Weight of Girder Concrete			=	0.15 kcf			
21	Unit Weight of Deck Concrete			=	0.15 kcf			
22	Unit Weight of Haunch Concrete			=	0.15 kcf			
23	Unit weight of Wearing Surface			=	0.15 kcf			
24	Unit weight of Parapet Concrete			=	0.15 kcf		Update	
25	Number of Supporting Piers			=	1			

Figure 3-1 Screen shot showing the input page of the excel sheet for calculating loads on top of footings

3.2.1 Input Parameters

- a) Girder type: The girder type or girder shape affects the dead load calculations and is varied based on span lengths. The girder type also gives the details of the shape selected for various span lengths. These are based on the maximum possible capacities of each of these sections. It should be noted that for this project, the girder shapes are limited to AASHTO standard I Beams (Type I – VI), BT-72 and BT-78.

Table 3-1 Selection of girder shape for various span lengths

Span length (ft)	Girder Shape
<40	AASHTO Type – I
40-70	AASHTO Type – II
70-100	AASHTO Type – III
100-120	AASHTO Type – IV
120-140	AASHTO Type – V
140-160	AASHTO Type – VI
160-165	BT-72
165-180	BT-78

- b) Span: The span lengths were varied from 40-180 ft in 10 ft intervals. Span length values affect all the load calculations.
- c) Girder Spacing: The girder spacing was kept at a constant value of 6 ft. This affects dead load and live load calculations.
- d) Width of the bridge deck: The width of the bridge deck measured from gutter to gutter is assumed as 28 ft for 2 lane configurations.
- e) Overhang width: An overhang width of 2 ft is assumed for all calculations.
- f) Deck Thickness: The thickness of the concrete deck is assumed to be 8 in for all cases. This is a conservative number, compared to the thickness of decks used by ALDOT.
- g) Average haunch thickness: The average haunch thickness is dependent on the geometry of the bridge but for the sake of uniformity, an average haunch thickness of 4 in is assumed for all the configurations.
- h) Wearing surface thickness: A wearing surface thickness of 2.5 in is assumed for all calculations
- i) Parapet height and cross-sectional area: Parapet height is utilized in the calculation of wind load on the structure and the cross-sectional area contributes to the dead load calculations. The

parapet geometry is as per the standard bridge barrier drawings of ALDOT and is shown in Figure 3-2. This geometry translates to a cross-sectional area of 2.7 sq. ft and a parapet height of 3 ft.

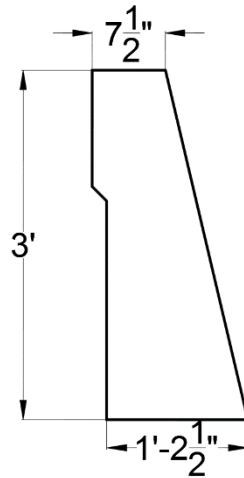


Figure 3-2 Geometry of parapet as per ALDOT standards

- j) Unit weight of concrete: The unit weight of concrete for all members is assumed to be 150 pcf.

3.2.2 Load calculations

After gathering all the required input data, calculations are performed to assess the following components.

a) Dead Loads

Calculating dead loads at girder support points according to the geometry of each part, including the girder, slab, haunch, wearing surface, and parapet. Where necessary, the computation of loads on the interior and external girder support has been differentiated. Additionally, the dead load has been separated into two parts: dead loads of components (DLC) and dead loads of wearing surfaces (DLW). Figure 3-3 shows a screenshot of these computations as they appear in an Excel spreadsheet.

27	2.1 Dead Load								
28									
29	Girder Cross Sectional Area			=	559.50	in ²			
30	DL _{Girder}			=	0.58	k/ft/girder			
31	DL _{Slab-interior}			=	0.60	k/ft/girder			
32	DL _{Slab-Exterior}			=	0.50	k/ft/girder			
33	DL _{Haunch}			=	0.09	k/ft/girder			
34	DL _{W.Sur.Int}			=	0.19	k/ft/girder			
35	DL _{W.Sur.Ext}			=	0.16	k/ft/girder			
36	DL _{Parapet}			=	0.20	k/ft/girder			
37									
38	DLC _{Interior Point}	(Components)		=	1.48	k/ft/girder			
39	DLC _{Exterior Point}			=	1.38	k/ft/girder			
40	DLW _{Interior Point}	(Wearing Surfaces)		=	0.19	k/ft/girder			
41	DLW _{Exterior Point}			=	0.16	k/ft/girder			
42									
43	DLC-Reaction @ Interior Support Points			=	66.46	kips/girder			
44	DLC-Reaction @ Exterior Support Points			=	61.96	kips/girder			
45	DLW-Reaction @ Interior Support Points			=	8.44	kips/girder			
46	DLW-Reaction @ Exterior Support Points			=	7.03	kips/girder			

Figure 3-3 Screenshot showing the dead load calculations performed in the excel sheet for calculating loads on top of footings

b) Live loads

Live load calculations are performed as per the AASHTO LRFD design specifications (2017). The loads computed in this section are for the HL93 design truck along with a design lane load of 640 plf as shown in Figure 3-4. It should be noted that for live load calculations, the truck position which results in the maximum possible end reactions are computed for each of the span lengths. The resulting end reactions for this truck position are then used with appropriate lane presence and distribution factors. The distribution factors for the live loads are calculated as per the clause 4.6.2.2 of AASHTO LRFD design specifications (2017). Figure 3-5 shows a screen shot of these calculations as performed in the excel sheet.

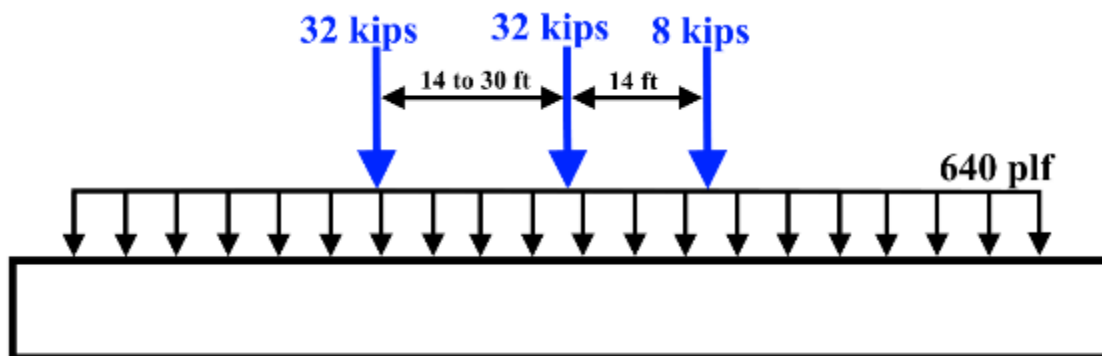


Figure 3-4 HL93 loading of design truck (Indicated in blue) and design lane load (indicated in black)

48	2.2 Live Load								
49									
50	Distribution Factors for shear								
51	Interior Beam -	One lane loaded	=	0.60					
52	Exterior Beam -	One lane loaded	=	1.00					
53									
54	Interior Beam -	Two or more lanes loaded	=	0.67					
55	Exterior Beam -	Two or more lanes loaded	=	0.53					
56									
57	Max. reaction for given span length		=	122.1	kips/lane				
58									
59	LL-Reaction @ Interior Support Points		=	40.94	kips/girder				
60	LL-Reaction @ Exterior Support Points		=	32.06	kips/girder				
61									

Figure 3-5 Screenshot showing the live load calculations performed in the excel sheet for calculating loads on top of footings

c) Braking force

The braking force is calculated as the maximum of 25% of axle weight of the design truck or 5% of the design truck + lane load. This is as per clause 3.6.4 of AASHTO LRFD design specifications (2017). These loads are calculated per pier and applied at a height of 6 ft above the roadway surface for the calculation of moments. Figure 3-6 shows a screen shot of this calculation in the excel sheet.

62	2.3 Braking Force								
63									
64	Multiple lane Presence Factor		=	1					
65	25 % of Axle weight of the design truck	BR_1	=	36.00	kips/pier				
66	5 % of Design Truck + Lane Load	BR_{2A}	=	18.72	kips/pier				
67									
68	Total braking force on one pier		=	36.00	kips/pier				
69	(@6ft above roadway surface)								
70									

Figure 3-6 Screen shot showing the braking force calculations performed in the excel sheet for calculating loads on top of footings

d) Wind loads

Wind loads are calculated as per section 3.8 of AASHTO LRFD design specifications (2017). Equation (3-1) shown below gives the expression for calculating the design wind velocity as per AASHTO specifications. In this equation, for the sake of uniformity all the calculations for different span lengths are performed assuming a pier height of 30 ft, thus $V_B = V_{30}$. The values of friction velocity (V_0) and friction length (Z_0) are assumed to be of 8.2 mph and 0.23 ft, respectively. These values correspond to an upstream surface condition of the open country.

$$V_{DZ} = 2.5V_0 \left(\frac{V_{30}}{V_B} \right) \ln \left(\frac{Z}{Z_0} \right) \quad (3-1)$$

Subsequent to this as per AASHTO specifications wind pressures are calculated using Equation (3-2) shown below. In this equation, V_B is assumed to be 100 mph and the base wind pressure P_B is assumed as .05 ksf. This corresponds to the worst-case wind pressures as per AASHTO LRFD specifications

$$P_D = P_B \left(\frac{V_{DZ}}{V_B} \right)^2 \quad (3-2)$$

71	2.3 Wind Force								
72	On structures (WS)								
73	Top most elevation of the bridge	=		30	ft				
74	Design Wind Velocity	=		99.85					
75	Design Wind pressure	=		0.050	ksf				
76	Exposed superstructure height	=		7.96	ft				
77									
78	WL Transverse to Super Struttre @ 0 Degrees	=		35.81	kips/pier				
79	WL Transverse to Super Struttre @ 15 Degrees	=		31.52	kips/pier				
80	WL Transverse to Super Struttre @ 30 Degrees	=		29.37	kips/pier				
81	WL Transverse to Super Struttre @ 45 Degrees	=		23.64	kips/pier				
82	WL Transverse to Super Struttre @ 60 Degrees	=		12.18	kips/pier				
83									
84	WL Longitudnal to Super Struttre @ 0 Degrees	=		0.00	kips/pier				
85	WL Longitudnal to Super Struttre @ 15 Degrees	=		4.30	kips/pier				
86	WL Longitudnal to Super Struttre @ 30 Degrees	=		8.60	kips/pier				
87	WL Longitudnal to Super Struttre @ 45 Degrees	=		11.46	kips/pier				
88	WL Longitudnal to Super Struttre @ 60 Degrees	=		13.61	kips/pier				
89									
90	Guiding case (both applied simultaneously)	=		37.96	kips/pier				
91		applied@	=	3.98	ft above road way				
92									
93	On moving load (WL)								
94									
95	WL Transverse to Super Struttre @ 0 Degrees	=		9.00	kips/pier				
96	WL Transverse to Super Struttre @ 15 Degrees	=		7.92	kips/pier				
97	WL Transverse to Super Struttre @ 30 Degrees	=		7.38	kips/pier				
98	WL Transverse to Super Struttre @ 45 Degrees	=		5.94	kips/pier				
99	WL Transverse to Super Struttre @ 60 Degrees	=		3.06	kips/pier				
100									
101	WL Longitudnal to Super Struttre @ 0 Degrees	=		0	kips/pier				
102	WL Longitudnal to Super Struttre @ 15 Degrees	=		1.08	kips/pier				
103	WL Longitudnal to Super Struttre @ 30 Degrees	=		2.16	kips/pier				
104	WL Longitudnal to Super Struttre @ 45 Degrees	=		2.88	kips/pier				
105	WL Longitudnal to Super Struttre @ 60 Degrees	=		2.88	kips/pier				
106									
107	Guiding case (both applied simultaneously)	=		9.54	kips/pier				
108		applied@	=	6.00	ft above road way				
109									

Figure 3-7 Screenshot showing the wind load calculations performed in the excel sheet for calculating loads on top of footings

The design wind pressure calculated using Equation (3-2) is then used to calculate the wind force on structures, designated as WS, and also on the moving load designated as WL. The wind loads are calculated in both transverse and longitudinal directions for wind skew angles of 0, 15, 30, 45, and 60 degrees, where the skew angle which generates the maximum load is taken as the guiding

a cap supported by two piers of height 30 ft. These assumptions are common for all the span ranges. It should be noted that the facilities at the Large-Scale Structures Lab, at the University of Alabama, limit the maximum load that can be applied on specimens to 1000 kips of vertical load. In this context the highlighted values in Table 3-3 represent the viable and practical span ranges for the prototype bridge, these span ranges result in limit states which can be conclusively tested without the need for interpretation or extrapolation of results.

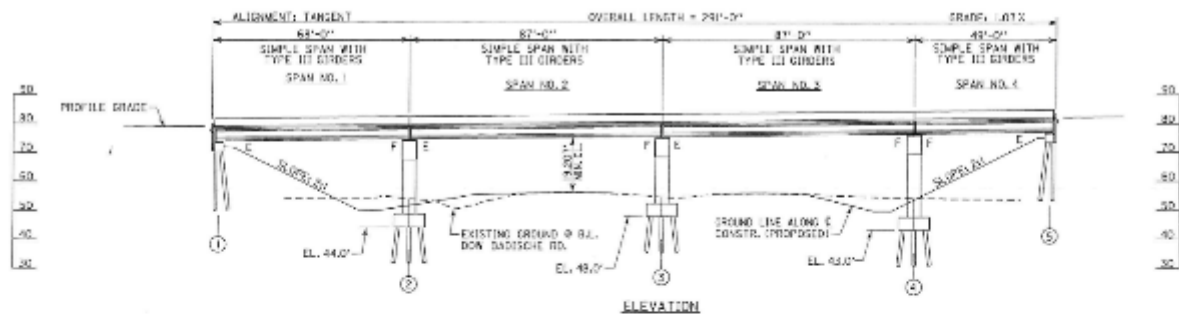
Table 3-3 Expected maximum vertical loads on footings for various spans

Span (ft)	Axial loads on top of footing (kips)					
	Strength				Service	
	I	II	III	V	I	II
40	477	438	308	438	340	315
50	533	490	344	490	380	348
60	587	539	379	539	418	380
70	639	587	414	587	455	411
80	733	678	493	678	526	467
120	1033	964	733	964	749	644
130	1192	1120	878	1120	873	739
140	1260	1185	932	1185	924	780
150	1357	1279	1015	1279	997	838
160	1428	1347	1072	1347	1050	880
170	1498	1414	1128	1414	1102	922
180	1569	1481	1185	1481	1155	963

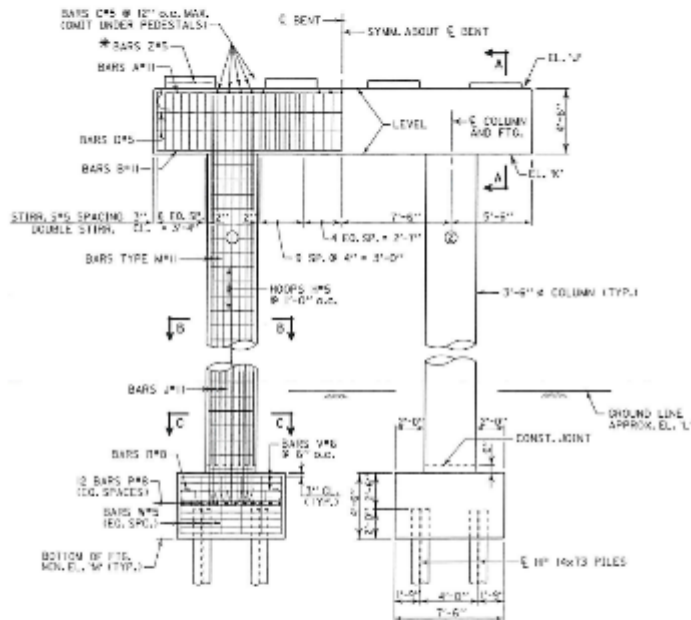
Thus, in consultation with ALDOT, the bridge constructed over US 43 on Dow Badische Road in Mobile County was selected as the prototype bridge. This bridge has a maximum span of 87 ft (see Figure 3-9a) and has a two-lane configuration with 4 girders placed at 7 ft spacing. The bridge cap is supported over two piers (see Figure 3-9b and c) and the foundation details in this bridge are very typical of the design and detailing practices of ALDOT. The foundation in this bridge consists of a 7.5 ft by 10.5 ft rectangular footing supported on 6 - HP 14 X 73 piles (see Figure 3-9d). The main reinforcement consists of #8 bars placed at approximately 7.5 in spacing in both directions. A clear cover of 4 in is left between the top of the pile to the main reinforcement layer. The expected loads for this prototype bridge are shown in Table 3-4.

Table 3-4 Expected loads on top of foundation for Prototype bridge

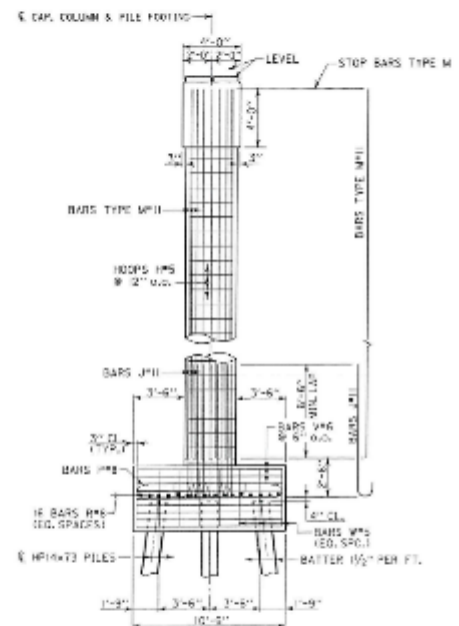
Load combinations	P (kips)	M _x (k-ft)	M _y (k-ft)
Strength I	887.8	27.4	661.5
Strength II	823.1	27.3	510.3
Strength III	604.6	335.7	90.2
Strength V	823.1	413.2	623.2
Service I	648.0	413.2	490.9
Service II	578.4	27.4	245.7



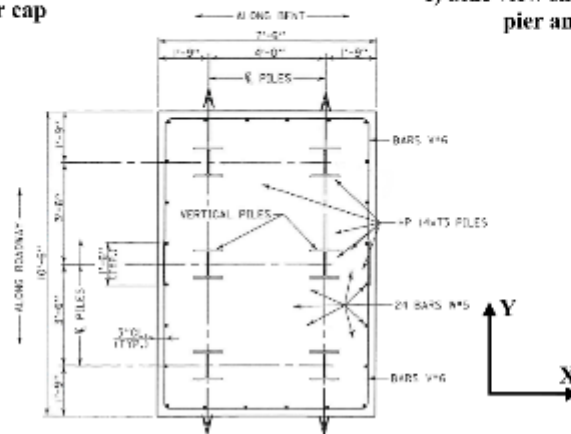
a) Elevation of the Prototype Bridge showing spans



b) Elevation showing foundation, pier and pier cap



c) Side view showing foundation, pier and pier cap



d) Plan view of the foundations

Figure 3-9 Figure showing details of the prototype bridge selected

CHAPTER 4: EVALUATION OF EFFECT OF PILE EMBEDMENT DEPTH USING 3D FINITE ELEMENT METHODS AND TEST SPECIMEN SELECTION

4.1 Introduction

One of the goals of this research is to investigate the feasibility of lowering the embedment depth of piles in footings. In accordance with this objective, detailed 3D finite element (FE) models of the prototype bridge's foundation are developed using the ATENA (2016) software. Three simulations are conducted utilizing three distinct pile embedment depths of 2 feet, which is the current ALDOT standard, 1 foot, and 0.5 foot. These are the objectives of this 3D FE models:

- Determine the influence of embedment length on the concrete stresses surrounding the pile.
- Stresses in the principal reinforcement layer in the footing above the piles
- Stresses in the Steel HP-Pile
- Examine and validate the design of large-scale test specimens
- Determine ideal locations for strain gauge placement in test specimens
- Analyze and correlation of experimental data to validate FE Models

The chosen material models and element types for piles, concrete, and steel rebar are first introduced in this chapter. The results of the analyses are then described in detail, and a comparison is made between the three models used. Next, the test specimens are described in detail, and then a FEA of those specimens is presented.

4.2 Finite element model properties

ATENA is a finite element analysis software developed specifically for simulation of reinforced concrete systems by Cervenka Consulting (Červenka, Jendele, & Červenka, 2016). The software allows for a realistic visualization of cracks and cracking patterns in reinforced concrete structures (see Figure 4-1) and includes options for simulating discrete reinforcement along with bond slip models. ATENA also has appropriate interface elements for modelling contact behavior between various objects such as steel piles and concrete.

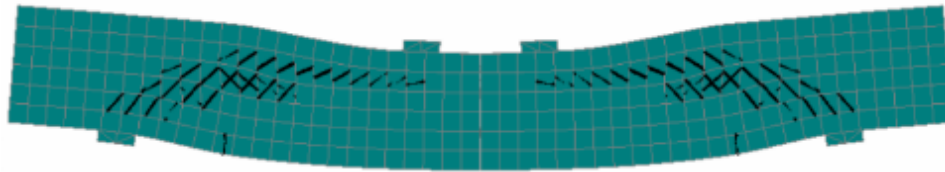


Figure 4-1 Expected cracking in an ATENA model of a simply supported beam failing in shear

4.2.1 Material models in ATENA

a) Concrete Material Model

In ATENA, two unique material models are available for modeling concrete. These are the Constitutive SBETA model and the Constitutive Fracture-Plastic model. Additionally, it should be noted that numerous variations of the Fracture-Plastic model exist within the ATENA framework for more specialized applications, including fatigue, restricted concrete, and fiber reinforced concrete. This study does not discuss these variants.

The Constitutive SBETA model is the most fundamental model of concrete available in ATENA. This model allows for nonlinear behavior in compression, including hardening and softening, as one of its properties. In this model, the tensile behavior of concrete is based on nonlinear fracture mechanics. In addition, it includes a biaxial strength failure criterion and permits a drop in compressive strength and shear stiffness following cracking. This model's shortcomings include a smeared approach to modeling both cracks and reinforcement. This results in the assumption that perfect bond between concrete and reinforcement is present. This model is therefore not used to model concrete in this study.

The Fracture-Plastic model is comprised of two separate models representing compressive and tensile behavior. This model can account for situations in which both compressive and tensile failure surfaces are active simultaneously. Consequently, this model is able to mimic concrete cracking, crushing under extreme confinement, and crack closure caused by crushing in various material orientations. This model enables the definition of an unloading factor that can be toggled to permit complete crack closure or permanent deformation. This approach also permits a decrease in tensile strength after crushing concrete and vice versa. Consequently, this model was used for modeling concrete materials in this study. Multiple parameters exist inside this model to characterize the needed behavior. The following are some of the crucial parameters employed in this particular study:

Compression strength (f'_c):

Compression strength is assumed as 4 ksi for the analysis of prototype foundation. In other places, measured concrete compressive strength from standard cylinder testing is used.

Elastic modulus (E)

Concrete elastic modulus was defined as per as per the following equation, taken from ACI 318-14 (ACI, 2014).

$$E = 57000 \sqrt{f'_c} \text{ (in psi)} \quad (4-1)$$

Poisson's ratio (μ)

A constant value of 0.2 is assumed for concrete

Tensile strength (f_t)

To characterize the tensile behavior of concrete, the ACI 318-14 (ACI, 2014) limit as per the following equation is used.

$$f_t = 7.5 \sqrt{f'_c} \text{ (in psi)} \quad (4-2)$$

Fracture energy (G_f)

The fracture energy parameter is used in the simulation of tensile behavior of concrete and is calculated as per the following relationship defined by Vos (1983). This value is automatically calculated in ATENA as per the provided input values of f'_c

$$G_f = 0.000025(0.24f'_c)^{\frac{2}{3}} \text{ (in psi)} \quad (4-3)$$

ATENA provides suggested values for other parameters which are suitable for concrete structure simulation based on other research sources and the CEB –FIP model code 90 (CEB-FIP, 1993). These parameters include; critical compressive displacement (W_d), plastic strain at compressive strength (ϵ_{cp}), reduction of compressive strength due to cracks ($r_{c,lim}$) and crack shear stiffness factor (S_F).

b) Reinforcement Material Model

In ATENA, reinforcement can be modeled in discrete or smeared form. The discrete modeling method is more precise and permits the specification of bond slip. In this study, discrete form reinforcement is used for the FEA models. Notably, the discrete type of reinforcement only permits modeling of reinforcing bars as uniaxial truss members. ATENA enables the constitutive relationship of the rebar to be specified as either elastic, bilinear, or multilinear. For the prototype foundation simulation, the reinforcement stress-strain response is modeled using a bilinear response with a maximum stress of 60 ksi at a strain of 0.00207 (see Figure 4-2). This approach is deemed suitable as the stresses in the foundation reinforcement are expected to be below the yield stress values under applied loading.

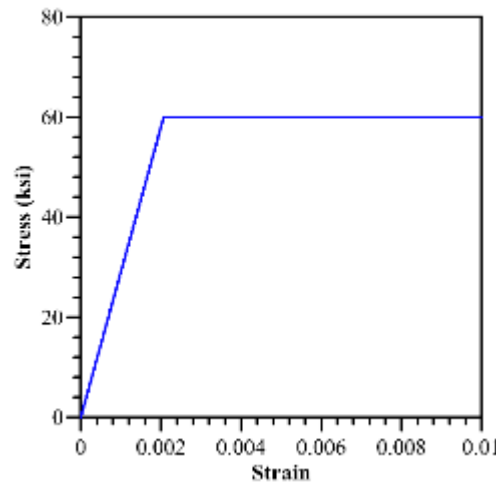


Figure 4-2 Bilinear stress-strain relationship used for rebar modelling

c) Interface Material Model

The interface material model is assigned to a fictitious interface element in structures to simulate the contact behavior. This interface material model is utilized in the post-construction analysis to simulate the behavior between the steel pile and concrete surfaces. The behavior of this contact

model is characterized by shear stiffness (K_{tt}), tensile stiffness (K_{nn}), cohesion strength (C), tensile strength (f_t), and coefficient of friction (μ) (see Figure 4-3).

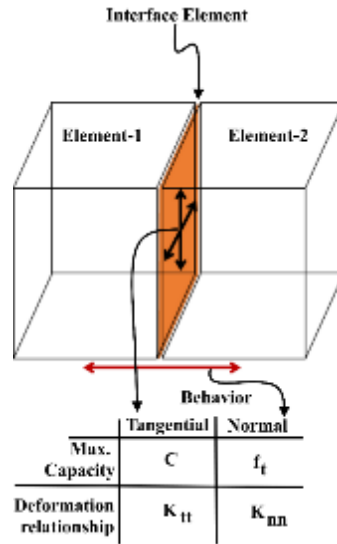


Figure 4-3 Figure showing interface element parameters

4.2.2 Element types in ATENA

ATENA's element types can be generically categorized into three primary groups: plane elements for 2D and 3D analysis, solid elements for 3D analysis, and special elements for modeling external cables, springs, etc. There are tetrahedral elements (see Figure 4-4a), brick elements (see Figure 4-4b), and wedge elements (see Figure 4-4c) in the 3D solid element library. In this study, these three sorts of elements are utilized to describe the specimens' concrete and pile geometry. For the geometry of rebar, 2-node 2D truss elements (see Figure 4-5) are utilized.

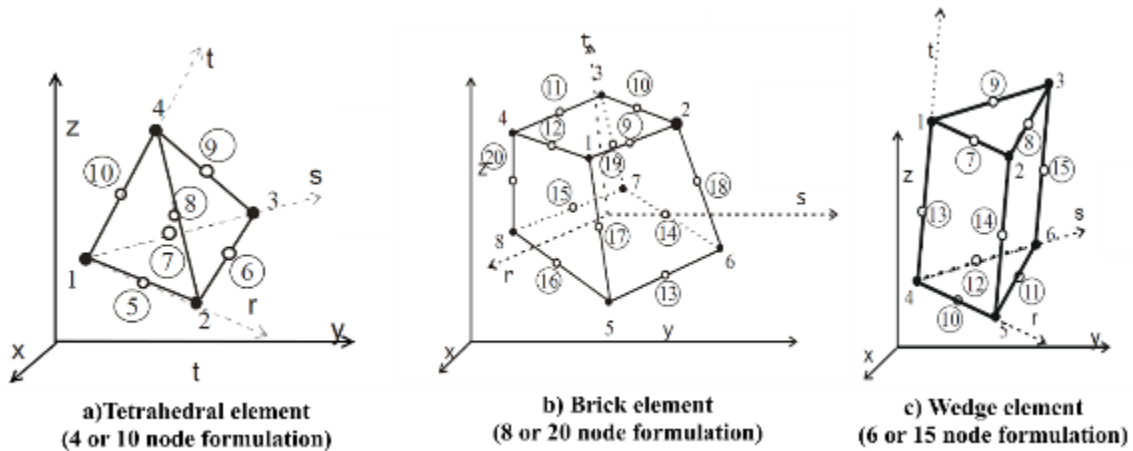


Figure 4-4 Figure showing element types in ATENA (2016)

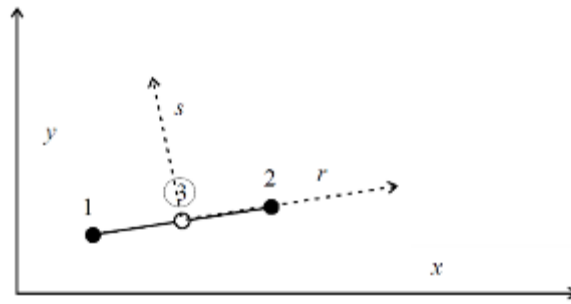


Figure 4-5 Truss element with 2 or 3 node formulations in ATENA (2016)

4.2.3 Material model verification and modelling of other concrete systems

To evaluate the reliability of ATENA software in modeling concrete behavior, a preliminary study was carried out by simulating a compression cylinder test, a dog bone coupon test, and a 3-point loading test of prestressed precast bulb-tee (BT-78) girders from a previous ALDOT-funded project, as detailed below.

a) Compression cylinder test and dog bone coupon tension test

A standard 3 in by 6 in cylinder that is typically used for characterizing the concrete compressive strength and a concrete dog bone coupon were modelled in ATENA using properties as described in Section 4.2.1. These 3D FE models of cylinder and dog-bone coupons were built using tetrahedral elements. They were subjected to uniaxial loading by applying uniform displacement in increments to the top surface, while the bottom surface is restrained. The meshing pattern of the FEM models can be seen in Figure 4-6. The FE model is analyzed to see if the constitutive relationships are consistent with prior assumptions. Figure 4-7a shows the results of the compression cylinder analysis along with stress strain relationship of a 4 ksi concrete as per well-established Mander model (Mander, Priestley, & Park, 1988). It can be seen from this graph that ATENA analysis very closely follows the stress strain relationship described by the Mander model. Figure 4-7b shows that the dog bone coupon test exhibits the standard concrete behavior of brittle tensile failure with an abrupt loss in load carrying capacity after cracking.

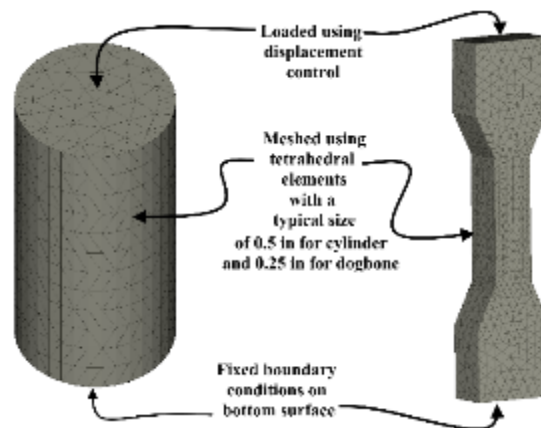


Figure 4-6 FE model details of the compression cylinder and dog bone coupon test

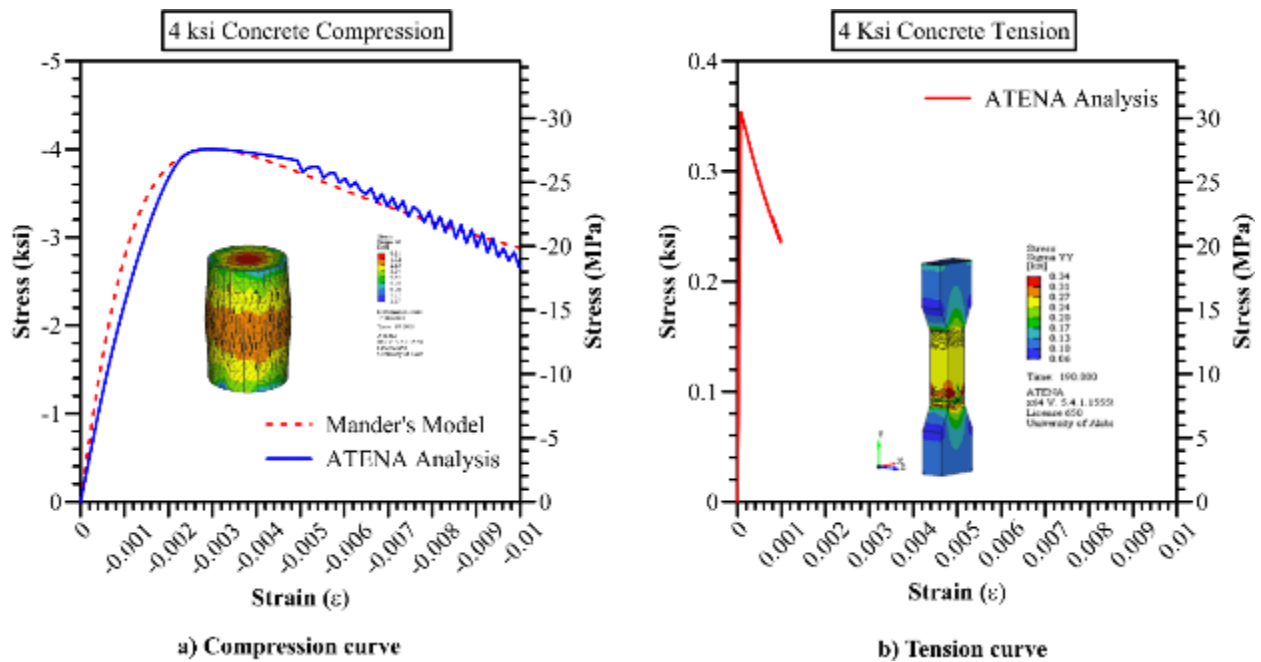


Figure 4-7 Figure showing output stress strain curves for compression and tension obtained from ATENA FEA

b) Verification of crack prediction capabilities of ATENA

Data from an earlier ALDOT funded research project on end zone cracking of BT-78 girders is used to evaluate ATENA's crack prediction capabilities. A finite element analysis (FEA) model is created to simulate the release stresses as well as the laboratory testing under 3-point loading. As illustrated in Figure 4-8, the FE models for the bulb-tee girder were developed utilizing tetrahedral elements with a characteristic element size of 4 in. In ATENA, prestressing is applied by the prestressing load module. A single FE analysis model was employed to simulate prestressing strand release and laboratory shear testing.

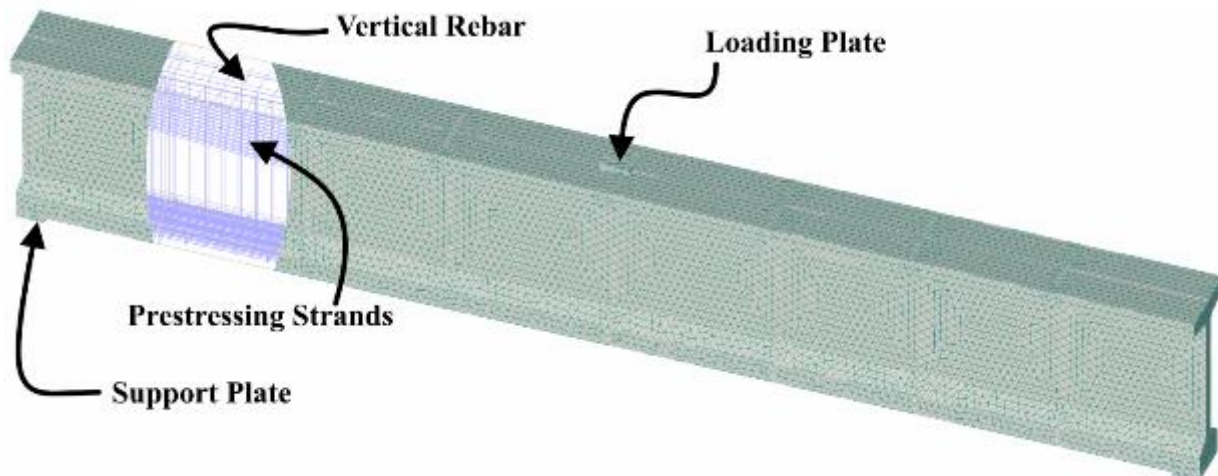


Figure 4-8 Finite element analysis model of a previously tested BT-78 girder

The results of this analysis are shown in Figure 4-9, it can be seen from this figure that ATENA can effectively simulate the complex structural system behavior such as end zone cracking and shear behavior.

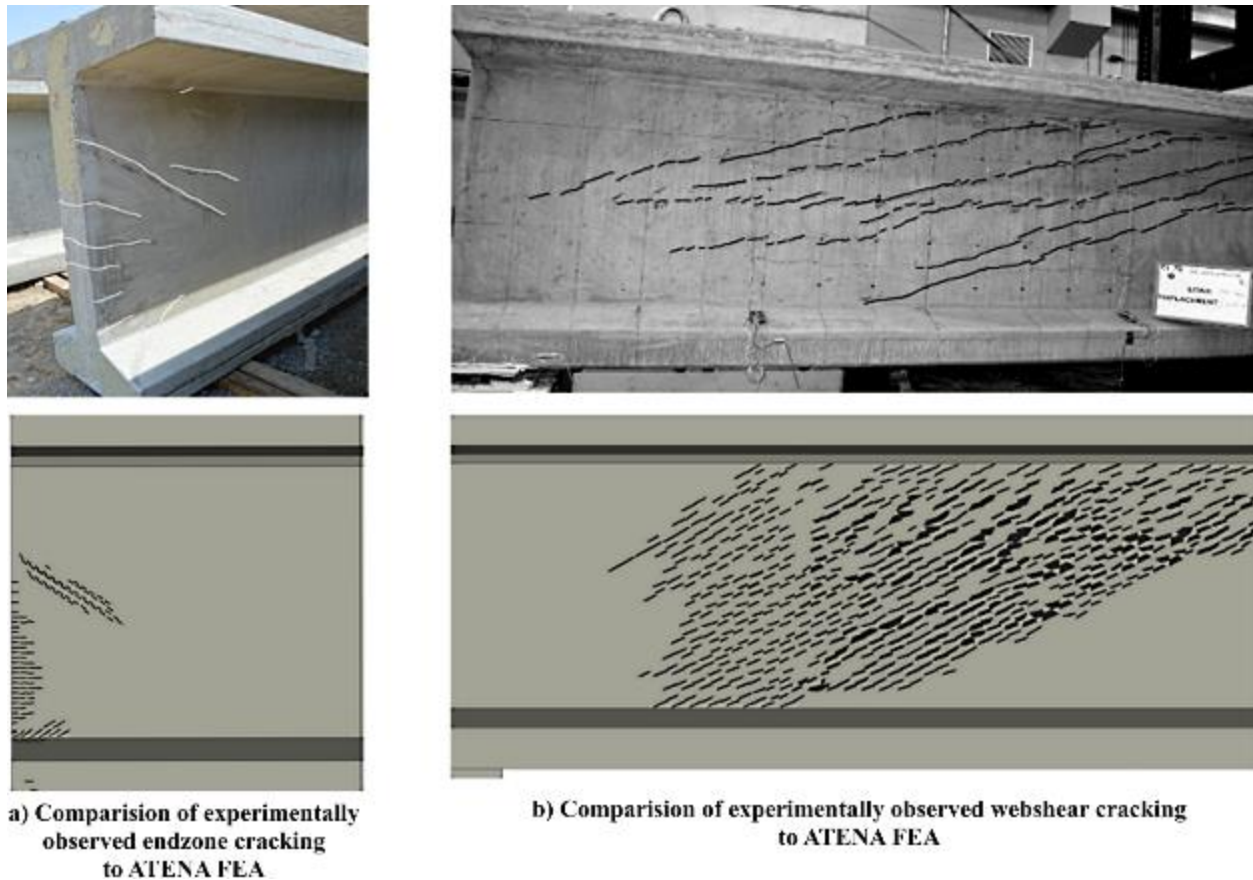


Figure 4-9 Figure showing comparison of experimentally observed cracking to results from ATENA FEA

4.3 Finite element model of Prototype Bridge foundation

This section describes the development of 3D finite element model of the Prototype Bridge foundation (see Figure 4-10a). The analysis model was divided in 5 distinct zones as shown in Figure 4-10b. Zone-1 consists of the steel HP piles. These piles are modelled as linear elastic as the stresses in these piles are not expected to go beyond yield for design loads. The characteristic mesh size used for constructing these elements was less than 0.5 in. This mesh size selection was largely dictated by the thickness of the pile webs and flanges. Zone-2 consists of the concrete layer in which the piles are embedded. In this zone for the regions surrounding the piles a very fine mesh size was employed to match the mesh size and pattern of the piles (Figure 4-10c). The rest of the general area of the footing transitions to a maximum element size of 3 in. The concrete material in this layer and all the other layers are modelled using nonlinear material model. Table 4-1 gives the complete details of the material properties used. Zone-3 is the foundation layer consisting of main reinforcement of the footing. The level of mesh refinement needed in this layer is not as high as in Zone-2 as there are no concentrated forces being applied to the members in this zone. Thus, a larger characteristic mesh size of 6 in is used for computational efficiency. Further, it should also

be noted that the using this mesh size results in having sufficient number of layers in this zone to allow for accurate capture of bending, shear, and deformation behavior. Zone-4 consists of a concrete column modelled to simulate the effects of column punching if any and column rebar interaction with the footings. The height of the column modelled in this zone is 3 ft. Zone-5 consists of a dummy steel column. This column was intended to avoid stress concentration in the load application nodes. The loads were applied on top of this stiff dummy column, this would ensure an even distribution of moments and forces on the concrete column. All the rebar as detailed in the prototype bridge foundation are modelled in this simulation. This includes the main reinforcement layer (#8 bars), the skin reinforcement (#5 and #6 bars), and column reinforcement (#11 bars) (see Figure 4-10d). A fixed boundary condition at the bottom surface of the piles is also applied in this model.

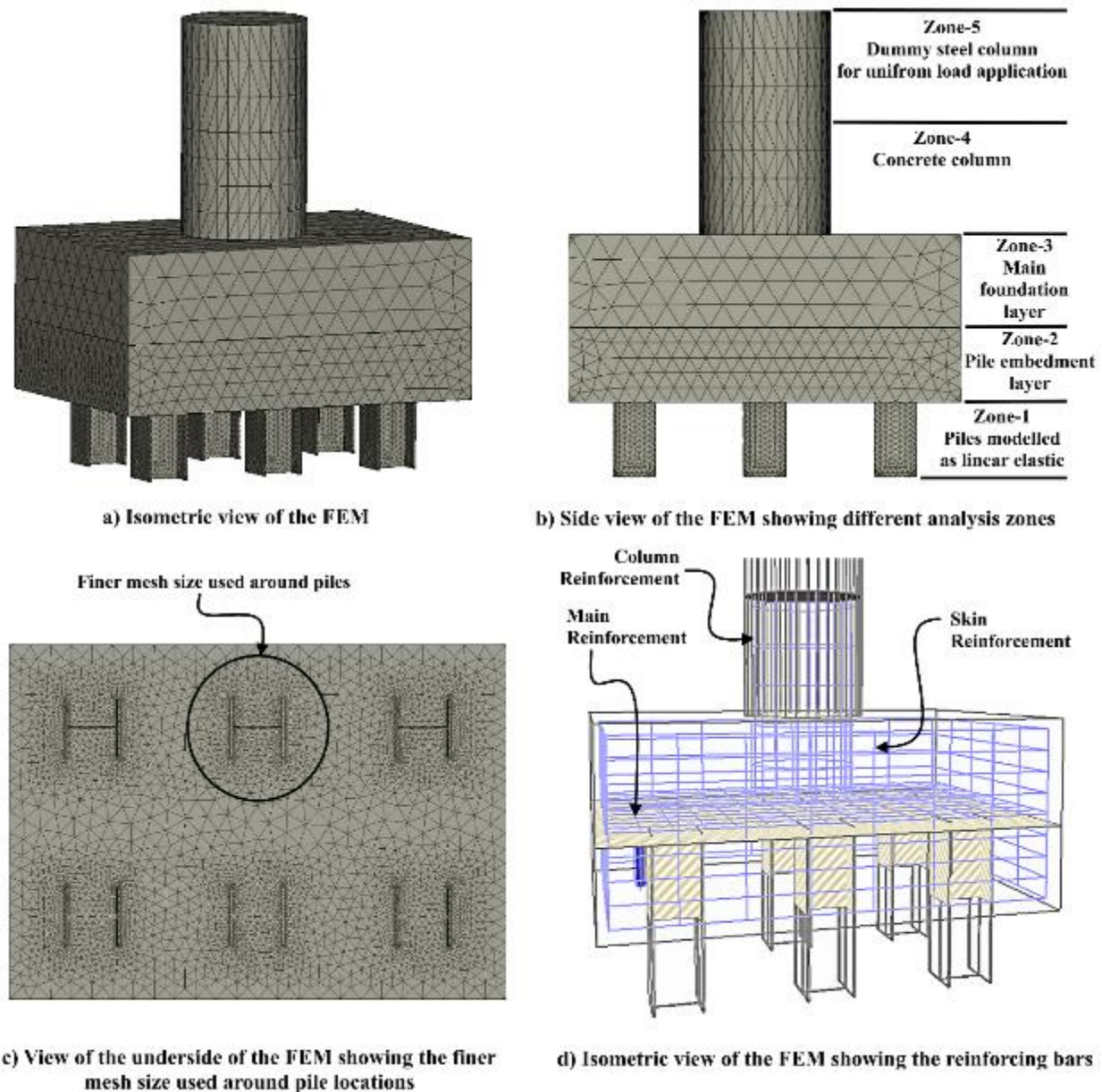


Figure 4-10 Figure showing details of the finite element model built in ATENA

Table 4-1 Material properties of concrete used in modelling of Prototype Bridge foundation

Material Characteristics	Value
E	4.54E+03
ALPHA	6.67E-06
RHO	8.68E-06
MU	2.00E-01
FC	-4.00E+00
FT	3.54E-01
GF	3.49E-04
WD	-1.97E-02
BETA	0.00E+00
EPS_CP	-8.81E-04
EXC	5.20E-01
FIXED	1.00E+00
FC0	-7.44E-01
FC_REDUCTION	8.00E-01
SHEAR_FACTOR	2.00E+01
AGG_SIZE	7.87E-01

It should also be noted that ALDOT standard practice precludes applying tensile stresses on piles through the footing. In this application, the contact mechanics between the footing and the piles can be modeled in two ways. One approach is to mimic no friction or cohesion between the pile and the footing, resulting in forces being transferred purely by pile bearing. All of the concrete beneath the bearing surface would be rendered useless by this mechanism. The second option is to take advantage of the foundation's interface properties with pile flanges and webs. This method would enable us to explore the effect of embedment depth on a number of parameters. This chapter's preconstruction analysis assumes a perfect connection between the piles and the foundation. After the specimens have been tested experimentally, this perfect state is replaced with acceptable values in the post-construction analysis.

4.4 Results of FEA of Prototype Bridge foundation

4.4.1 Principal stress contours

This section gives the FEA results for the prototype bridge foundation. This section looks at a variety of factors, starting with the maximum principal stresses observed in Zones 2 and 3. The maximum principal stress contours are an excellent predictor of cracking in a concrete structure. The significant contributing stress contours for this analysis are analyzed at six critical locations (cuts), as shown in Figure 4-11a. Cuts 1–3 are planes along the transverse direction cut at the flange edge position of piles, cuts 4–6 are planes along the longitudinal direction cut at the web location of piles, and cut 5 is the plane along the longitudinal direction cut at the foundation center line. This figure shows that 92 percent of the area examined in these planes had principal tensile stresses less than 100 psi. This number equates to $1.5 \sqrt{f'_c}$. Tensile stresses less than 385 psi have been reported in various sections of cuts 2, 4, and 5. This number equates to $6.5 \sqrt{f'_c}$ and is less than the prescribed tensile stress limit of concrete. This means that no cracking is expected in the prototype bridge foundation, even though the applied design loads are for the ultimate strength limit state. This is largely owing to the fact that the normal design of these footings is performed as a beam supported on piles, ignoring the concrete below the main reinforcement layer.

Furthermore, the existence of material and load safety factors enhances on this conservative design.

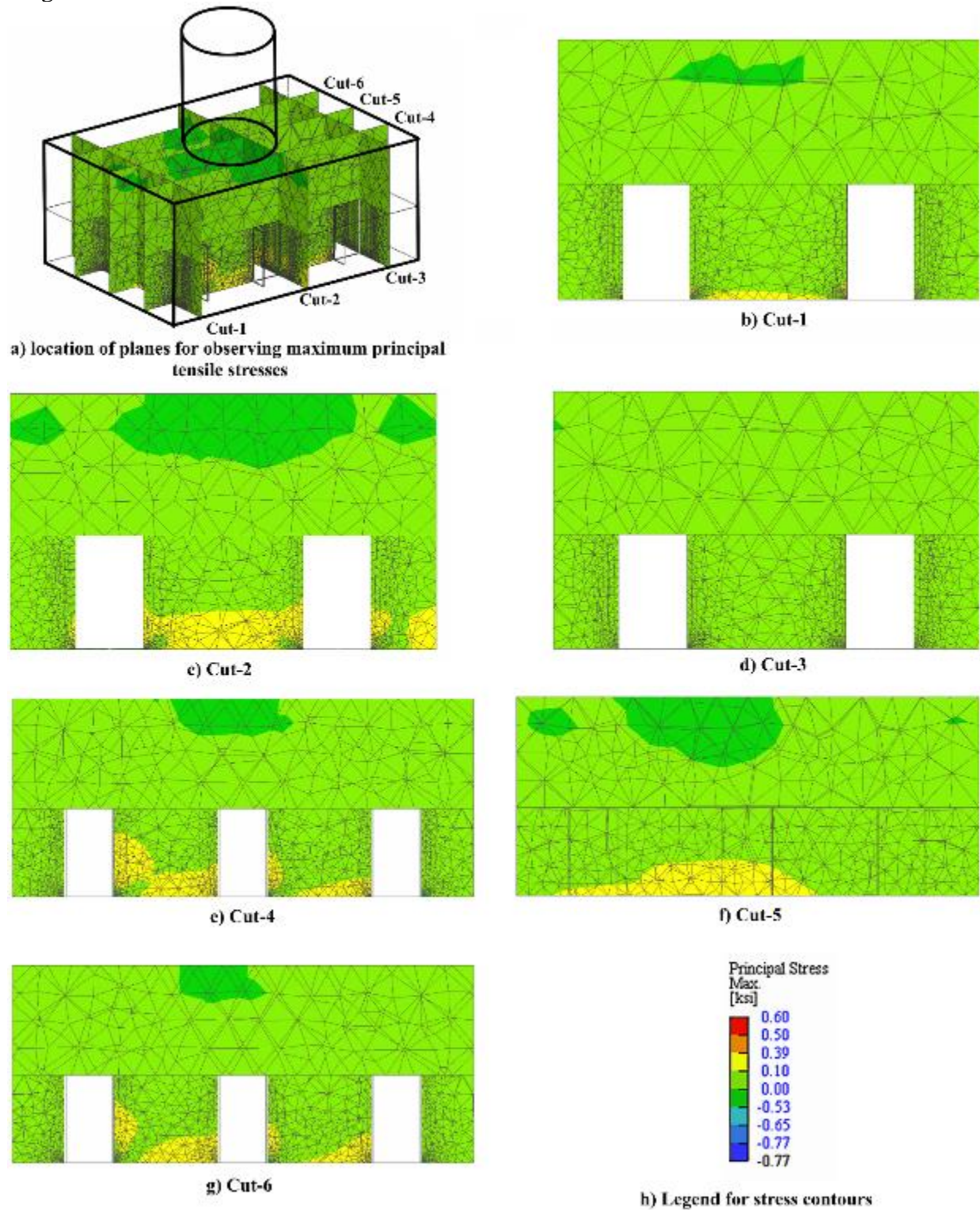


Figure 4-11 Figure showing principal stress contours in Prototype Bridge foundation

4.4.2 Reinforcement Stresses

Figure 4-12 shows the stresses observed in the primary reinforcement layer above the piles. It can be seen from this figure that the reinforcement has stresses of less than 1 ksi. This is due to the fact that the foundation design is not controlled by reinforcement requirement. The high amount of reinforcement (#8 bars @ 7" spacing) had to be provided to satisfy the minimum reinforcement criteria.

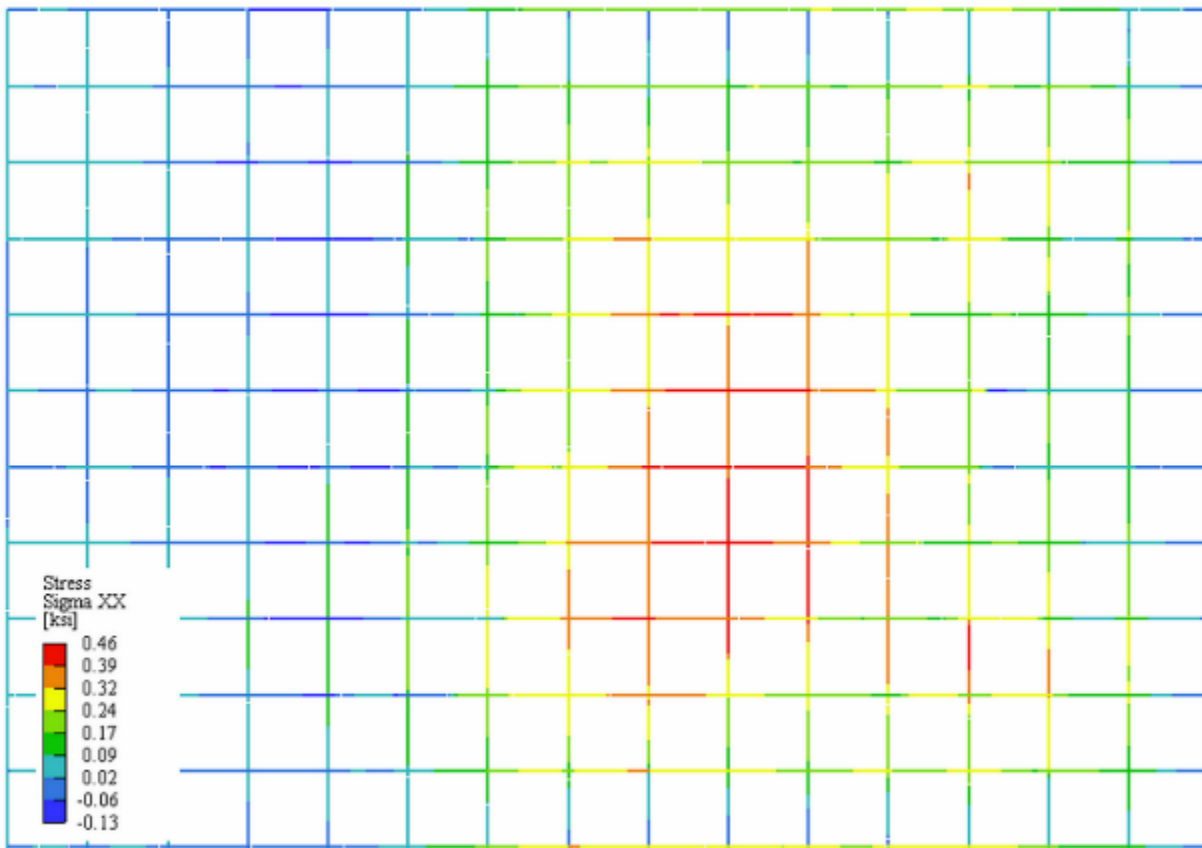


Figure 4-12 Stresses in main reinforcement layer above the piles

4.4.3 Shear stresses in main foundation

Pile foundation designs are often controlled by shear due to the presence of large, concentrated loads. The shear stress contours along the critical longitudinal direction are shown in Figure 4-13. It can be observed from this figure that maximum shear stresses near the face of the column are less than the limit of 0.25 ksi (equivalent to $4 \sqrt{f'_c}$, punching shear limit) and the one-way shear stresses in the footing are within the limit of 130 psi (equivalent to $2 \sqrt{f'_c}$).

It should be noted that any shear failure would have also shown up in the form of principal stresses exceeding the cracking limits. The purpose of this particular section on shear is to provide an

additional visual parameter of the stress state of the foundation. This visual parameter is also later used in comparing the effects of reducing the embedment depth.

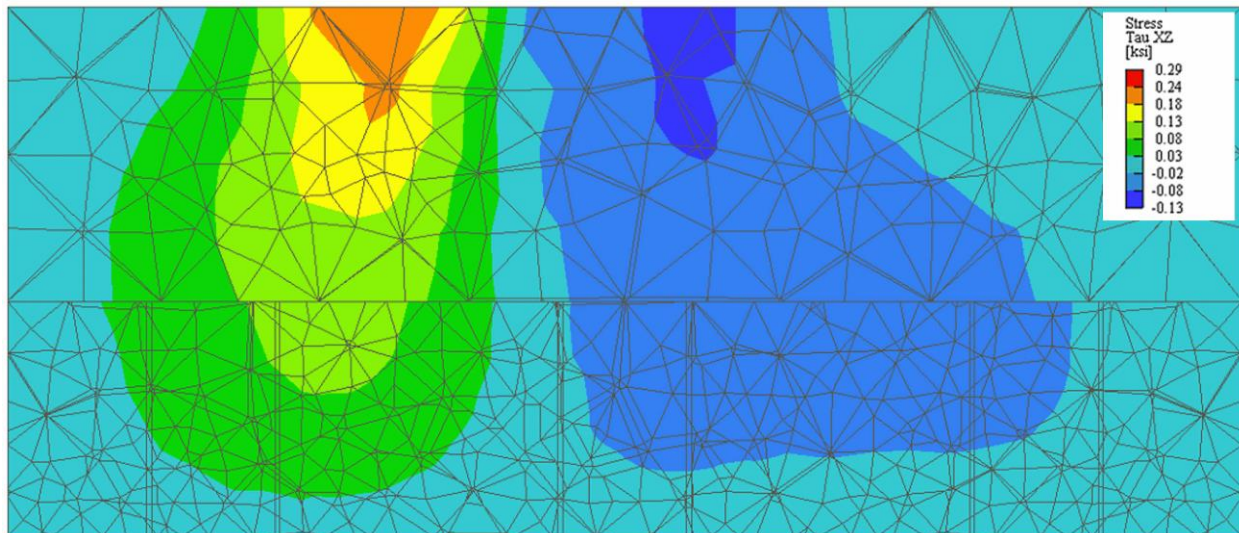


Figure 4-13 Shear Stresses in foundation

4.5 Effect of reducing the pile embedment length

Subsequent to the analysis of the Prototype Bridge two more models are prepared with a pile embedment depth of 1 ft and 0.5 ft. The modelling of these two variations followed the exact same procedures as the Prototype Bridge foundation. A comparison of various parameters between all three models is presented in this section.

4.5.1 Comparison of maximum principal stresses in concrete

Figure 4-14a to Figure 4-14b compares the principal stress contours of the three foundation configurations with embedment depths of 2 ft, 1 ft and 0.5 ft. This comparison is made at each of the six cut locations as discussed previously in section 4.4.1 and are shown in Figure 4-11a. These figures also follow the same stress contour legend as shown in Figure 4-11h. It is observed from these figures that all three foundation configurations have stress contours within permissible tensile stress limits for cracking even though the applied design loads are for the ultimate strength limit state. It should also be noted that with decreasing embedment depth the foundation moves towards a higher stress state. This is clearly observed in cut-2 (see Figure 4-14b below), in which the area indicated in yellow (stress between 0.1 ksi – 0.39 ksi); is limited to the bottom portion of the footing for 2 ft embedment length model; is in the entire region of the embedment depth for the 1 ft embedment length model; and extends into the main foundation zone for the 0.5 ft embedment length model.

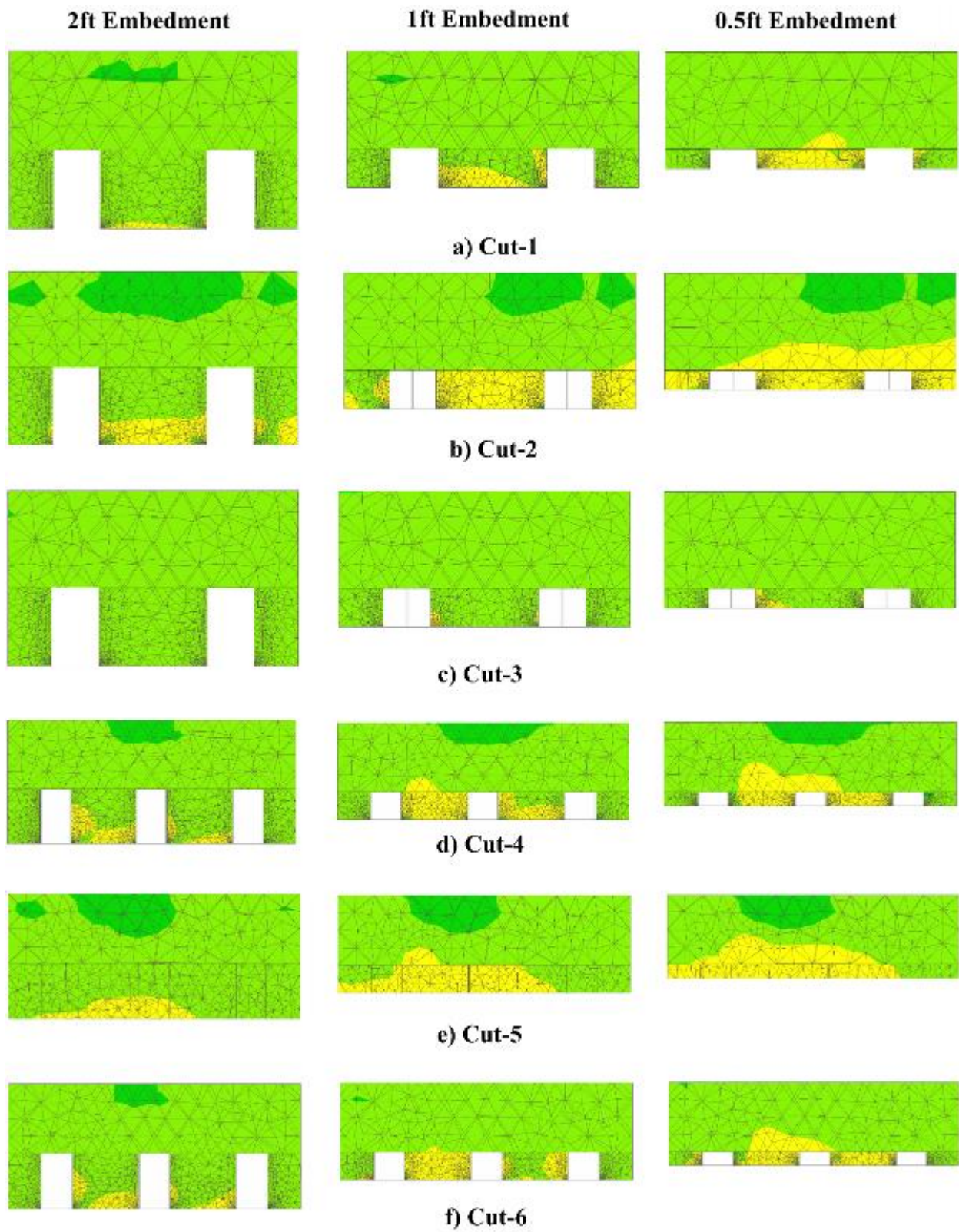


Figure 4-14 Figure comparing principal stresses in foundation for different embedment depths

4.5.2 Comparison of rebar stresses

Figure 4-15 shows a comparison of the rebar stresses. The maximum stress in rebar observed in model with 2 ft pile embedment depth is 0.46 ksi. In the model with 1 ft and 0.5 ft embedment depth the maximum observed rebar stresses were 1.1 ksi and 1.5 ksi respectively. This change in rebar stresses is very minor and it can be stated that changes to pile embedment depth for these design loads is not expected to cause any changes to reinforcement stresses.

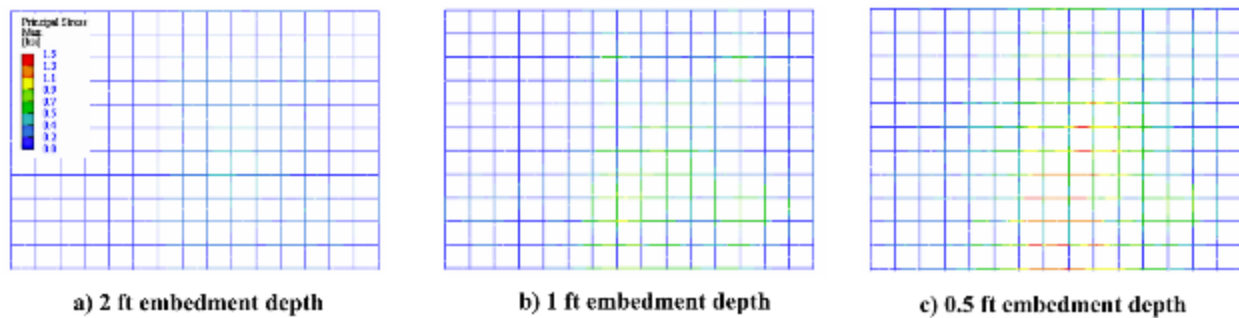


Figure 4-15 Figure comparing stresses in bottom reinforcement layer for different embedment depths

4.5.3 Comparison of shear stresses

The maximum shear stresses observed largely remained the same across all three models. This can be seen in Figure 4-16. A slight increase of 0.02 ksi is observed in isolated nodes near the face of the column.



Figure 4-16 Figure comparing shear stresses in foundation for different embedment depths

4.6 Selection of test specimens

Following the finite element analysis, the following objectives were established in order to choose test specimens that would aid in this investigation.

- 1) The test specimens should be able to quantify the amount of force transferred from the foundation to the pile via bearing at the pile ends and skin friction of the pile web and flanges.
- 2) The test specimens must enable for the evaluation of the adequacy of 1 ft embedment depth for ALDOT standard design and detailing process.
- 3) The test specimens should be in the same stress state as the prototype foundation.
- 4) The design of the test specimen should allow for the creation of a precast foundation specimen with appropriate tolerances to allow for straight and battered pile placement.

In meeting the first objective test specimen #1 and specimen #2 as shown in Figure 4-17a and b are chosen. These specimens consisted of a single HP 12 X 53 pile embedded into a 3 ft 6 in square foundation block. These specimens would provide the necessary data for modelling of a more refined finite element model. The reinforcement details of these specimens are shown in Figure 4-17c. Reinforcement (#4 bars) below the pile is provided to resist the compressive loads coming from the piles. Minimal number of confining hoops (#3 bars) are also provided. The steel pile is provided with a 1 in thick end plate welded all around to the pile for load application.

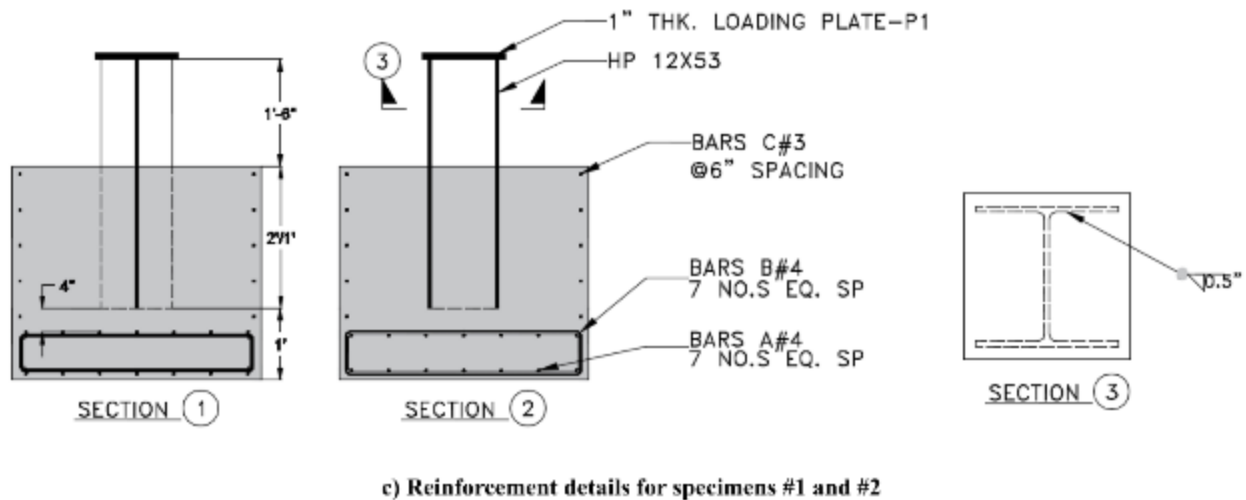
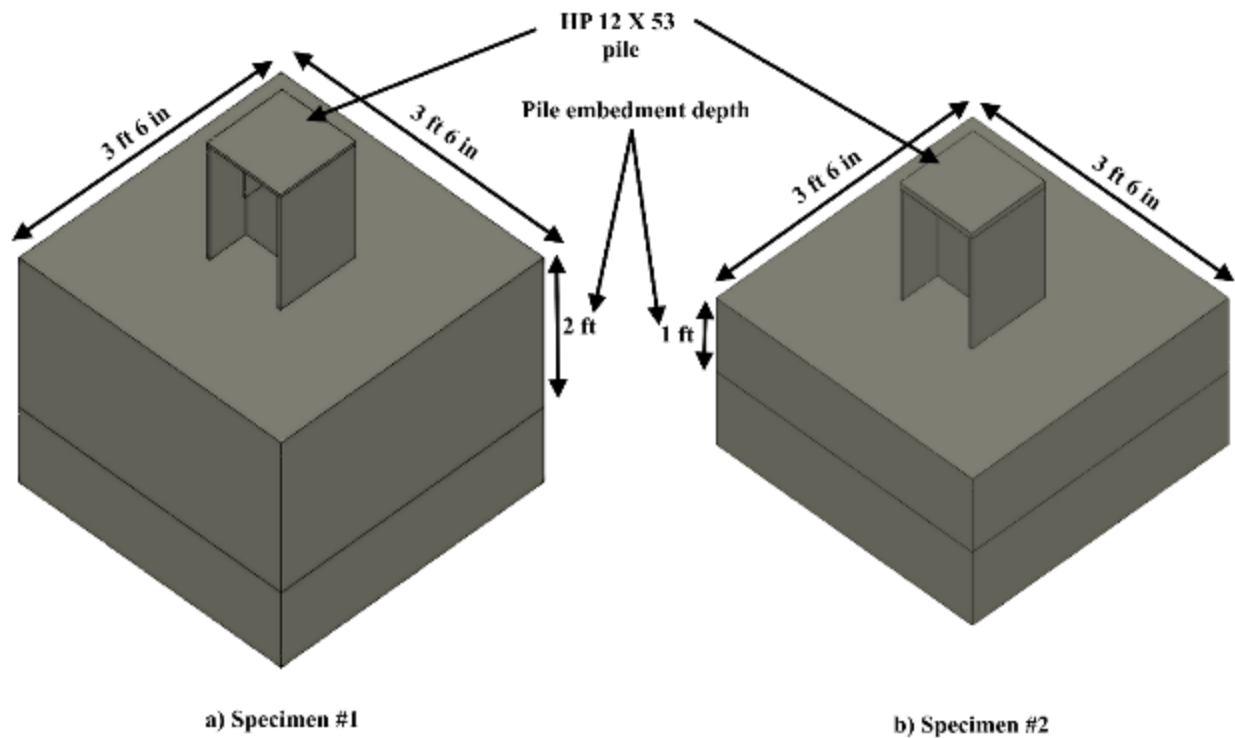


Figure 4-17 Figure showing details of specimen #1 and specimen #2

In order to verify the adequacy of 1ft embedment length a test specimen as shown in Figure 4-18a is developed. This specimen consists of a 3 ft 6 in by 7 ft 6 in rectangular block supported on two HP 12 X 53 piles placed at a center to center distance of 4 ft. The reinforcement details of this foundation are similar to Prototype foundation (see Figure 4-18b). The main reinforcing bars consist of # 8 bars at approximately 7.5 in spacing in both directions. The skin reinforcement bars consisted of #6 bars spaced at 6 in spacing.

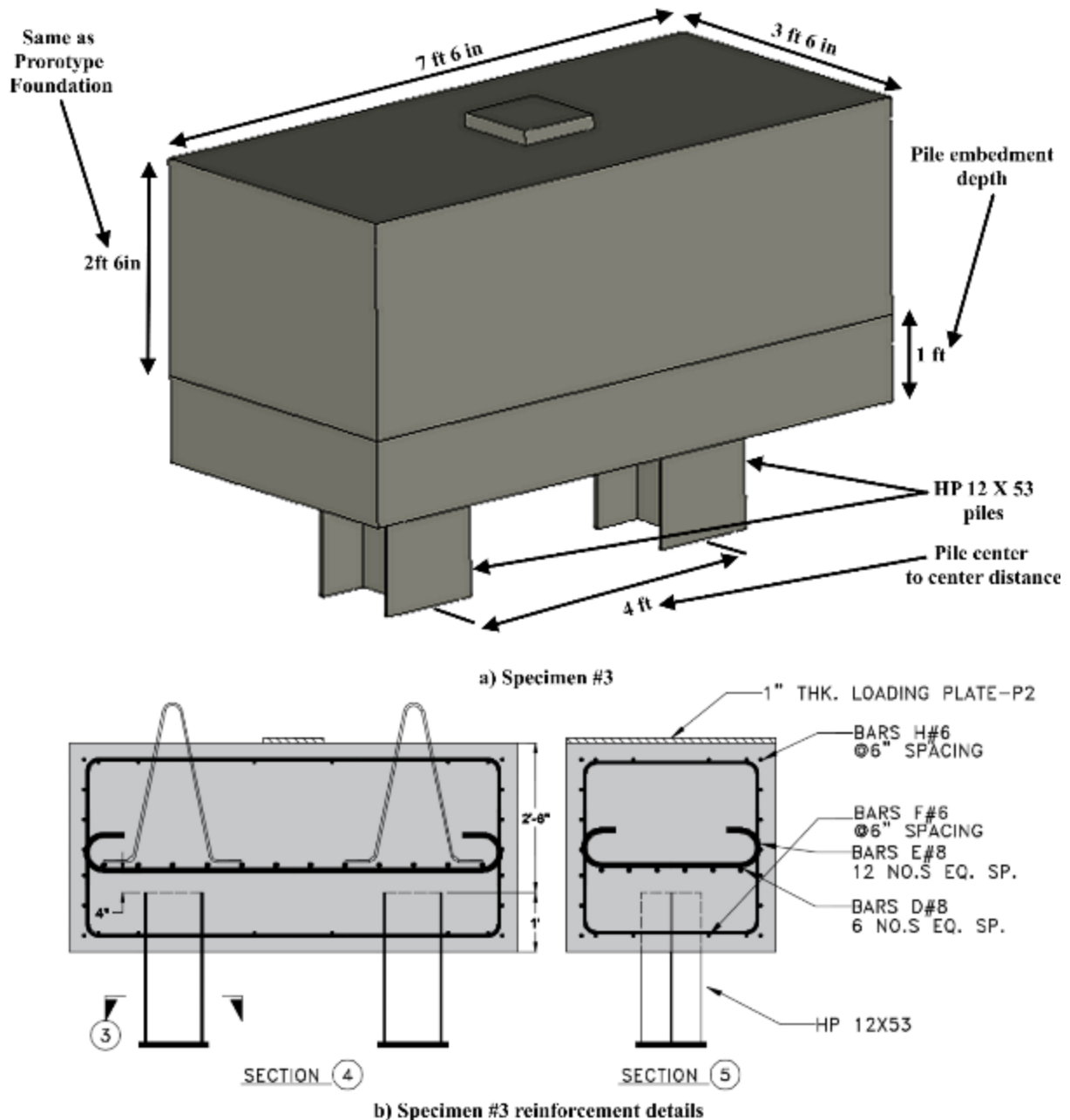


Figure 4-18 Figure showing details of specimen #3

One of the objectives of this study was also to develop and examine the feasibility of a precast foundation detail, specimen #4 having the exact outline dimension and reinforcement details as specimen #3 was thus developed. This specimen would allow for a comparison between cast-in-situ foundation (Specimen #3) and a precast foundation. The details of this precast test specimen are shown in Figure 4-19. The specimen consists of grout holes and voids to allow for placement of cast-in-situ grout. The voids left for placement were 16 in square shaped and 15 in deep, which would allow for battering of HP 12 X 53 piles and have a 4 in. tolerance on the pile positioning.

Equation (4-4) shown below is the AASHTO LRFD formula for calculating interface shear of two different materials. In this equation V_{ni} is the nominal shear resistance, c is the cohesion capacity of the interface, μ is the friction coefficient of the interface, A_{vf} is the reinforcement going across the interface and P_c is the normal compressive force on the interface. This equation was used to check the adequacy of the grout-concrete interface to carry the pile forces, without engaging the bearing mechanism. In this equation, the interface cohesion capacity was assumed as 0.24 ksi as per Cl. 5.8.4.3 of AASHTO LRFD (2017) code. This corresponds to an interface which is roughened to an amplitude of 0.25 in and is free of laitance. It should also be noted that there is no reinforcement or normal force across the interface and hence the second part of this equation reduces to naught. For the dimension of the grout void provided in this specimen the nominal shear resistance works out to be a value of 280 kips and the factored capacity is 252 kips. The maximum allowable factored load on a HP 12 X 53 pile is 200 kips. Thus for a 16 in square shaped and 15 in deep void the interface has sufficient capacity to carry the pile forces without having to rely on the bearing mechanism.

$$V_{ni} = cA_{cv} + \mu(A_{vf} + P_c) \quad (4-4)$$

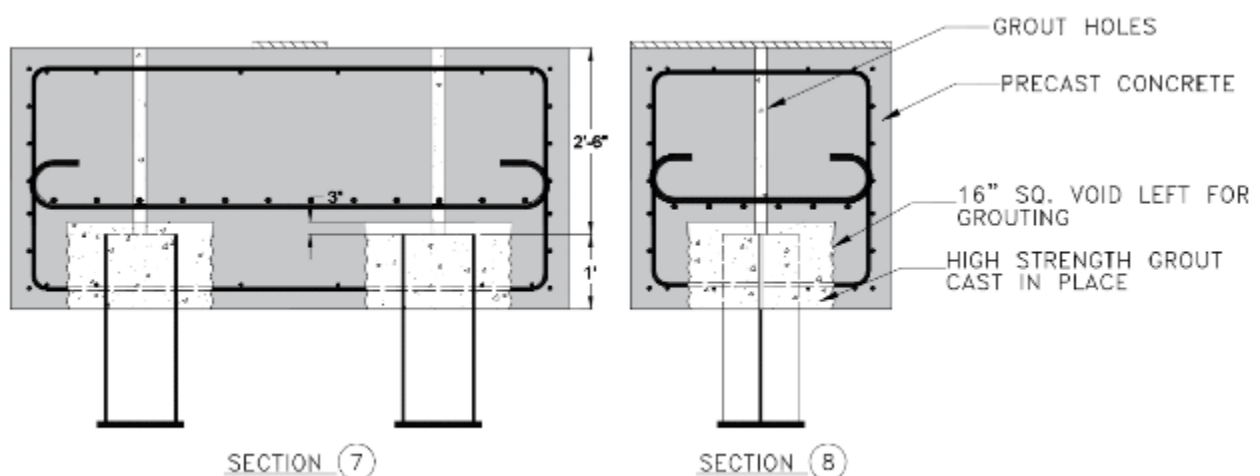


Figure 4-19 Figure showing precast foundation details

All these specimen details were discussed with ALDOT project advisory committee and were finalized after taking their inputs. The fabrication drawings giving complete details of all the test specimens is provided in Appendix A.

CHAPTER 5: FABRICATION AND TESTING OF EXPERIMENTAL SPECIMENS

5.1 Introduction

A total of four different test specimens were finalized. Specimen #1 and Specimen #2 were intended to help characterize the force transfer mechanism between the steel piles and the concrete foundation. Specimen #1 had an embedment depth of 2 ft, and Specimen #2 had an embedment depth of 1 ft. Specimen #3 and Specimen #4 were full scale specimens containing a two pile set with 1 ft embedment depth. These specimens were designed to test the adequacy of the 1 ft embedment depth and the performance of the precast foundation, respectively. All four test specimens were fabricated in the Large Scale Structures Lab at the University of Alabama, Tuscaloosa. This chapter presents, properties of materials used, fabrication details of the test specimens and experimental test program details.

5.2 Material Properties

5.2.1 Steel

All the steel reinforcement used in this investigation was grade 60 mild steel reinforcement. The main reinforcing bars used in the study were of three different diameters: #4, #6, and #8. Tensile tests were conducted on all the rebar (see Figure 5-1a) and dog bone coupons cut from unused steel pile sections. A yield plateau was observed in all three rebar tests and dog bone coupon tests, and the eventual failure of the specimens was through tensile rupture (see Figure 5-1b). The measured properties are given in Table 5-1. This table also includes the details of the rebar deformations. The deformation pattern on these rebar can be seen in Figure 5-2.

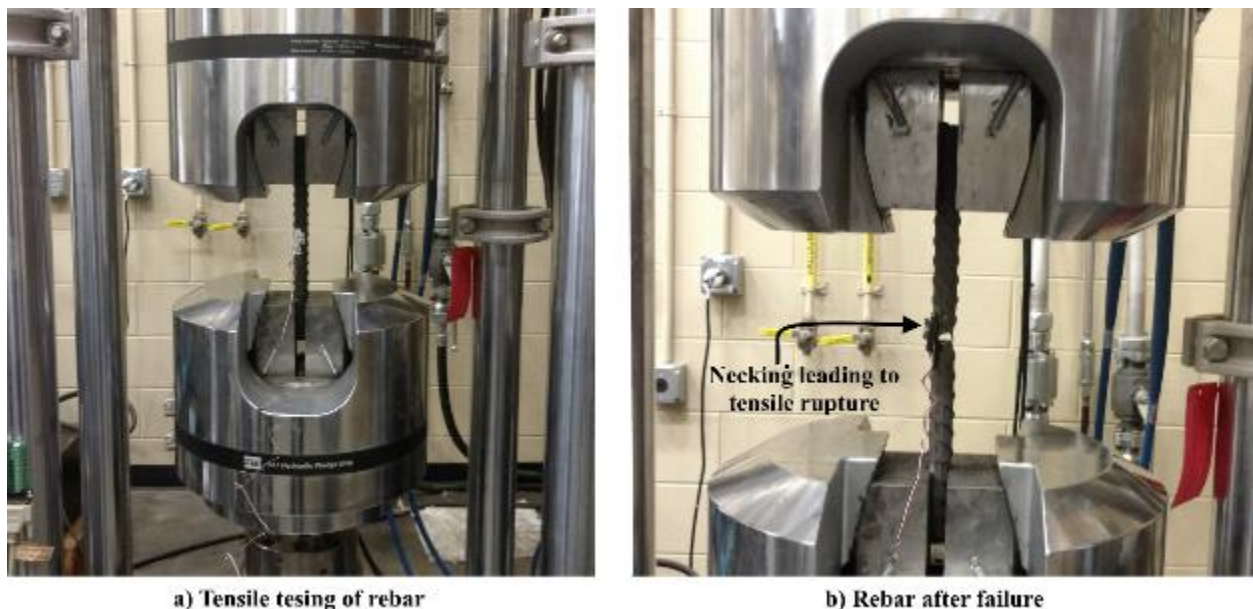
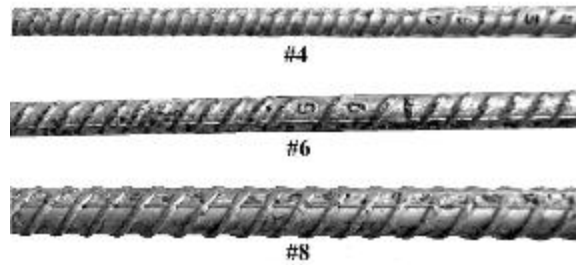


Figure 5-1 Figure showing tensile testing of rebar

Table 5-1 Reinforcing bar and structural steel properties

Bar Size (US)	Yield Strength (ksi)	Tensile Strength (ksi)	Young's Modulus (ksi)	Deformation Details (in.)	
				Mean Spacing	Mean Height
#4	64	94	29090	0.150	0.041
#6	63	96	29032	0.280	0.050
#8	67	101	28510	0.300	0.059
Steel piles	61	83	30526	NA	NA

The bar bend diameters and hook lengths for all the reinforcing bars were as per the standard details adopted by Concrete Reinforcing Steel Institute (CRSI) and ACI-318-14.

**Figure 5-2 Figure showing the rebar deformation pattern**

5.2.2 Concrete

All four test specimens were designed with a target concrete strength of 4000 psi. Class B concrete (as per ALDOT specifications) was used in all the specimens. The properties of this concrete are as shown in Table 5-2. Two different pours were used for this investigation. The measured 7 day, 28 day, and test day compressive strengths are shown in Table 5-3. The compressive tests were performed on 6 in by 12 in cylinders which were stored in a curing room.

Table 5-2 Concrete material Properties

Property	Value
Maximum water/cementitious materials ratio	0.45
Total air content	2.5-6.0 %
Slump	3.5 in
Largest nominal aggregate size	1 in

Table 5-3 Measure concrete compressive strengths

Day of measurement	Compressive strength (psi)	
	Pour-1	Pour-2
7 days	3297	3468
28 days	4798	5257
46 days (Testing of Specimen#1 and #2)	4849	5339
81 days (Testing of Specimen#3 and #4)	5927	6265

5.2.3 Grout

Grout was used to fill the voids and establish the force transfer mechanism between the steel piles and the precast foundation in Specimen #4. The grout used in this project was supplied by CTS cement with a product name “Ultraflow 4000/8”. This grout was selected due to its non-shrink properties, high early strength characteristics and its flowability properties. This grout also has high resistance to freeze thaw cycles (99% as per ASTM C666). The grout was mixed in a standard concrete mixer such as the one shown in Figure 5-3.



Figure 5-3 Figure showing grout preparation in a concrete mixer

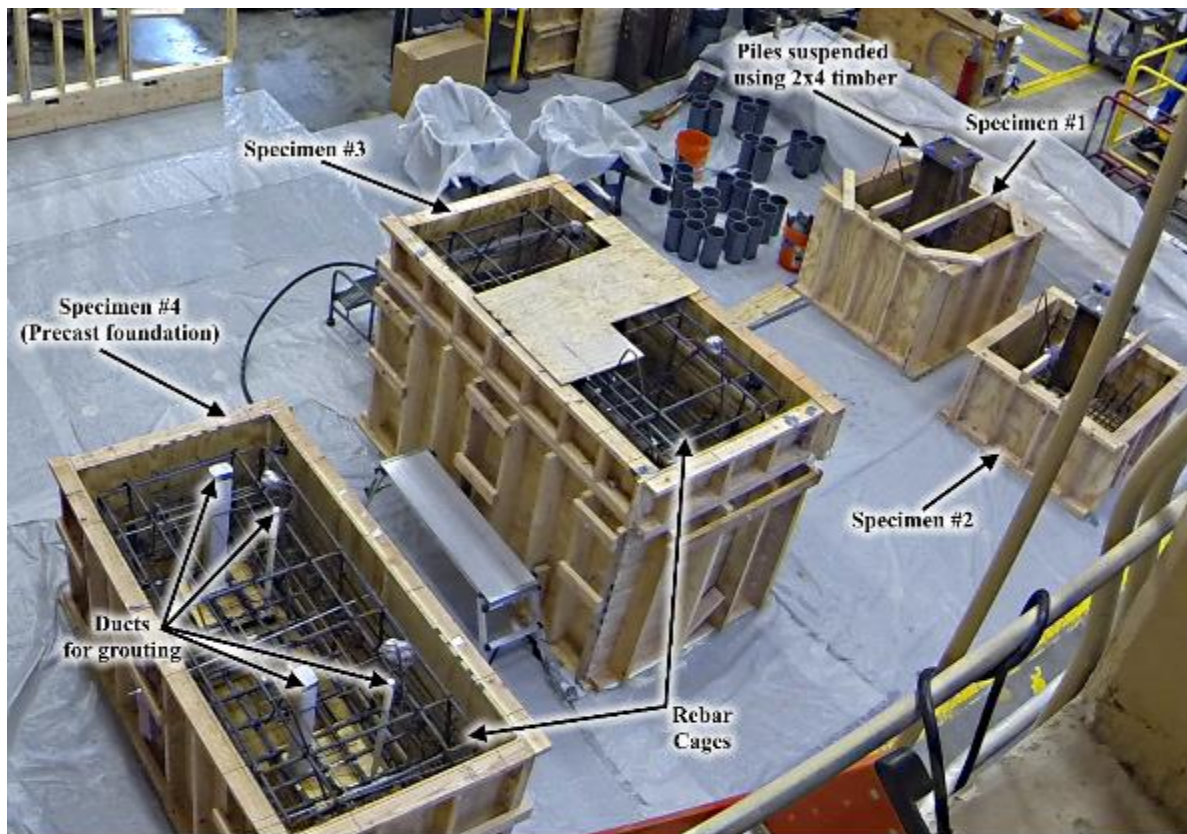
The measured 12 hour, 3 day, and test day compressive strengths are provided in Table 5-4. These strengths were measured through the testing of 2 in cubes. The material data sheet for the grout is provided in Appendix-B

Table 5-4 Measured compressive strengths of grout	
Time of measurement	Compressive strength (psi)
12 hours	7509
3 days	10980
41 days (Testing of Specimen #4)	11445

5.3 Fabrication of test specimens

The specimens were cast in wood formworks built using $\frac{3}{4}$ in plywood sheets and reinforced using 2x4 and 2x6 timber pieces. The opposite faces of the formwork were also tied together internally using threaded rods to avoid bowing out of the forms. Figure 5-4a shows the formwork of all four specimens. Also notice in the figure the rebar cages placed inside the form work. The rebar cages for Specimen #3 and Specimen #4 were identical (see Figure 5-4b). These rebar cages were

assembled outside the forms and then lowered using the crane (see Figure 5-4c). Prior to placement of the rebar cages the forms were adequately coated with form release to ensure smooth removal of formwork. For the fabrication of Specimen #3, piles were first placed inside the form work as shown in Figure 5-5a, subsequent to this Styrofoam was used to fill the height so as to leave a 1 ft length of free pile sticking out. This was finished with a plastic sheeting to create a moisture barrier and the concrete pour was then carried out. For the casting of Specimen #4, the voids were created using a plywood box with a texture on all four sides. The details of the texture can be seen in Figure 5-5c and Figure 5-5d. These boxes were then placed in the form work prior to concrete casting as shown in (Figure 5-5e). Figure 5-5f shows the details of the interior of the void after concreting.



a) Figure showing formwork for all the specimens



b) Rebar cages for Specimen #3 (foreground) and Specimen #4 (background)

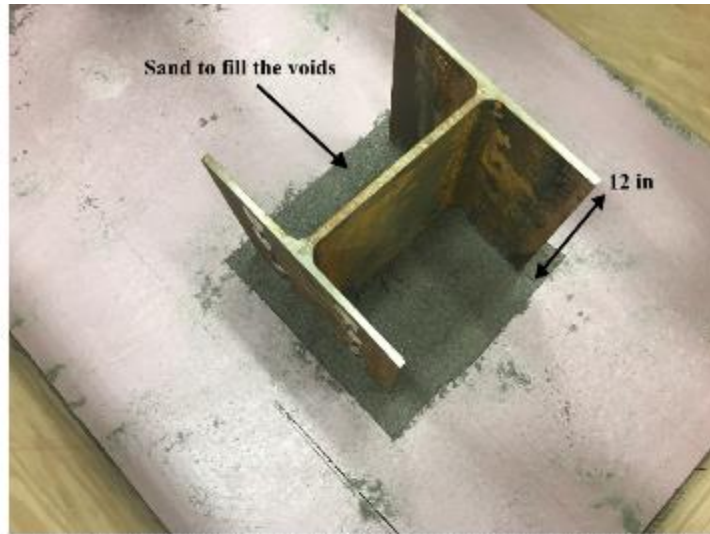


c) Rebar cage being lowered into Specimen #4

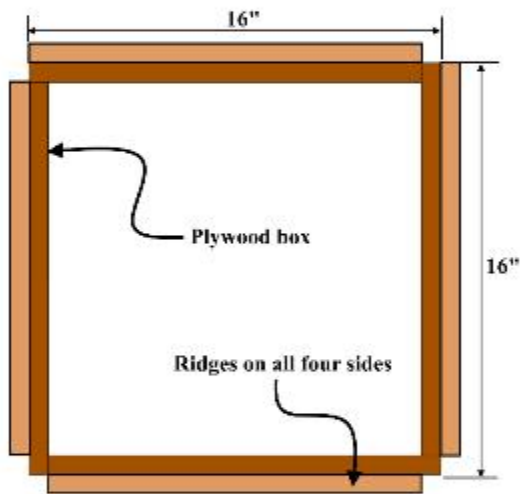
Figure 5-4 Figure showing the form work of all the test specimens



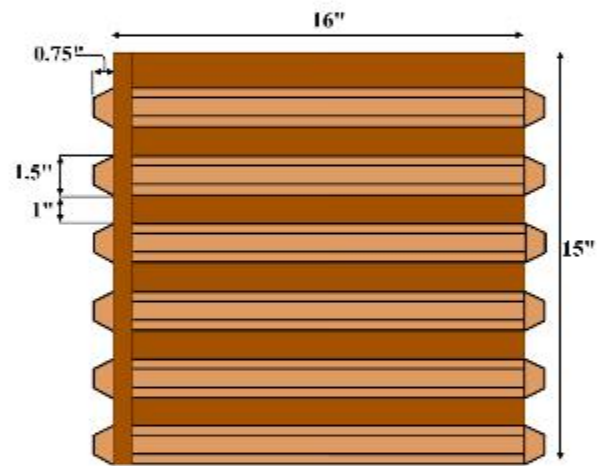
a) Piles placed in formwork



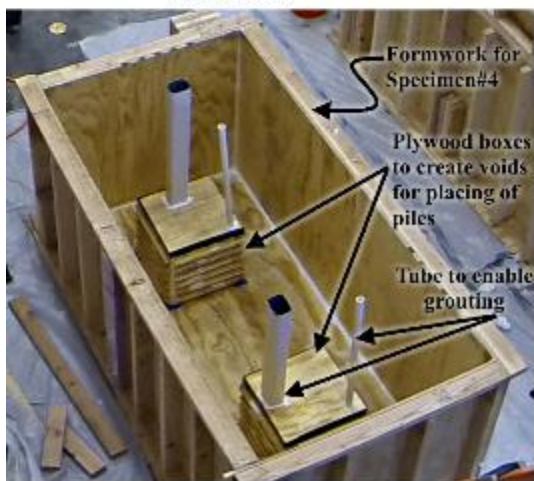
b) Specimen filled with styrofoam leaving 1ft of free pile sticking out



c) Plan View



d) Side View



e) Specimen #4 formwork



f) Interior of the void after casting

Figure 5-5 Figure showing casting details of Specimen #3 and Specimen #4

The concrete pour for all the test specimens was carried out on July 2nd, 2018. The test specimens were cast using two pours of concrete obtained using a truck mixer (see Figure 5-6a). A vibrator was used during the concrete pouring to ensure proper distribution of the concrete mix (see Figure 5-6b). Separate sets of 6 in x 12 in cylinders were cast for each of the two concrete pours. Once the casting was finished the specimens were covered with a plastic sheeting. The formwork was removed after 3 days and the specimens were stored at ambient temperature until testing.



Figure 5-6 Figure showing details of concrete casting

Subsequent to the casting of all the specimens, grouting of Specimen #4 was taken up. Styrofoam was placed around the piles and the specimen was lowered on this setup using a crane. It should be noted that difficulty was experienced during the grouting of East side void. It was noticed that the grout was starting to harden in the grout hole itself, using a pressure grouting may have helped in avoiding this issue.

5.4 Test Setup and Instrumentation

5.4.1 Specimen #1 and Specimen #2

Specimen #1 and Specimen #2 with a single pile were tested using the same test setup as shown in Figure 5-7. Compressive loads were applied using a stub column bolted to the ends of the piles. A load cell and a pressure sensor were used to monitor the loading. The test specimens were instrumented with LED markers which help measure the surface strains and displacement. The LED markers were used both on the concrete block and the steel piles above the concrete block. The LED markers were placed on a 6 in grid on the concrete block. A DCDT was also attached to the pile flanges as a secondary source for measuring the pile movement. It should also be noted that these specimens were cast in the same orientation as they were tested in, i.e. concrete block at the bottom and piles sticking out from the top, as shown in Figure 5-7. This resulted in a bottom surface which was flat enough to allow for full bearing contact thus no surface preparation underneath the foundation blocks was required.

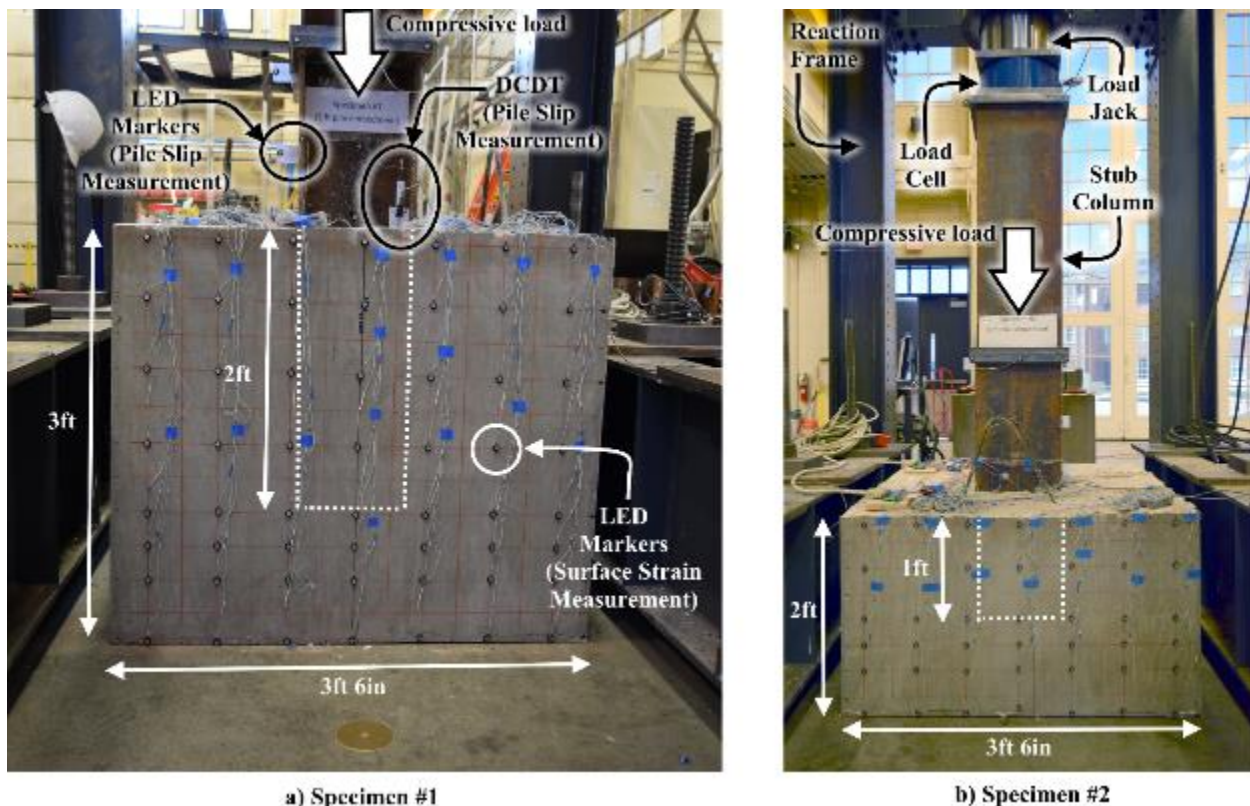


Figure 5-7 Figure showing test setup for specimens #1 and #2

Steel strain gauges were also placed on the pile flanges. Figure 5-8 shows the details of the placement of these gauges. A total of 16 gauges were placed on each pile. The placement of the steel gauges at multiple locations along the embedment depth enabled us to characterize the amount of force transferred through skin friction between the pile flanges and concrete.

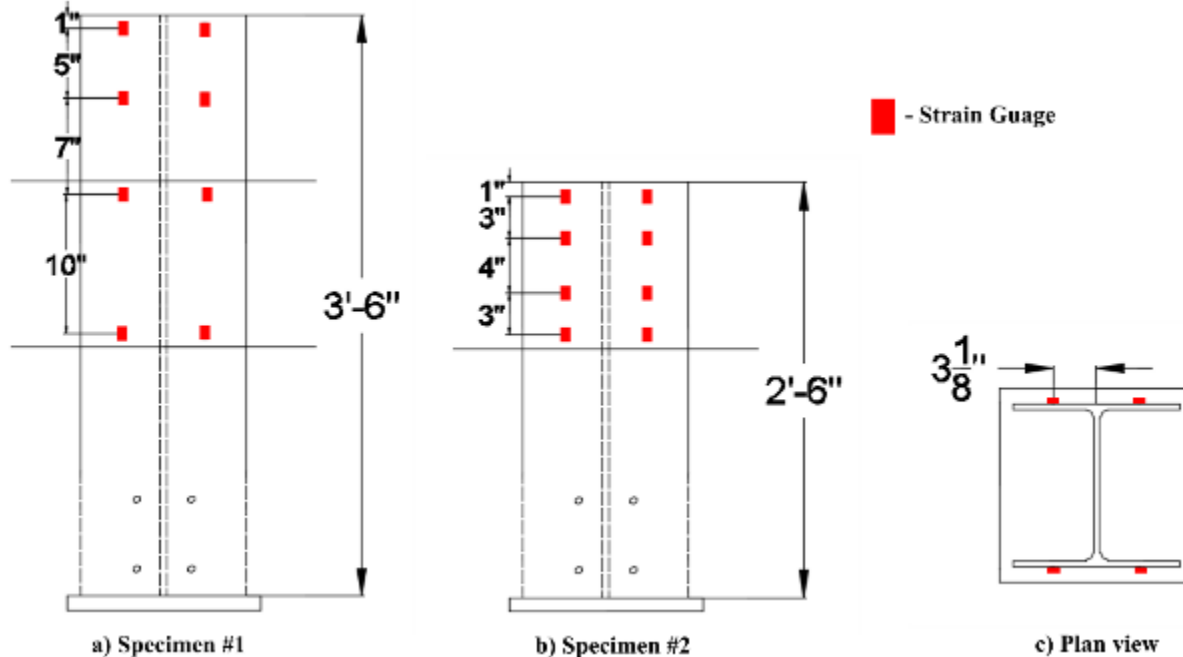


Figure 5-8 Figure showing strain gauge locations for piles in specimens #1 and #2

5.4.2 Specimen #3 and Specimen #4

Specimen #3 and Specimen #4 had two piles embedded 1 ft into the foundations. The test setup for both specimens was the same and is shown in Figure 5-9. The front view of the setup is shown in Figure 5-9a, it can be seen from this figure that force from the load jack is transferred using a UHPC block sandwiched between steel plates to the spreader beam which is resting on an 8 in wide, 1 in thick plate spanning the entire width of the foundation. Figure 5-9b shows the side view of the test setup. In this figure two channels can be seen, these are running along the length of the foundations and are bolted to the pile flanges. These channels are intended to resist horizontal forces that will be generated in the piles. Additionally, in order to provide resistance to unexpected overturning forces, the channels are held in place by two hold down plates which are bolted to the strong floor. A schematic with these details is also shown in Figure 5-10. Both the specimens were instrumented with LED surface strain and displacement measurement system (see Figure 5-9a) and DCDTs (see Figure 5-9c). These specimens were also instrumented with concrete and steel strain gauges. Figure 5-11a shows the locations of the concrete gauges along with the individual designation. A total of 8 concrete gauges were placed in each of the specimens. The location of the concrete gauges was based on the expected critical stress locations from the FEA. The gauges labelled “Inc.T” and “Inc.C” were intended to capture the stresses along the compressive strut that would form between the load point and the support. Steel gauges were placed at three locations on the main longitudinal reinforcing bars, two at the location of each pile center and one at the midpoint of the rebar. For the transverse reinforcing bars a single strain gauge was placed at the

middle of the rebar. These details are also shown in Figure 5-11b. The strain gauges on the steel piles for these specimens are placed at the same locations as Specimen #2 (see Figure 5-8b above).

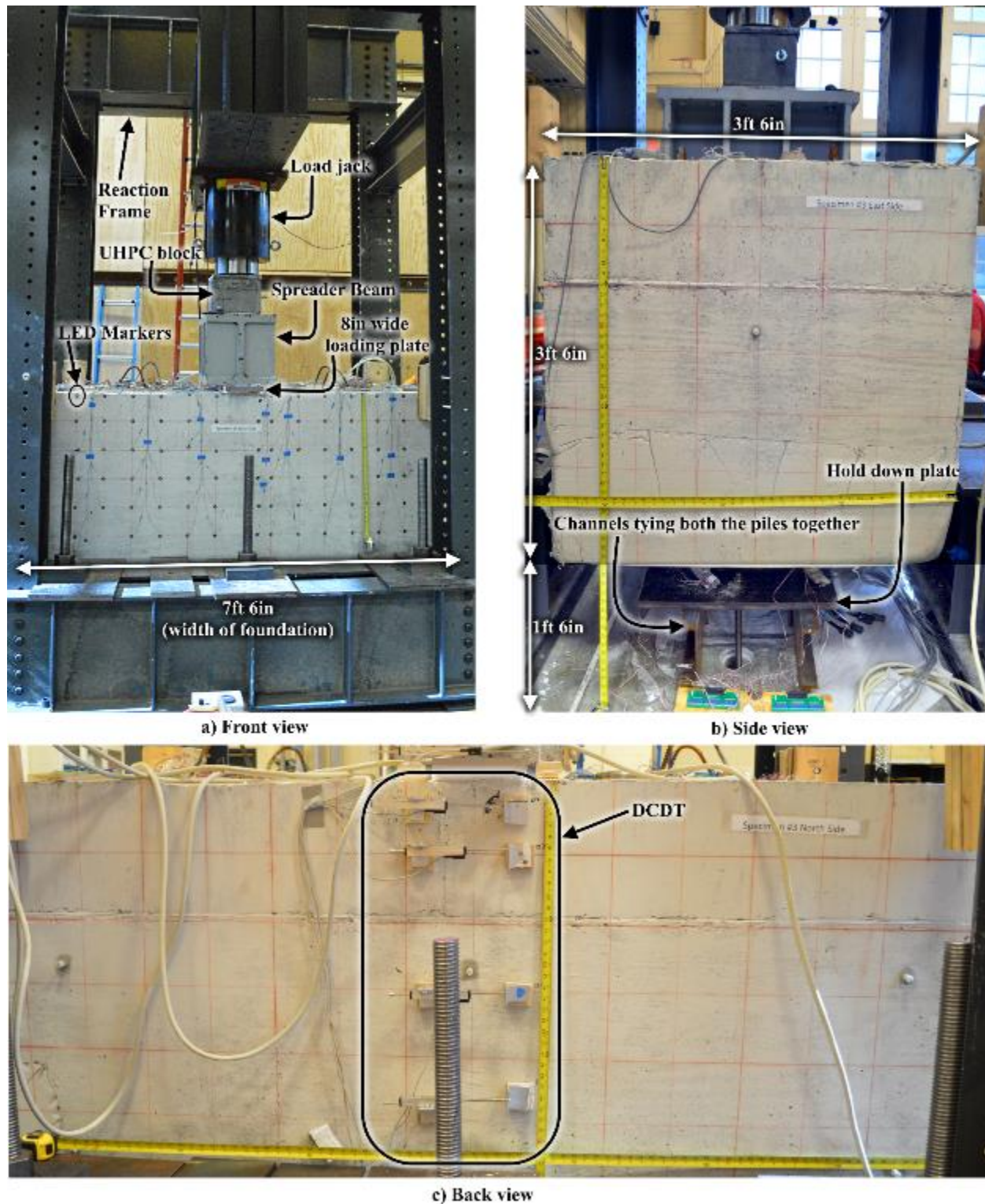


Figure 5-9 Figure showing typical test setup for specimens #3 and #4

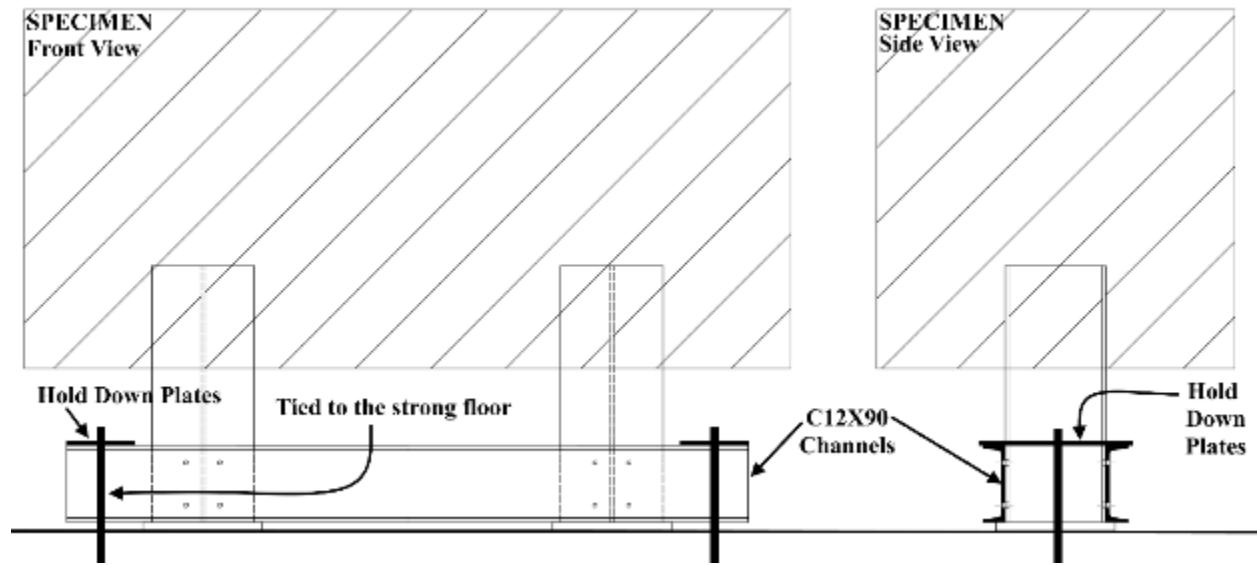


Figure 5-10 Details of the hold down plates

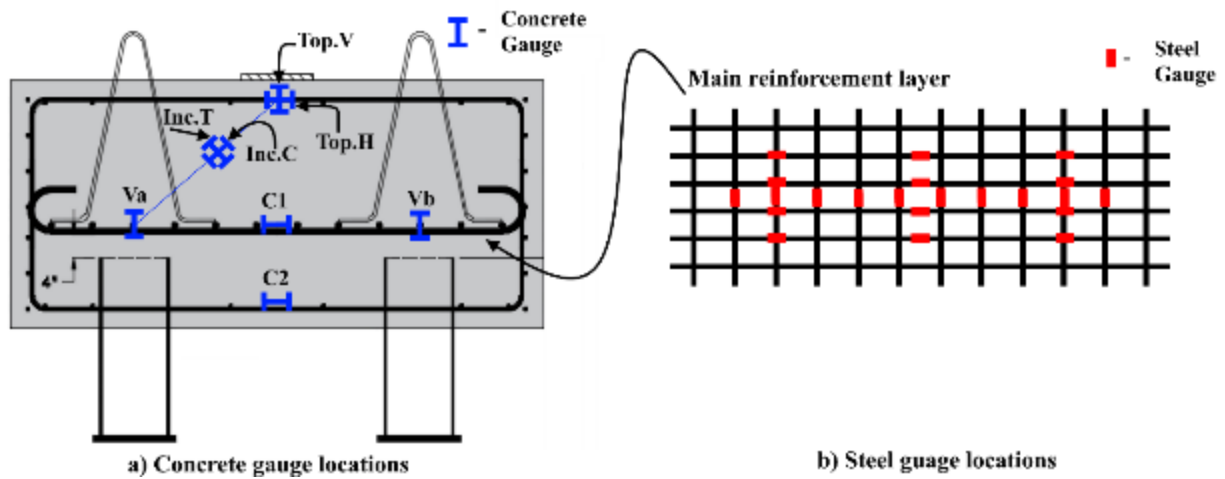


Figure 5-11 Location of concrete gauges

5.4.3 Gauge placement

a) Steel Strain Gauges

The steel strain gauges were placed on the rebars and the piles using the following process.

- 1) The surfaces of the rebar and the piles were grinded to obtain a flat and smooth surface. It was ensured that minimal amount of surface grinding was done so as to ensure that strength of the rebar or pile remains is not significantly affected.
- 2) Two different grits of sandpaper (100 and 150) were then used to obtain an even smoother finish and clear the surface of any remaining rust.

- 3) The area was then cleaned using a neutralizer and a conditioner to remove any contaminants.
- 4) The strain gauges were subsequently placed in the cleaned area. A clear tape was used to handle the strain gauges. It was ensured that orientation of the strain gauge is parallel to the rebar length.
- 5) Glue was then applied to the strain gauge and it was held in place firmly using a light application of pressure from the fingers.
- 6) The clear tape was then pulled away leaving the strain gauge in place on the rebar (see Figure 5-12a)
- 7) Subsequently, 3 layers of protection were applied, the first layer of protection was a poly urethane coating followed by application of rubberized tack, and this was all wrapped using aluminum tape. (see Figure 5-12a)

b) Concrete strain gauges

The concrete strain gauges were held in place by tying them to a smooth #2 bar spanning between the main reinforcing bars (see Figure 5-12b)

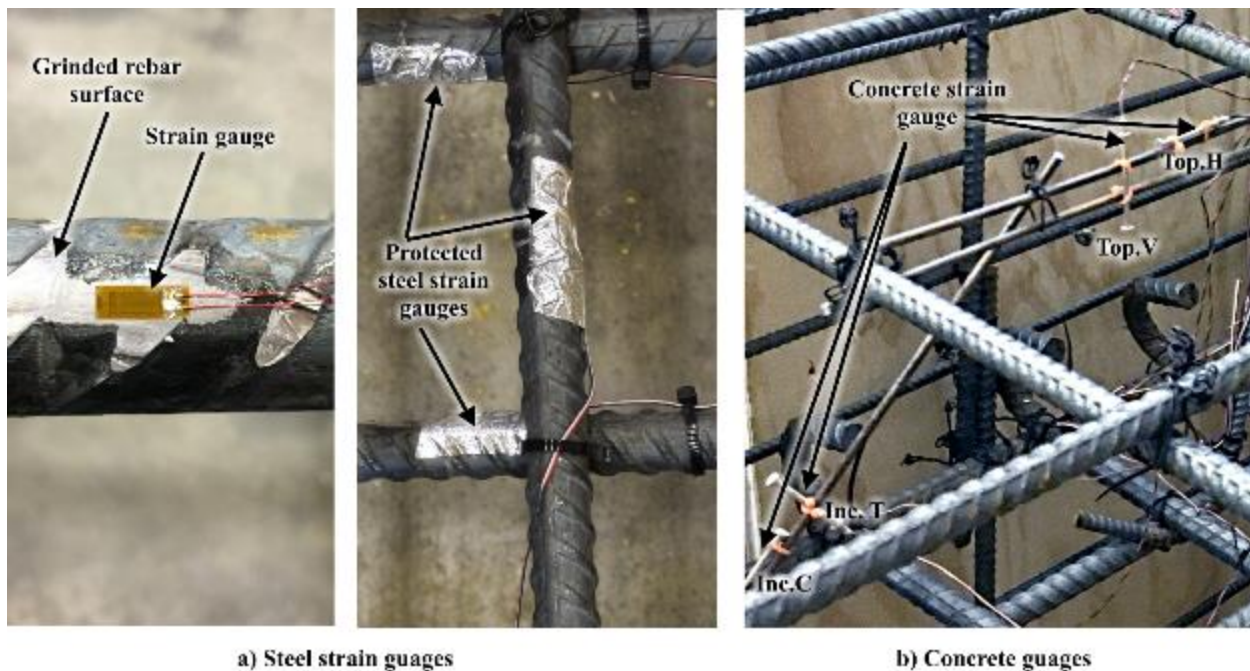


Figure 5-12 Figure showing placement of steel and concrete gauges

5.4.4 Load Application

All the specimens were loaded using a hydraulic jack which was controlled using a hand pump. The allowable maximum load on a single HP 12 X 53 piles as per ALDOT specifications is 200 kips. The specimens were all loaded to go beyond this value. For specimen #1 and #2 the load was monotonically increased till the peak load of 400 kips was reached. For specimen #3 and Specimen #4 the load was cycled from 0 to 200 kips, 0 to 400 kips and then 0 to 600 kips.

CHAPTER 6: RESULTS AND DISCUSSION

6.1 Introduction

This chapter presents the results of the investigation carried out. The results from each specimen are first examined and subsequently a comparative discussion is presented. This chapter also presents the details of the post construction finite element analysis carried out. The results from this FEA are also compared with experimental results.

6.2 Specimen #1 Test Results

The maximum load applied on this specimen was 398 kips. No cracking was visible around the pile concrete interface for this maximum load level (see Figure 6-1). A maximum average strain of 0.0008495 was observed in the pile. This strain value corresponds to a load of 402 kips as per the measured Young's Modulus of the piles provided in Table 5-1. This value is very close to the values measured from the load cell, indicating that the strain gauges are working as expected.

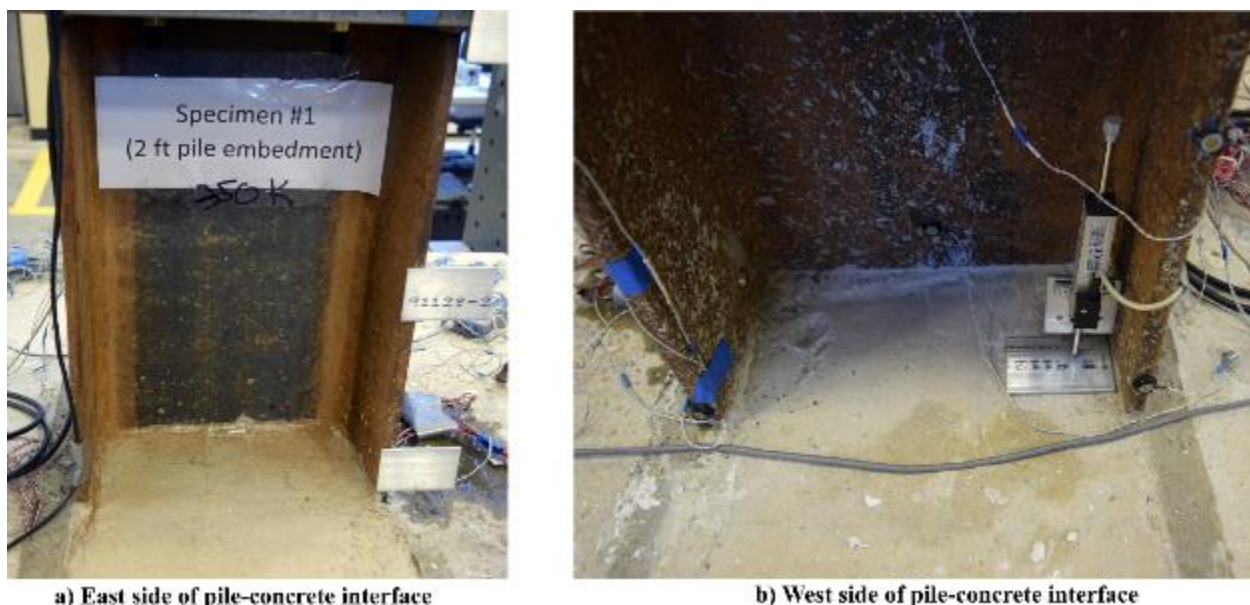


Figure 6-1 Figure showing the condition of pile concrete interface for specimen #1 at maximum loading

The measured pile displacement vs load is shown in Figure 6-2. The pile displacement is measured approximately 1 in above the top of concrete. It should be noted that $\frac{3}{4}$ in thick Styrofoam pieces were glued to the embedded end of the piles. Due to presence of this Styrofoam, as soon as there is a loss of cohesion between the steel piles and concrete, it is expected that the pile will start bearing on the Styrofoam pieces. Styrofoam being a material with low stiffness will thus allow for a considerably large slip values while holding the load. This mechanism is observed for this specimen at a value of 392 kips. In Figure 6-2, it can be noticed that the pile displacement is linear up to this value and the pile starts slipping subsequent to reaching this load. Upon unloading it is observed that a slip value of 0.0035 in remains as the permanent displacement of the pile.

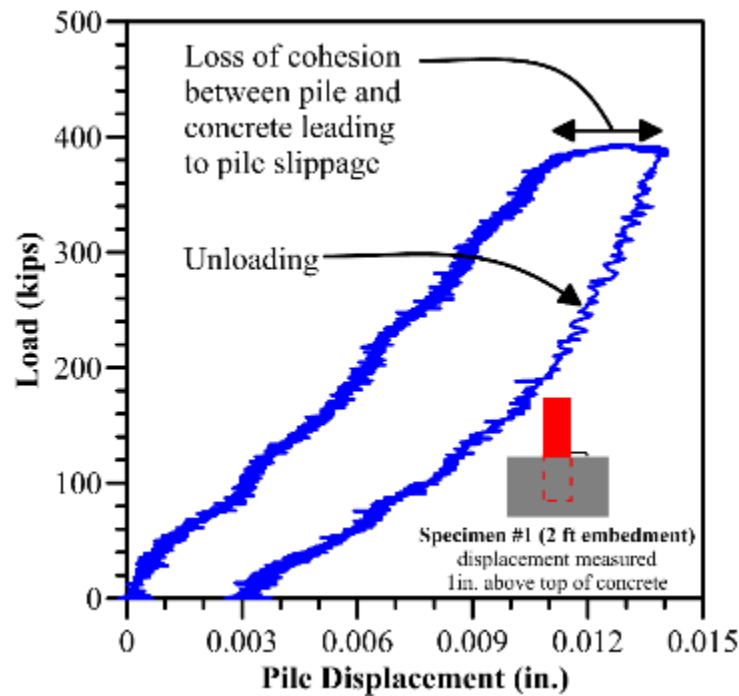


Figure 6-2 Graph showing the experimentally obtained load vs pile displacement data for Specimen #1

Figure 6-3 shows the strains recorded in the pile strain gauges present on all four sides of the pile. Each of the different colored lines represent the strain gauge readings at different embedment depth as shown in the legend. In these graphs the unloading curve has not been shown for the sake of clarity. For side-1 and side-4 only 3 out of the 4 strain gauges were functioning, for side-2 and side-3 all four gauges were functioning. It can be observed from these graphs that the strains recorded on the piles decreases with increasing embedment depth. For example, in Figure 6-3b it can be seen that at peak load the strains recorded at an embedment depth of 1 in. have strains in excess of 0.001 and at an embedment depth of 23 in. a negligible value of less than 0.00005 is recorded. This is indicative of the fact that a majority of the force transfer is happening through skin friction between the pile surface and concrete. This phenomenon can be quantified as shown in Figure 6-4. This figure plots the recorded strain values at different embedment depths as a percentage of maximum strain observed. It can be seen from this figure that the strain values vary linearly with embedment depth.

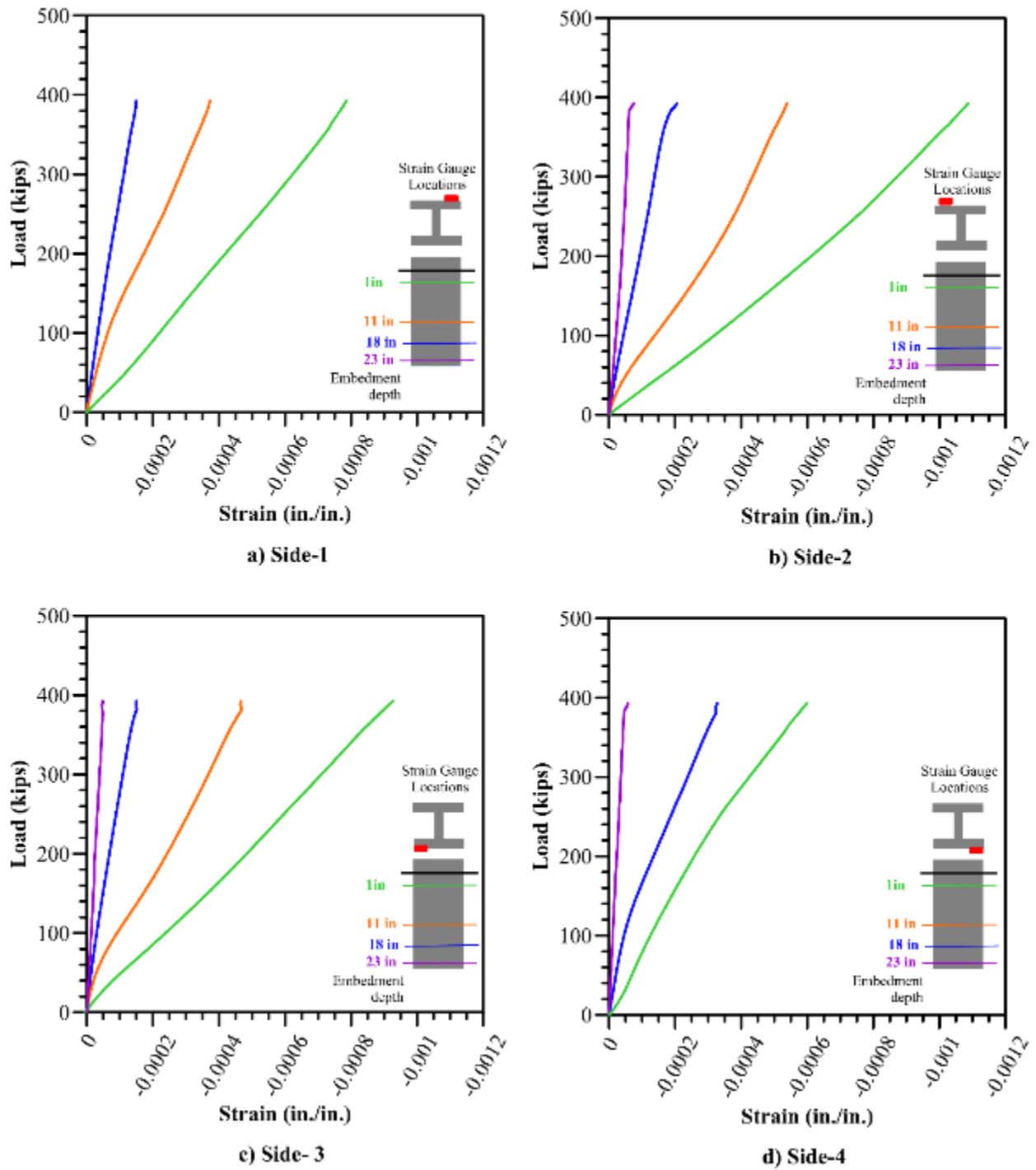


Figure 6-3 Figure showing the strains recorded at various embedment depth on the pile in specimen #1

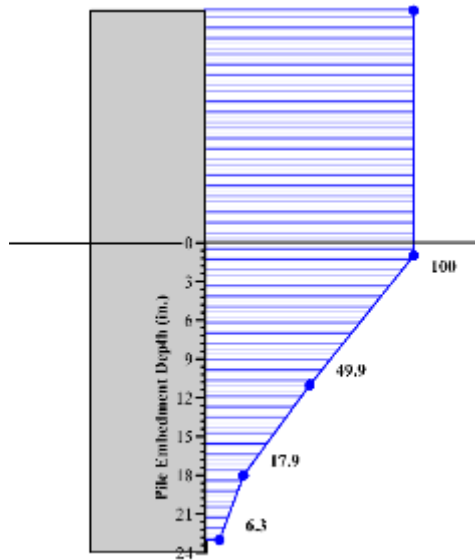


Figure 6-4 Figure showing the strains recorded along the depth of the pile for Specimen #1

6.3 Specimen #2 Test Results

The maximum load applied on this specimen was 390 kips. No cracking was visible around the pile concrete interface for this maximum load level (see Figure 6-5). A maximum average strain of 0.00084 was observed in the pile. This strain value corresponds to a load of 397 kips as per the measured young's modulus of the piles provided in Table 5-1. This value is very close to the values measured from the load cell, indicating that the strain gauges are working as expected. It should also be noted that these values are in the same range of values observed in Specimen #1.

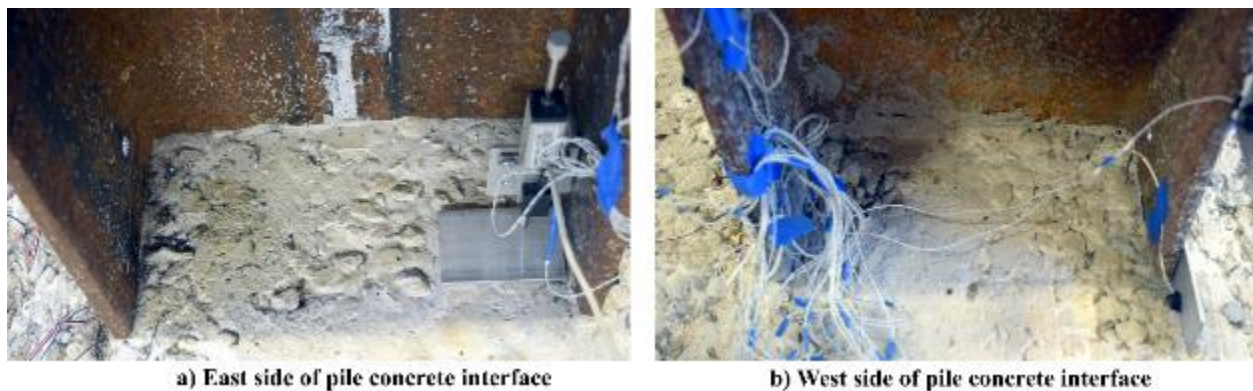


Figure 6-5 Figure showing the condition of pile concrete interface for specimen #2 at maximum loading

The measured pile displacement vs load is shown in Figure 6-6. The pile displacement is measured approximately 1 in above the top of concrete. The pile slippage in this specimen starts at a load value of 205 kips, indicated by the change in slope observed in Figure 6-6. A permanent displacement of 0.007 in is observed in the pile after unloading.

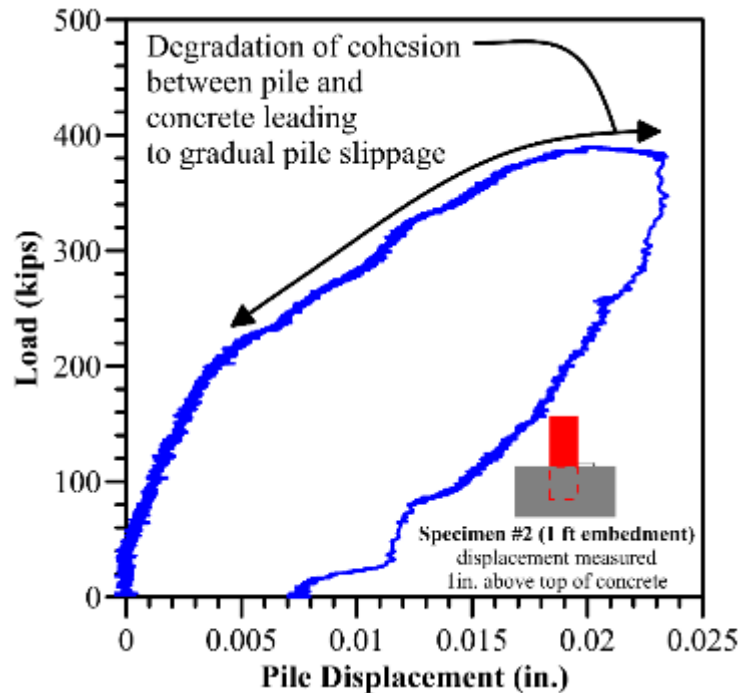


Figure 6-6 Graph showing the experimentally obtained load vs pile displacement data for Specimen #2

Figure 6-7 shows the strains recorded in the pile strain gauges present on all four sides of the pile. Each of the different colored lines represent the strain gauge readings at different embedment depth as shown in the legend. In these graphs the unloading curve has not been shown for the sake of clarity. For side-3 and side-4 only 2 out of the 4 strain gauges were functioning, it is also observed that the difference in strains recorded on this pile flange at different embedment depths on these sides is negligible. This is indicative of a bearing action. This is possibly because of the displacement of the Styrofoam piece provided underneath this flange during the concrete pour. It can be observed from these graphs that the strains recorded on the piles decreases with increasing embedment depth. It is also of particular interest that, on side-2 the strains recorded at 8 in and 12 in embedment depth have just started to plateau (Figure 6-7b). This is indicative of the force transfer mechanism transitioning from skin friction to bearing. The strain distribution observed along the embedment depth is also shown in Figure 6-8. It can be seen from this figure that the strain values vary linearly with embedment depth. It should be noted that while the strain values have plateaued at 8 in. and 11 in. embedment depth these are not appropriately reflected in the strain distribution diagram because of the small values of the strain. At higher loads than those applied here, this affect could have been observed in a pronounced manner in which the linear strain distribution would transition to a uniform strain distribution across the embedment depth.

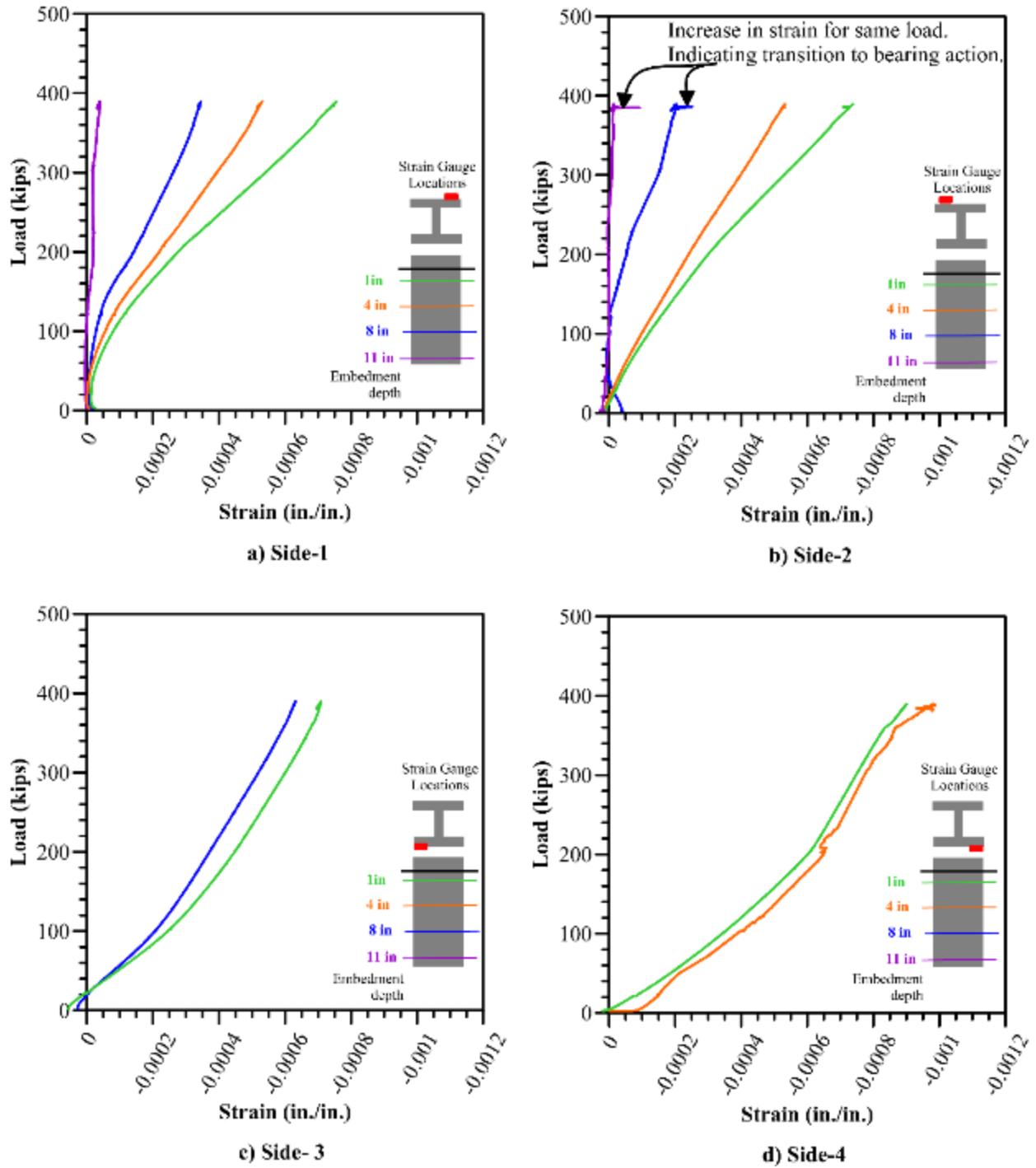


Figure 6-7 Figure showing the strains recorded at various embedment depth on the pile in specimen #2

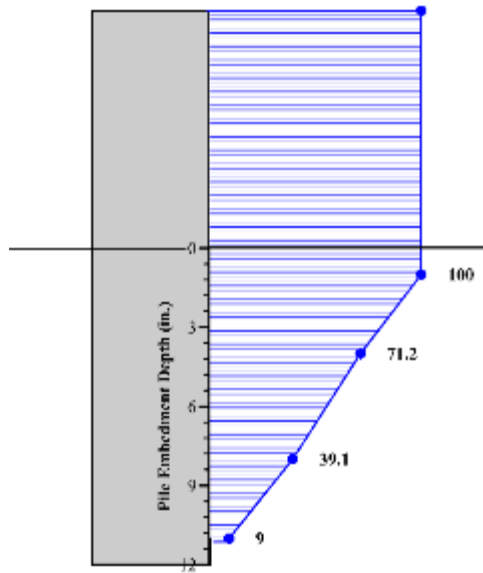


Figure 6-8 Figure showing the strains recorded along the depth of the pile for Specimen #2

6.4 Pile-concrete interface properties and post construction analysis

Based on the results from Specimen #1 and Specimen #2 presented above, the pile – concrete interface properties can be obtained. These properties are then utilized in performing a post construction analysis of specimen #3. The experimental results are then compared with the results from the finite element analysis to check for the adequacy and limitation of the finite element model in predicting the behavior.

The main properties required to model the pile concrete interface are cohesion, represented as “C” and tangential stiffness represented as “ K_{tt} ”. The cohesion value defines the maximum load an interface can sustain before failure occurs. For determining this value we have two data points, we observed that; for Specimen #1 which had an embedment depth of 2 ft, the cohesion failure occurred at a load of 392 kips and for Specimen #2 with an embedment depth of 1 ft, the cohesion degradation started at load of 194 kips. Considering the fact that surface conditions of the both piles were nearly identical, these results are in agreement with each other. The available cohesion strength for 2 ft embedment is nearly double that of 1 ft embedment. Based on this we can determine the cohesion strength as shown in Table 6-1 shown below. This value is obtained as 0.233 ksi for specimen #1 and 0.231 ksi for specimen #2. For the purposes of modelling, the value of 0.23 ksi is used. For the calculation of stiffness parameter “ K_{tt} ”, the obtained value of C is divided by the observed pile displacement at the respective load points. In this context it should be noted that for specimen #2, due to the loss of the Styrofoam piece on one of the flanges the pile displacement response was stiffer than what was to be expected. Hence the displacement value obtained for Specimen #1 alone is used to obtain a K_{tt} value of 19.1 kci.

Table 6-1 Table showing calculation of cohesion value, C

Specimen #1	Specimen #2
Load = 392 kips	Load = 194 kips
Depth of embedment = 24 in	Depth of embedment = 12 in
Perimeter of HP 12 X 53 = 69.85 in	Perimeter of HP 12 X 53 = 69.85 in
Area of contact = 24 * 69.85 = 1676.4 in ²	Area of contact = 12 * 69.85 = 838.4 in ²
$C = \frac{\text{Load}}{\text{Area of contact}} = \frac{392}{1676.4}$	$C = \frac{\text{Load}}{\text{Area of contact}} = \frac{194}{838.4}$
C = 0.233 ksi	C = 0.231 ksi

Using the cohesion properties obtained above and the material properties as discussed in section 5.2, a finite element model for specimen #3 is created. This model was created using the techniques discussed previously in Chapter 4. Figure 6-9 shows the details of this model. In discussing the results of Specimen #3, the post-construction results are also presented alongside the experimental results.

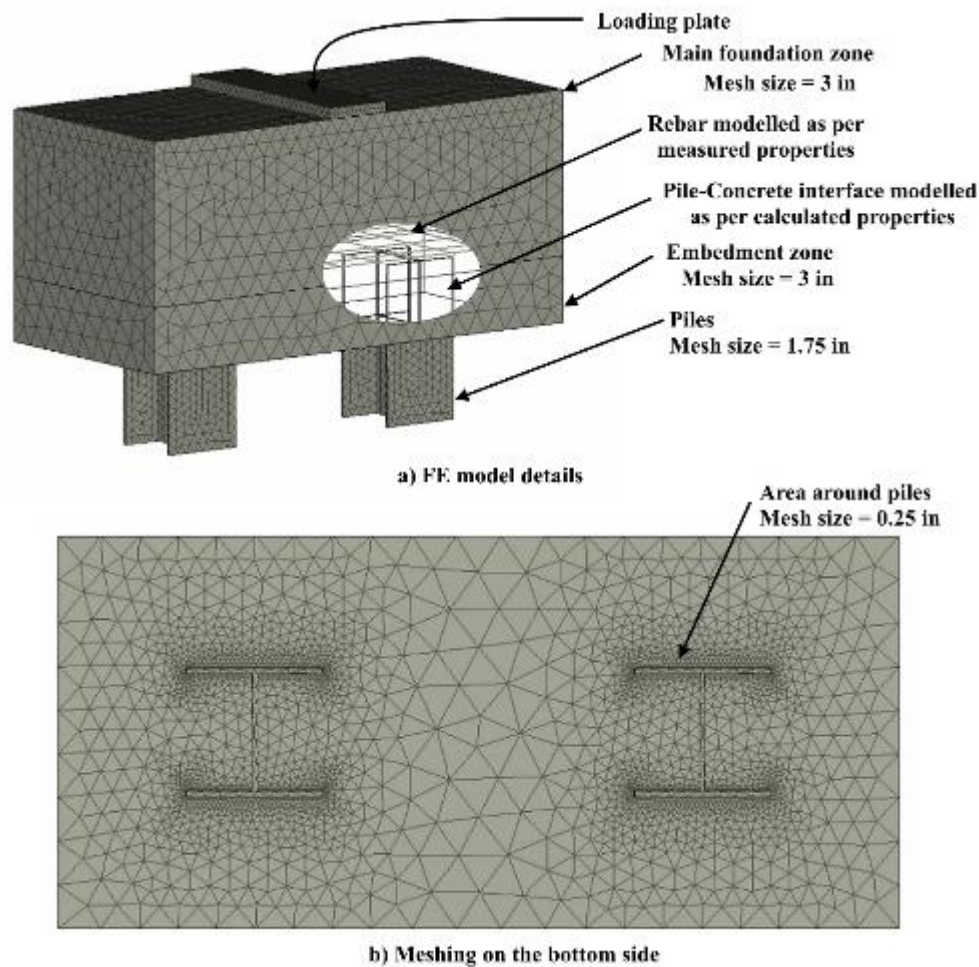


Figure 6-9 Figure showing post-construction Finite Element Analysis details of Specimen #3

6.5 Specimen #3 Test Results

A maximum load of 600 kips was applied on specimen #3, which corresponds to 1.5 times the maximum allowable load on each of the HP 12 X 53 piles. This specimen was intended to verify the adequacy of providing a pile embedment depth of 1 ft into the footing along with ALDOT design and detailing practices.

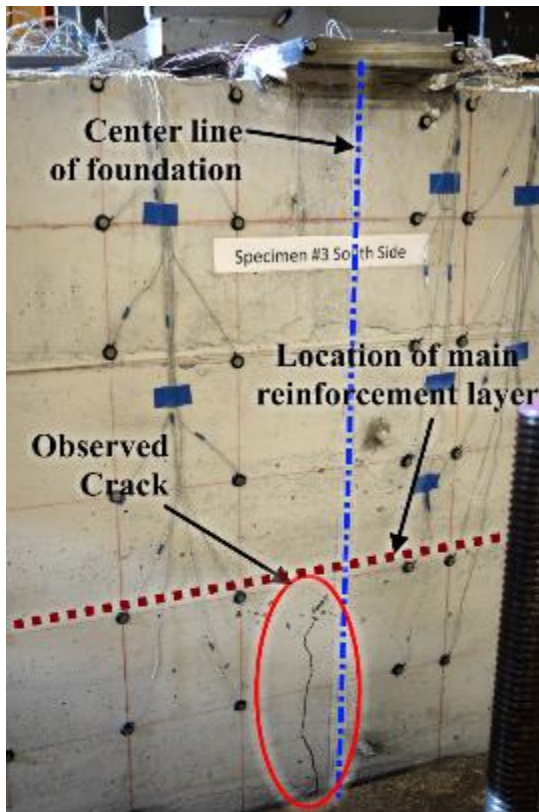
Upon applying a load of 600 kips the limit state of cracking was reached in the footing. A single crack in the middle region of the footing as shown in Figure 6-10a was observed at this loading. This crack extended from the bottom of the footing to the level of main reinforcement layer indicated by the dotted line in Figure 6-10a. A close-up view of this crack, along with a crack gauge is provided in Figure 6-10b. It was observed that at a depth of approximately 6 in below the main reinforcement layer, the crack widths were in the range of 0.007 in to 0.009 in. It should also be noted that this crack appeared suddenly at a load between 550 kips and 600 kips and was not a gradual progression from the bottom. This can be explained by the fact that little to no reinforcement is present in the bottom 1 ft of the foundation and thus as soon as the cracking stresses were reached, the crack zipped through till it reached resistance in the form main reinforcement layer. The crack locations and crack widths as per the finite element analysis is shown in Figure 6-10c. It can be seen from this figure that the finite element analysis predicts the crack widths to be in between 0.006 in to 0.010 in, which is within the range of values experimentally observed. In this context, it should also be noted that the crack width values predicted by ATENA (2016) are extremely sensitive to the input fracture energy (G_F) values provided. For this study the G_F value is taken as per the discussions provided in 4.2.1

At 600 kips the region surrounding the piles remained visibly intact and showed no signs of distress, thus indicating that even for 1 ft embedment depth the foundation reaches the limit state of cracking before the concrete surrounding the piles reaches its service limit state. This is a desirable condition and indicates the adequacy of the 1 ft embedment length for carrying compressive loads.

Results from the steel strain gauges at the midspan of the longitudinal rebar are shown in Figure 6-12a. This graph also shows the data from the finite element analysis (dashed lines). It can be observed that all the rebar remained in the elastic zone, the maximum stress observed was 20 ksi, while the maximum rebar stresses obtained from FEA was 22 ksi. It should also be observed that the steep increase in rebar stresses seen around the load of 570 kips is consistent with the fact that the cracks observed in the foundation appeared suddenly around this same load value. The FE model predicts the same behavior and shows a steep increase in rebar stresses at a value of 500 kips.

Figure 6-12 shows the load vs mid span deflection for specimen #3. This graph also presents the results from finite element analysis. The experimentally observed deflection at maximum load was 0.036 in, the FEA expected a deflection of 0.034 in. In this graph the change in of slope of the load vs deflection curve, which is an indicator of cracking load was observed at 525 kips as per the tests and 500 kips as per the FEA. It should be noted that the considerably small values of deflection are due to the large depth of foundation. The authors would also like to note that this

deflection value should not confused with foundation settlement values which are a function of soil-pile interaction.



a) Observed cracks in Specimen #3



b) Closeup view showing crackwidth

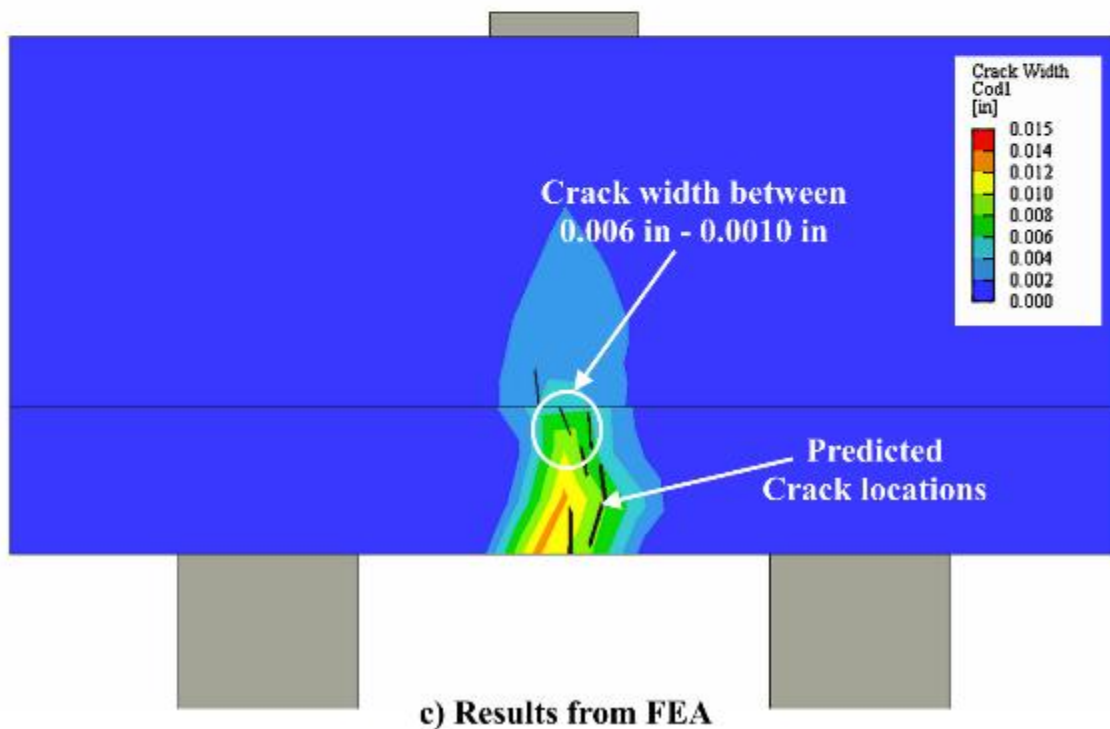


Figure 6-10 Comparison of experimental results with FEA for Specimen #3



Figure 6-11 Figures showing no visible damage to the concrete surrounding the pile in Specimen #3

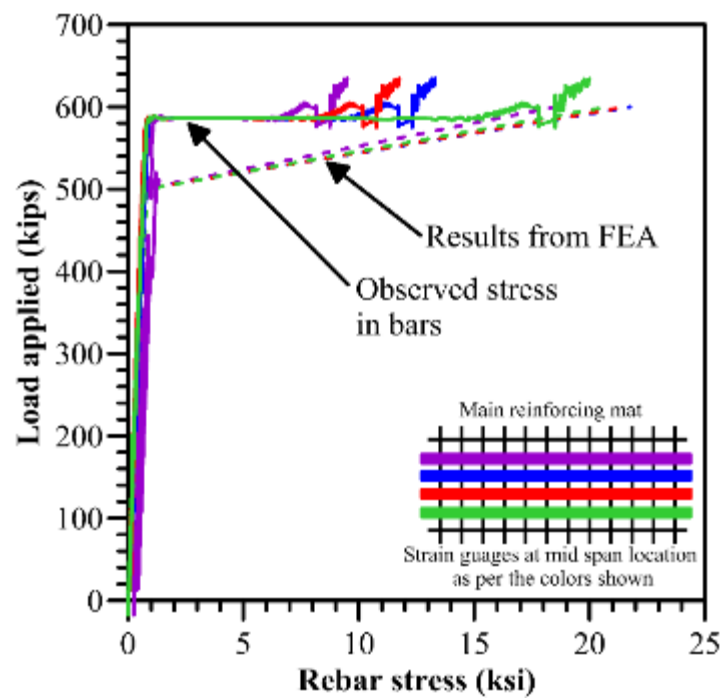


Figure 6-12 Graph showing the experimentally observed longitudinal rebar stresses and comparing with FEA in Specimen #3

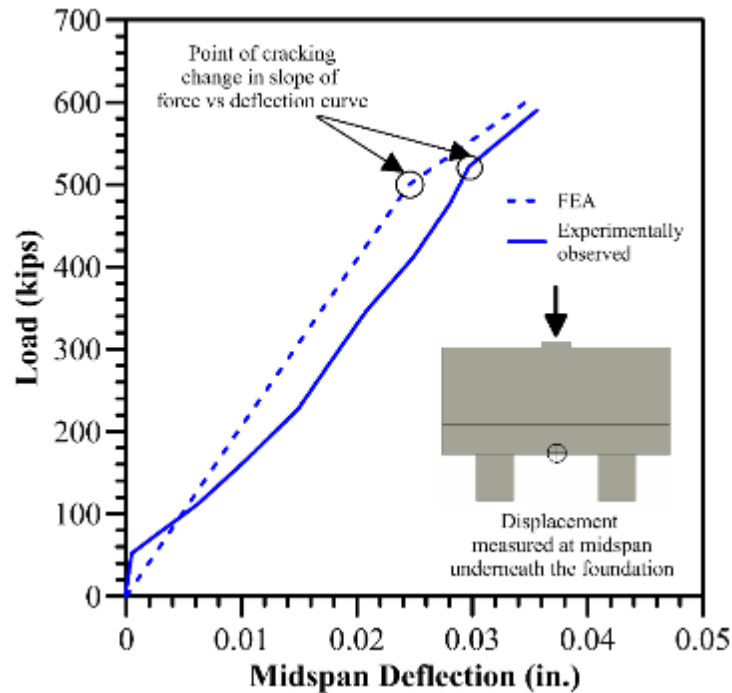


Figure 6-13 Graph showing load vs deflection from experimental observations and FEA for Specimen #3

To further verify the accuracy of the finite element model in predicting the behavior of this foundation, the strains from concrete gauges at critical locations are also compared. Figure 6-14a shows the concrete strain values at midspan and at the same height as the main reinforcement layer. It can be seen from this graph that this trend is similar to the strains observed in steel rebar discussed above. The experimentally obtained concrete gauge readings at peak load was 0.00044 and from FEA it was obtained as 0.00048. Figure 6-14b shows the strain gauge data obtained at the top of the foundation. It can be observed from this graph that while the initial stiffness is accurately predicted by the FEA, a deviation from the trend is observed around the 200 kip mark, wherein the strains remain stagnant with increasing load. This is possibly due to the presence of mortar stone in the vicinity of the strain gauge affecting its response. The strain values obtained using the strain gauge and FEA at peak load are 0.00018 and 0.00023.

The results presented in this section for specimen #3 and its comparison to the finite element model should be carefully weighed with the consideration that, the position of the strain gauge and the rebar itself are subject to variation during the concrete pour. Presence of air voids or cracks adjacent to a strain gauge can considerably affect the data. In this experimental investigation, care was taken to maintain the tolerances for the positioning of the strain gauges and rebar, as well as prevent air voids and cracks.

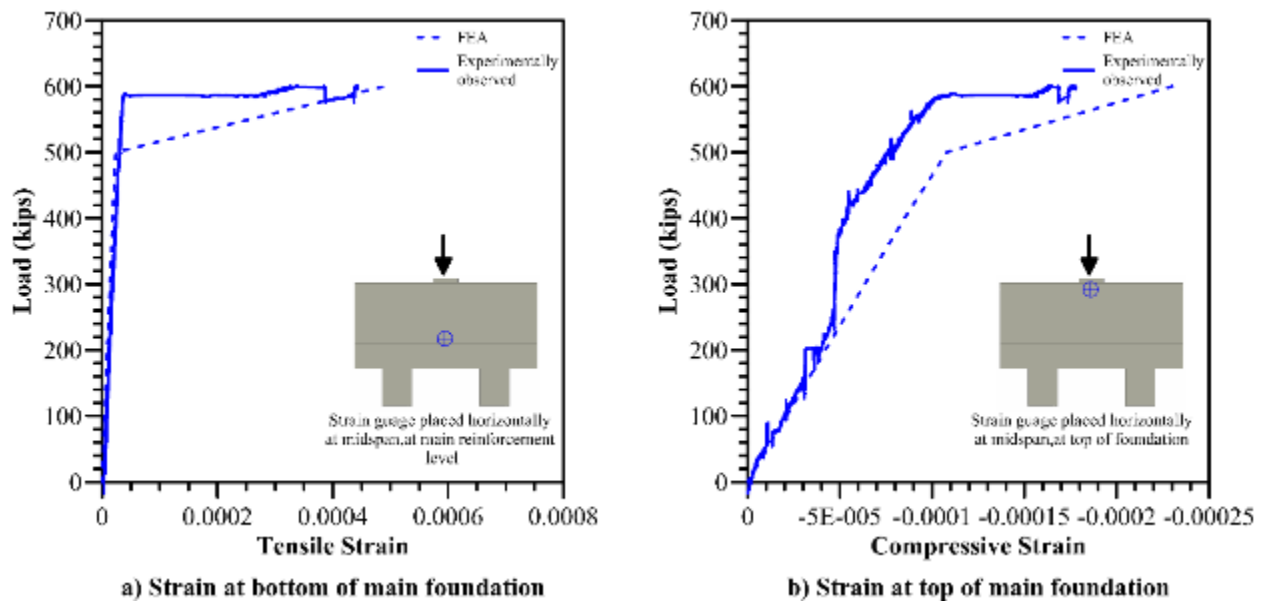


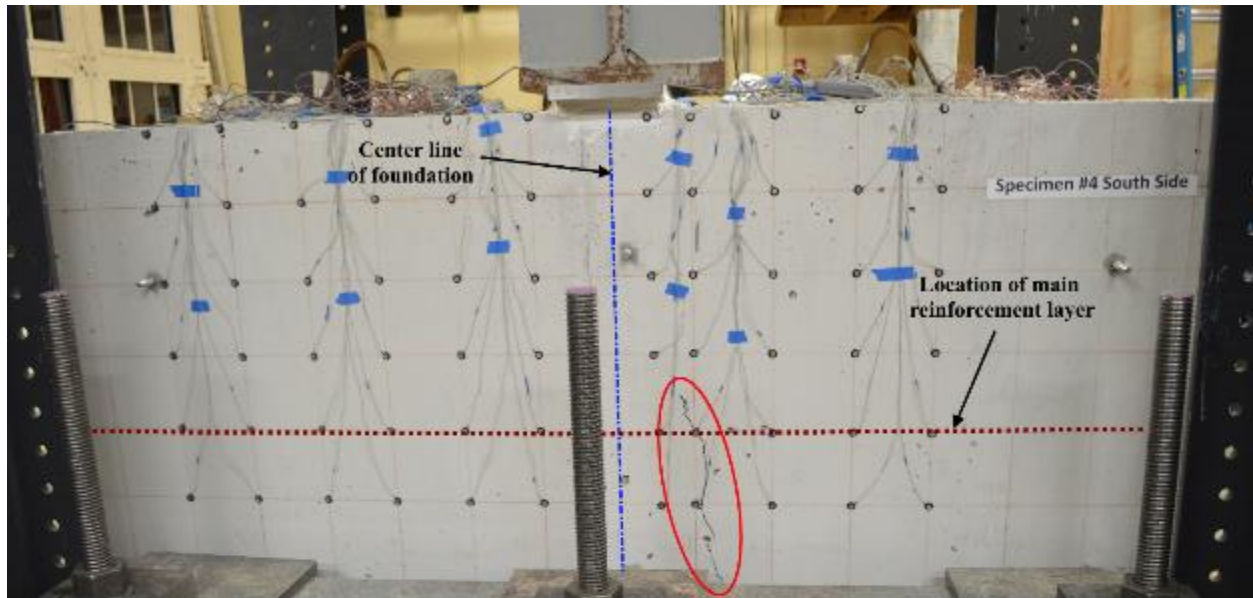
Figure 6-14 Figure showing graphs of concrete strains observed at critical locations for Specimen #3

6.6 Specimen #4 Test Results

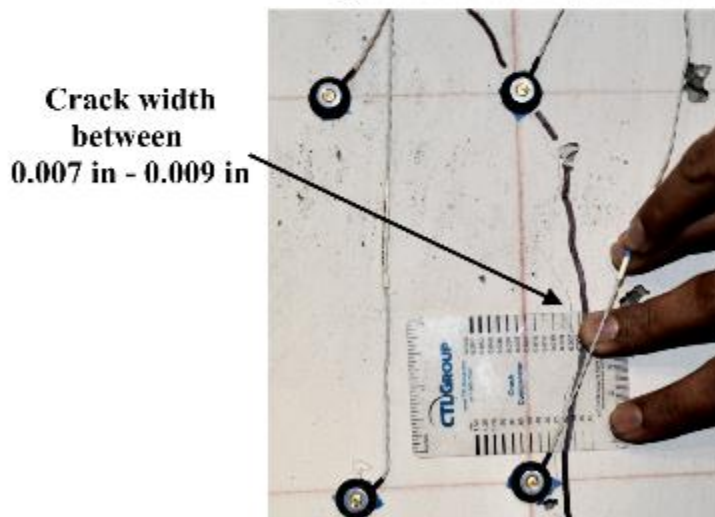
Specimen #4 was intended to check the performance of a precast pile foundation when compared to a cast-in-situ foundation (Specimen #3). The details of Specimen #4 and Specimen #3 were identical except for the presence of a void which was filled with grout. In presenting the results for this specimen the performance of various factors will be compared with Specimen #3.

This foundation was subject to a maximum load of 600 kips. A single crack at the middle of the foundation was observed at the load of 550 kips (Figure 6-15a). The crack width measured at approximately 6 in below the reinforcement layer was found to be in the range of 0.007 in to 0.009 in. These values are same as those observed in Specimen #3. The load displacement graph for specimen #4 is shown in Figure 6-16a. It can be seen from this graph that this specimen has a much higher displacement value of 0.12 in. at 600 kips compared to 0.036 in. in Specimen #3. This was because the failure of this specimen was through the settling of the foundation on the east side by 1 in. This settlement occurred possibly because of an air void in the grout fill. As explained previously in section 5.3, the grouting operation for the east side had issues and this might have led to the void not being completely filled with grout as intended. Figure 6-16b shows the tensile response of both Specimen #3 and Specimen #4 at the main reinforcement level. It can be seen from this graph that Specimen #4 exhibits a tensile response as Specimen #3. In this context the following things must be noted; Specimen #4 was capable of carrying 500 kips of load in the same manner as Specimen #3; the load of 500 kips is larger than the maximum allowable load on the HP 12 x 53 piles. Thus, it can be stated that the foundation reached the service limit state of the piles before failure. Based on the behavior of the foundation prior to 500 kips it is possible that if there were no air voids in the grout, Specimen #4 would have performed at the same level as the cast in situ specimen #3. To further verify that the performance of the precast foundation (Specimen #4) and cast-in-situ (Specimen #3) are similar, the strain gauge data at the middle of the compressive strut between the loading point and the pile support location are also compared in Figure 6-16c. It can be seen from this figure that the strains recorded in Specimen #3 are within

25 % of the strains recorded in Specimen #4. Figure 6-16c shows the strains recorded on the east side piles of Specimen #3 and Specimen #4. Specimen #4 also exhibited a similar strain distribution as that of Specimen #3, but as the material surrounding the piles for both the specimens is considerably different, i.e grout for Specimen #4, and normal concrete for Specimen #3, an exact comparison is not possible.

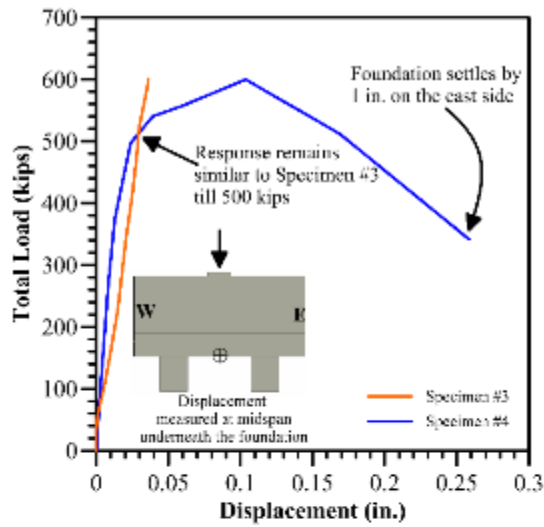


a) Observed cracks in Specimen #4

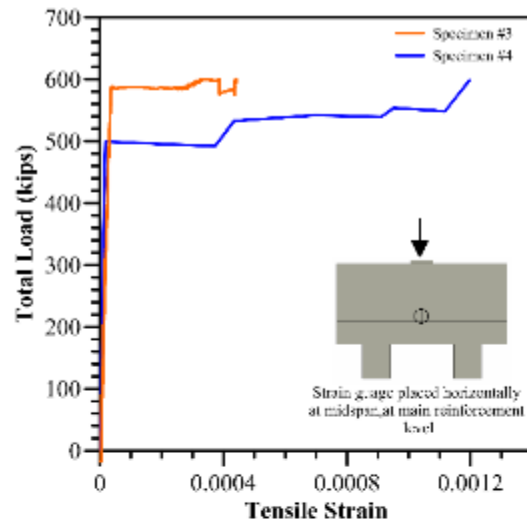


b) Closeup view showing crackwidth

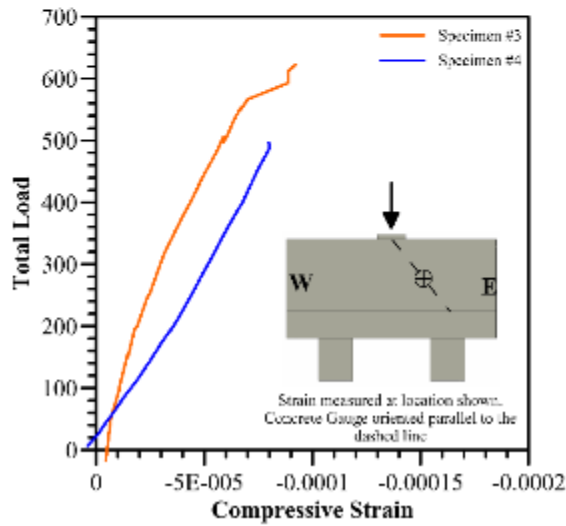
Figure 6-15 Figure showing cracking in Specimen #4



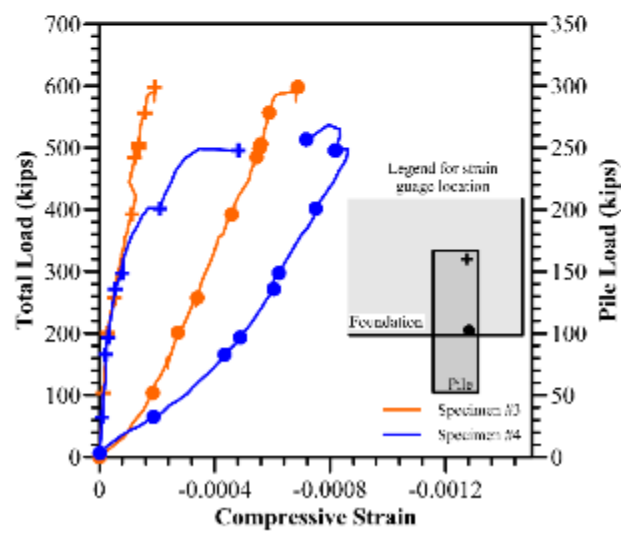
a) Displacement response at midspan, bottom of foundation



b) Tensile Strain response at main reinforcement level



c) Compressive strain response at the middle of the compressive strut



d) strain response in piles at different locations along the pile

Figure 6-16 Figure comparing the critical parameters of Specimen #3 and Specimen #4

CHAPTER 7: SUMMARY AND CONCLUSIONS

7.1 Summary

The objectives of this experimental and analytical study were to examine the feasibility of reduction in the minimum embedment depth requirements of steel piles into foundations and also to provide ALDOT Bridge Bureau with dependable and cost-effective substructure system which can be implemented as an accelerated bridge construction solution.

Existing research on the performance and behavior of several different types of pile to footing connections along with the requirements for minimum embedment length of state DOT's in the USA were examined and reviewed in Chapter 2 of this report.

In Chapter 3 an analysis is carried out to examine the range of loading values to be expected on top of foundations, subsequently a prototype bridge foundation was finalized in consultation with ALDOT.

In order to understand the effect of reducing the pile embedment, a finite element model of the prototype bridge was developed in ATENA software. Three different models were prepared with embedment lengths of 2 ft, 1 ft, and 0.5 ft. The other details of these footings were kept exactly the same. The objectives of the 3D FEA were to understand the effect of embedment length on concrete stresses surrounding the pile and stresses on the main reinforcement layer. Subsequent to the analysis it was found that by reducing the embedment depth to 1ft, the performance of the footing is not substantially affected. Chapter 4 presents the details of the techniques implemented in this Finite Element Analysis.

Based on this understanding, four different test specimens were prepared and finalized. Specimen #1 and Specimen #2 were intended to characterize the behavior of the pile – concrete interface. Specimen #3 was designed to check the adequacy of 1 ft embedment depth. Specimen #4 was intended to check the performance of a cast-in-situ foundation to a precast foundation. All these specimens were cast in the Large Scale Structures Lab in University of Alabama. The details of the specimen fabrication along with information on test setup and instrumentation were provided in Chapter 5

Chapter 6 presented the results of the experimental program, using the data from test specimens #1 and #2 the necessary properties required to characterize interface behavior were obtained. The results from Specimen #3 indicated that a footing with 1 ft embedment length can safely carry the maximum loads that can be expected of HP 12 X 53 piles. The finite element model was also compared and validated with Specimen #3. Specimen #4 results indicated that the performance of the precast footing is similar to that of a cast-in-situ footing, but due to grouting issues this specimen failed by the foundation settling on one pile by 1 in.

7.2 Conclusions

The following conclusions were reached based on the analytical and experimental investigation carried out:

- Majority of the state department of transportations in the US specify a minimum embedment length of 1 ft.
- The results from the finite element study of the prototype foundation indicate that for loads which exert only compressive stresses, pile embedment depth does not affect the characteristics of the foundation and its behavior.
- Based on the finite element study of the prototype foundation it was found out that decreasing the embedment length of pile into footing to 1 ft or 0.5 ft does not increase rebar stresses, flexural stresses, or shear stresses in the footing.
- Based on the experimental investigation of Specimen #1 and Specimen #2, it can be concluded that for a pile surface condition such as the one used in this study:
 - The steel pile-to-concrete skin friction capacity increases linearly with increasing depth.
 - The cohesion capacity is 0.23 ksi. For a HP 12 X 53 pile this translates to a load of up to 190 kips which can be transferred using only skin friction for 1 ft embedment.
- Based on the experimental investigation of Specimen #3 it can be concluded that:
 - The connection between a HP 12 X 53 pile embedded 1 ft into the footing has more capacity than the pile service limit state.
 - The finite element analysis techniques developed as part of this study can accurately predicted the behavior of a pile to foundation connection. These FE methods can be used in the future investigate further design changes.
- Based on the experimental investigation of Specimen #4, it can be concluded that a precast footing with grout details as given in this report may perform just as well as a cast-in situ foundation, provided no air voids are left during the grouting procedure.

7.3 Recommendations for Future Research

Based on the findings from the research conducted in this study further research on the following topics is recommended:

- The effect of decreasing embedment depth should also be studied for lateral and tensile loads.
- A comprehensive study categorizing the pile surface condition at the time of casting should be carried out to determine the cohesion value more effectively between the steel piles and concrete.
- A precast detail utilizing the main footing thickness for embedding the piles should be examined using advanced materials such as UHPC.

CHAPTER 8: REFERENCES

- Aaleti, S., Heine, J., & Sritharan, S. (2012). Experimental evaluation of UHPC piles with a splice and pile-to-abutment connection performance. Nashville, TN: Prestressed/precast concrete institute.
- ACI. (2011). *Building Code Requirements for Structural Concrete*. American Concrete Institute.
- ACI. (2014). *ACI 318-14: Building Code Requirements for Structural Concrete*. American Concrete Institute.
- American Association of State Highway and Transportation Officials. (2017). AASHTO LRFD Bridge Design Specifications. Washington, DC.
- ASTM. (2015). Standard Test Method for Resistance of Concrete to Rapid Freezing and Thawing. C666. ASTM.
- CEB-FIP. (1993). CEB-FIP Model Code 1990: Design Code. Thomas Telford.
- Červenka, V., Jendele, L., & Červenka, J. (2016). ATENA Program Documentation Part 1 Theory. Prague: Červenka Consulting.
- Colorado State DOT. (n.d.). *Bridge Design Manual*. Retrieved from https://www.codot.gov/library/bridge/bridge-manuals/lrfd-bridge-design-manual/lrfd_bridgedesignmanual_june2017/at_download/file
- Connecticut DOT. (n.d.). *Bridge Design Manual*. Retrieved from <http://www.ct.gov/dot/lib/dot/documents/dpublications/bridge/bdm.pdf>
- Culmo, M. P. (2009). *Connection Details for Prefabricated Bridge Elements and Systems*. Federal Highway Administration.
- Delaware DOT. (n.d.). *Bridge Design Manual*. Retrieved from https://www.deldot.gov/information/pubs_forms/manuals/bridge_design/2016/bridge_design_manual.pdf
- Georgia DOT. (n.d.). *Bridge and Structures Policy Manual*. Retrieved from http://www.dot.ga.gov/PartnerSmart/DesignManuals/BridgeandStructure/GDOT_Bridge_and_Structures_Policy_Manual.pdf
- Graybeal, B. (2014). *Design and construction of field-cast UHPC connections*. McLean, VA: Fedral Highway.
- Idaho DOT. (n.d.). *Bridge Design Manual*. Retrieved from <http://apps.itd.idaho.gov/apps/bridge/manual/11%20Abutments%20Piers%20and%20Walls/11.6.1.3%20Integral%20Abutments.pdf>
- Illinois DOT. (n.d.). *Bridge Manual*. Retrieved from <http://www.idot.illinois.gov/Assets/uploads/files/Doing-Business/Manuals-Guides-&-Handbooks/Highways/Bridges/Bridge%20Manual%202012.pdf>
- Indiana DOT. (n.d.). *Design Manual*. Retrieved from http://www.in.gov/indot/design_manual/files/Ch409_2013.pdf
- Iowa DOT. (n.d.). *LRFD Bridge Design Manual*. Retrieved from <http://www.iowadot.gov/bridge/policy/06-02-00PileLRFD.pdf>
- Kansas DOT. (n.d.). *Construction Manual*. Retrieved from <https://www.ksdot.org/Assets/wwwksdotorg/bureaus/burStructGeotech/ConstructionManual/pile.pdf>

- Kentucky DOT. (n.d.). *Structural Design Manual*. Retrieved from <https://transportation.ky.gov/StructuralDesign/Documents/Chapters3.pdf>
- Mander, J. B., Priestley, M. J., & Park, R. (1988). Theoretical Stress-Strain Model for Confined Concrete. *Journal of Structural Engineering*, 1804-1825.
- Marcakis, K., & Mitchell, D. (1980). Precast Concrete Connections with Embedded Steel Members. *PCI Journal*, 88-116.
- Michigan DOT. (n.d.). *Bridge Manual*. Retrieved from <http://mdotcf.state.mi.us/public/design/englishbridgemanual/>
- Minnesota DOT. (n.d.). *LRFD Bridge Design Manual*. Retrieved from <https://www.dot.state.mn.us/bridge/pdf/lrfdmanual/lrfdbridgedesignmanual.pdf>
- Montana DOT. (n.d.). *Structures Manual*. Retrieved from http://www.mdt.mt.gov/other/webdata/external/bridge/structures-manual/part_II/chp-20-final.pdf
- Nevada DOT. (n.d.). *Structures Manual*. Retrieved from <https://www.nevadadot.com/home/showdocument?id=1733>
- New Hampshire DOT. (n.d.). *Bridge Design Manual*. Retrieved from <https://www.nh.gov/dot/org/projectdevelopment/bridgedesign/documents/CompleteChapter6Mar2016.pdf>
- North Carolina DOT. (n.d.). *Structures Design Manual*. Retrieved from https://connect.ncdot.gov/resources/Structures/Structure%20Design%20Manual/02%20Design%20Manual%20Changes_Metric.pdf
- North Dakota DOT. (n.d.). *Design Manual*. Retrieved from <https://www.dot.nd.gov/manuals/design/designmanual/Chapter%204.pdf>
- NY State DOT. (n.d.). *Bridge Manual*. Retrieved from https://www.dot.ny.gov/divisions/engineering/structures/repository/manuals/brman-usc/NYSDOT_bridge_manual_US_2014.pdf
- Ohio DOT. (n.d.). *Bridge Design Manual*. Retrieved from http://www.dot.state.oh.us/Divisions/Engineering/Structures/standard/Bridges/BDM/BD M2007_07-15-16.pdf
- Oregon DOT. (n.d.). *Bridge Design Manual*. Retrieved from <https://www.oregon.gov/ODOT/Bridge/Pages/Bridge-Design-Manual.aspx>
- Rhode Island DOT. (n.d.). *LRFD Bridge Manual*. Retrieved from <http://www.dot.ri.gov/documents/doingbusiness/RILRFDBridgeManual.pdf>
- Rollins, K. M., & Stenlund, T. E. (2010). *Laterally Loaded Pile Cap Connections*. Salt Lake City, UT: Utah Department of Transportation.
- Shama, A. A., Mander, J. B., & Aref, A. J. (2002). Seismic Performance and Retrofit of Steel Pile to Concrete Cap Connections. *ACI Structural Journal*, 51-61.
- Silva, P. F., & Seible, F. (2001). Seismic Performance Evaluation of Cast-in-Steel-Shell (CISS) Piles. *ACI Structural Journal*, 36-49.
- South Carolina DOT. (n.d.). *Bridge Design Manual*. Retrieved from https://www.scdot.org/business/pdf/structural-design/SCDOT_Bridge_Design_Manual.pdf
- Stephens, J. E., & Mckittrick, L. R. (2005). *Performance of Steel Pipe Pile-to-Concrete Bent Cap Connections Subject to Seismic or High Transverse Loading Phase II*. Helena, MT: Montana Department of Transportation.

- Steunenbergh, M., Sexsmith, R. G., & Stierner, S. F. (1998). Seismic Behavior of Steel Pile to Precast Concrete Cap Beam Connections. *ASCE Journal of Bridge Engineering*, 177-185.
- Vermont DOT. (n.d.). *Structures Design Manual*. Retrieved from http://vtrans.vermont.gov/sites/aot/files/highway/documents/structures/Structures_Design_Manual.pdf
- Vos, E. (1983). *Influence of loading rate and radial pressure on bond in reinforced concrete*. Delft University Press .
- Washington State DOT. (n.d.). *Bridge Design Manual*. Retrieved from <http://www.wsdot.wa.gov/publications/manuals/fulltext/M23-50/BDM.pdf>
- West Virginia DOT. (n.d.). *Bridge Design Manual*. Retrieved from <http://www.transportation.wv.gov/highways/engineering/files/WVBDML%203-8-16.pdf>
- Wisconsin DOT. (n.d.). *Bridge Manual*. Retrieved from <http://wisconsindot.gov/dtsdManuals/strct/manuals/bridge/ch11.pdf>
- Xiao, Y., & Chen, L. (2013). Behavior of model steel H-pile-to-pile-cap connections. *Journal of Constructional Steel Research*, 153-162.
- Xiao, Y., Wu, H., Yaparak, T., Martin, G., & Mander, J. (2006). Experimental studies on seismic behavior of steel pile-to-pile-cap connections. *ASCE Journal of Bridge Engineering*, 151-159.